Development of a Rectenna Adapted to Ultra-wide Load Range for Microwave Power Transmission

Yong Huang

Kyoto University

Doctoral Thesis

Development of a Rectenna Adapted to Ultra-wide Load Range for Microwave Power Transmission

Author:
Yong Huang

Supervisor:
Prof. Naoki Shinohara

A thesis submitted in fulfilment of the requirements for the degree of Doctor of Philosophy

in the

Department of Electrical Engineering
Graduate School of Engineering
Kyoto University

February 2015

Acknowledgments

I would like to express my sincere gratitude to my supervisor, Professor Naoki Shinohara. I am so thankful to him for giving me an important opportunity to study my Ph.D. course in Shinohara Lab. of Research Institute for Sustainable Humanosphere (RISH) of Kyoto University. In this three years, he has provided continuous guidance, encouragement, useful advice for the present study. Specially, he is also concerned about my living as I am an international student studying in Japan. In addition, His enthusiasm for research and education will inspire me in my whole life. I have been extremely lucky to have a supervisor like him.

I am also grateful to Professor Osami Wada of Kyoto University for our fruitful discussions and his rigorous scholarship. I greatly appreciate his many helpful comments and suggestions as a reviewer of this thesis. I am very grateful to Professor Hiroshi Yamakawa of RISH of Kyoto University. I have to greatly thank him for reviewing this thesis and giving many useful comments and valuable advice. I also want to thank Associate Professor Hirotsugu Kojima of RISH of Kyoto University. I would like to give great thanks to him for affording enough time to discuss with me even he is very busy with his researches.

I must thank Associate Professor Tomohiko Mitani of RISH of Kyoto University. He provided us a convenient experiment environment and also gave me many valuable comments every time in the meeting of Shinohara Lab.. He has taught me many knowledge about microwave circuits and the usage of experiment equipment. I cannot thank him enough for his continuous support and constant interest in my study.

I am grateful to Professor Yoshiharu Omura, Associate Professor Yusuke Ebihara, and Assistant Professor Yoshikatsu Ueda for their great encouragement and helpful suggestions and advice on the present study. I greatly thank Dr. Takaki

Ishikawa, Dr. Naoki Hasegawa, Dr. Takayuki Matsumuro for their heartfelt discussions on my study and for kindly teaching me Japanese. I am very grateful to the countless others for their kind support including Dr. Yasumasa Ashida, Dr. Yoh Nagasaki, Dr. Kouhei Yamaguchi, Dr. Yohei Nakayama, Mr. Yuta Kubo, Mr. Ken Hatano, Mr. Akihito Nagahama and all of the space group members of RISH for many helpful discussions.

I wish to express my special gratitude to Ms. Yukiko Ueoka, secretary of Professor Shinohara, for her secretariat help and continuous careful support. I wish to thank Dr. Keiichiro Kashimura and Dr. Yao Yao for their kind support and encouragement.

Finally, I can hardly express my gratitude to my dear wife Hoho for her love, support, care and encouragement. I would also like to express my appreciation to my mother Xiurong and my older sister Min for their understanding and strong support for my Ph.D. course. I wish to thank my entire extended family for their support.

Abstract

Numerous studies have been carried out on the wireless power transmission (WPT) technologies, which transfers power to the electrical loads without man-made wires. As one mean of WPT, microwave power transmission (MPT) has attracted lots of attention due to its long-distance power transmission capability. A notable problem among these technologies is that the RF to DC conversion efficiency could be easily affected by the load resistance and the input power. Therefore, an impedance matching circuit becomes crucial to realize the wireless power transmission with high efficiency. Moreover, most of the impedance matching circuits in microwave circuits utilize distributed-constant circuits, whereas, the rectenna is a special distributed-constant circuit yielding a DC output. This present thesis aims at developing an ultra-wide load range rectenna for microwave power transmission and a resistance matching circuit from the viewpoint of DC, which is easy to design since it is unnecessary to consider high harmonics.

Different from the conventional DC-DC converters used for voltage conversion, in the present thesis, a resistance conversion DC-DC converter is proposed and validated in the following procedures:

Firstly, with aid of the simulator of advanced design system (ADS), a common pulse-width modulation (PWM) controlled boost converter is checked as an impedance matching circuit for rectifying circuit. For the validation a simulation model of RF-DC-DC circuit is built which consists of a simple single shunt rectifying circuit and the boost converter. The simulation results show that the overall efficiency of the RF-DC-DC circuit is almost constant over 70 % in the load range from 370 to 1300 Ω. Moreover, it is also found that the boost converter can prevent the reverse voltage applied on the rectifying diode from exceeding breakdown voltage and then the rectifying circuit can keep acting at the peak efficiency point. However, this PWM controlled boost converter can only convert

a wide load range into a narrow input resistance range which is insufficient for an impedance matching requirement of rectenna.

Next, according to the previous simulation results, an RF-DC-DC circuit is shown to be useful for impedance matching application. Therefore, an externally-powered RF-DC-DC circuit, consisting of a negative output rectifying circuit and a DC-DC converter, is designed. To choose a more suitable type of DC-DC converter, the input/output resistance relationships of three major DC-DC converter topologies (i.e. buck converter, boost converter and buck-boost converter) are investigated in continuous conduction mode (CCM) and discontinuous conduction mode (DCM), respectively. Only the DCM buck-boost converter is found to exhibit constant input resistance characteristic independent of the input voltage and the load resistance. Therefore, an inverting DCM buck-boost converter is adopted with an extra DC power supply for the control-pulse circuit, and the input resistance of the buck-boost converter is set to be close to the optimal load of the rectifying circuit. The experimental results show that the overall efficiency of this externally-powered RF-DC-DC circuit is approximately constant and over 60 %, despite the load resistance ranging from 100 to 5000 Ω.

However, the externally-powered RF-DC-DC circuit is difficult for the practical applications because of the requirement of an extra DC power supply. To solve this problem a self-powered RF-DC-DC circuit consisting of a positive output rectifying circuit and a non-inverting self-powered buck-boost converter is proposed. It can obtain a positive output voltage with a single positive input voltage. Furthermore, the input resistance of the buck-boost converter is designed to be equal to the optimal load of the rectifying circuit. The experimental results show that the overall efficiency of the self-powered RF-DC-DC circuit is constant and over 66 %, despite an ultra-wide load ranging from 200 to 10000 Ω.

Finally, several experiments are carried out on driving a DC motor using MPT with a compact designed power-receiving device which consists of a rectenna array (including some antennas and rectifiers) and an improved buck-boost converter. There exits four types of power-receiving devices combined by two different rectenna arrays and two different buck-boost converters. With these four power-receiving devices, some experiments are conducted by driving a dynamic load resistance device such as a DC motor with continuous-wave (CW) power transmission and pulsed-wave power transmission. In the CW case, the overall efficiency of the compact power-receiving device is above 50 % in a wide power density ranging from 0.25 to 2.08 mW/cm^2. In the pulsed-wave case, the overall efficiency is above 44 % in the duty ratio ranging from 0.2 to 1 for a power density of 0.98 mW/cm^2. Moreover, at a fixed duty ratio of 0.5, the overall efficiency is almost constant at 59 % with the pulsed-wave frequency changing from 0.33 to 41.7 kHz.

Therefore, tested by both load resistances and a dynamic load resistance device, the proposed rectenna is found to be excellent in a relatively high efficiency for an ultra-wide load range. As a novel application of DC-DC converter, the proposed buck-boost converter, with constant input resistance characteristic, is also expected to be valuable for other WPT applications.

Contents

List of Figures

List of Tables

Nomenclature

δ	off-state ratio
ε_{r}	dielectric constant
$\tan\,\delta$	dissipation factor
η_{all}	overall efficiency
$\eta_{\mathrm{dc-dc}}$	DC-DC converter efficiency
$\eta_{\mathrm{rf-dc}}$	RF-DC conversion efficiency
η_{prd}	overall efficiency of power-receiving device
η_{track}	tracking efficiency
η'_{track}	tracking efficiency
η'_{prd}	overall efficiency of power-receiving device
λ	wavelength
ΔI_{Lon}	inductor current variation at on-state
ΔI_{Loff}	inductor current variation at off-state
Δt	time variation
∞	infinity
B_{V}	reverse breakdown voltage
C_{J0}	junction capacitance
C_{in}	input capacitance
C_{o}	output capacitance
D	duty-on ratio
D_{pw}	pulsed-wave duty-on ratio
D_{h}	high frequency duty-on ratio
D_{ι}	low frequency duty-on ratio
dB	decibel
dBi	decibels over isotropic
E_{g}	activation energy
f	frequency
f_{sw}	switching frequency

f_{h}	high frequency
f_{ι}	low frequency
H	dielectric substrate thickness
I_{d}	diode current
I_{dc}	inductor allowable dc current
I_{inave}	converter average input current
I_{in}	converter input current
I_{L}	inductor current
I_{LP}	inductor peak current
I_{m}	DC motor input current
I_{o}	output current
I_{s}	saturation current
I_{SS}	power supply current
I_{BV}	reverse breakdown current
L	inductance
M	junction grading coefficient
N	emission coefficient
P_{RF}	microwave input power
P_{d}	diode loss ratio
P_{rall}	received RF power of antenna array
P_{m}	DC motor input power
P_{mos}	mosfet loss ratio
P_{o}	output power
R_{dc}	inductor dc resistance
$R_{\mathrm{DS(on)}}$	static drain-source on-resistance
R_{L}	load resistance
R_{in}	emulated input resistance of converter
$R_{\mathrm{in}}^{'}$	emulated input resistance of converter
R_{m}	emulated input resistance of DC motor
R_{out}	output load resistance
R_{s}	series resistance of diode
t	copper thickness
T	period
T_{on}	switch-on period
T_{off}	switch-off period
V_{d}	reverse voltage on diode

V_{DC}	dc output voltage
V_{DDmin}	minimum supply input
V_{DSS}	drain-source voltage
V_{FM}	peak forward voltage
V_{gate}	gate control-pulse voltage
V_{GS}	gate-source voltage
V_{h}	high frequency pulse voltage
V_{in}	input voltage
V_{j}	junction potential
V_{L}	inductor voltage
V_{ι}	low frequency pulse voltage
V_{rated}	rating voltage
V_{RRM}	repetitive peak reverse voltage
V_{m}	DC motor input voltage
V_{out}	output voltage
V_{SSmin}	minimum operating supply
Z_{out}	rectifier output impedance
Z_{opt}	rectifier optimal load
Z_{sw}	input impedance of control-pulse circuit

Chapter 1

Introduction

1.1 Wireless Power Transmission

Wireless power transmission (WPT) is the transmission of electrical energy from a power source to an electrical load without man-made conductors, which is useful in cases where interconnecting wires are inconvenient, hazardous, or impossible. Maxwell's equations, which were formulated in 1864, are essentially the first theoretical basis of WPT [1]. The concept of the Poynting vector elucidates the radio wave as representing the energy flux of an electromagnetic field. After Maxwell and Poynting, Nikola Tesla had a dream over a hundred years ago that all electricity would be provided without wires. He carried out the first WPT experiments via 150 kHz radio wave at the end of 19^{th} century [2]. However, his experiments ended in failure because they were far ahead of the high frequency technologies at that time. As the wireless communications and radar remote sensing technologies developing, William C. Brown developed a rectifying antenna named a "rectenna" and restarted WPT experiments with high-efficiency microwave technologies in 1960s [3]. The efficiency of the first rectenna developed by Brown was 50 % at an output of 4 WDC and 40 % at an output of 7 WDC, respectively [4]. With the rectenna, Brown's team had conducted many experiments on WPT such as the successful application of microwave power transmission (MPT) to a wired helicopter in 1964 and a free-flying helicopter in 1968 as shown in Fig. 1.1 [5].

Based on Brown's works, P. E. Glaser proposed a Space Solar Power Satellite (SSPS) system in 1968 [6], which is a huge satellite designed as an electric power

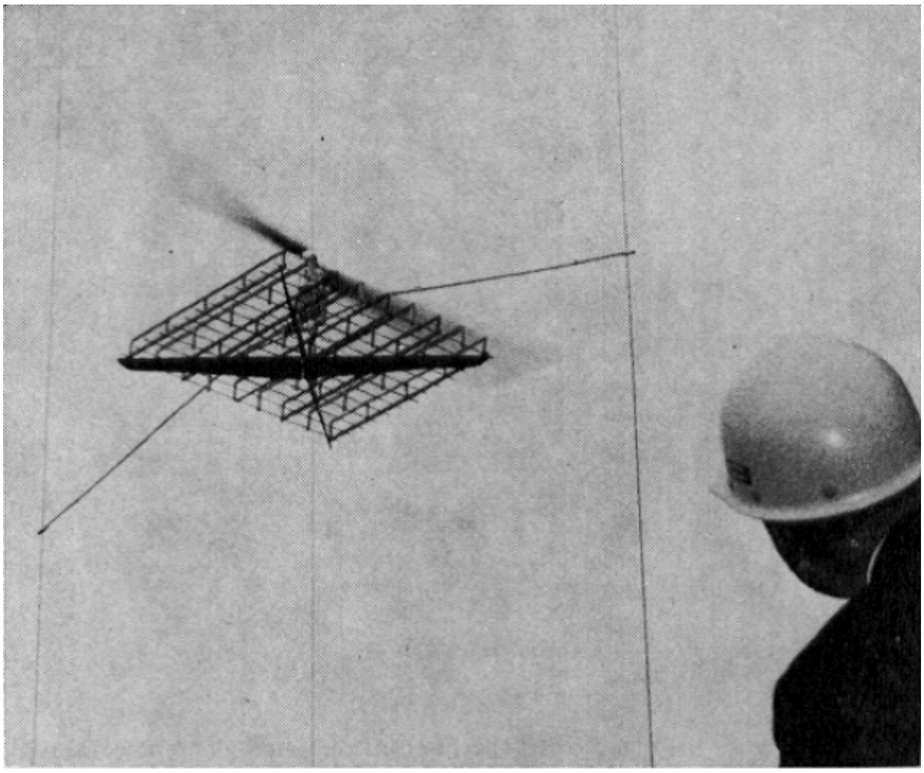

Figure 1.1: MPT experiment by W. C. Brown in 1964: the view of microwave-powered helicopter in flight at an altitude of 50 ft [5].

plant orbiting in the Geostationary Earth Orbit (GEO). Numerous Japanese scientists developed MPT technologies and researches throughout the 1980s [7]-[9]. Hiroshi Matsumoto's team carried out the first MPT experiment in space. The rocket experiment called MINIX (Microwave Ionosphere Nonlinear Interaction eXperiment) was conducted in 1983 as shown in Fig. 1.2, and ISY-METS (International Space Year - Microwave Energy Transmission in Space) was conducted in 1993 and so on.

The historical summary of WPT from Maxwell's times to nowadays is shown in Fig. 1.3 [10]. Over a hundred years development, WPT seems to be difficult for the commercial applications until recent years. A. Kurs's group, from MIT (Massachusetts Institute of Technology) of USA, proposed an efficient WPT via strongly coupled magnetic resonances at 9.9 MHz radio wave which was published on Science in 2007 [11]. They succeeded to transfer 60 watts with the efficiency of 40 % between two coils over distances in excess of 2 meters. Due to their success, it seems that resonant coupling WPT is more suitable for commercial needs. Therefore, there appears a worldwide upsurge of WPT researches in universities and companies.

(a) (b)

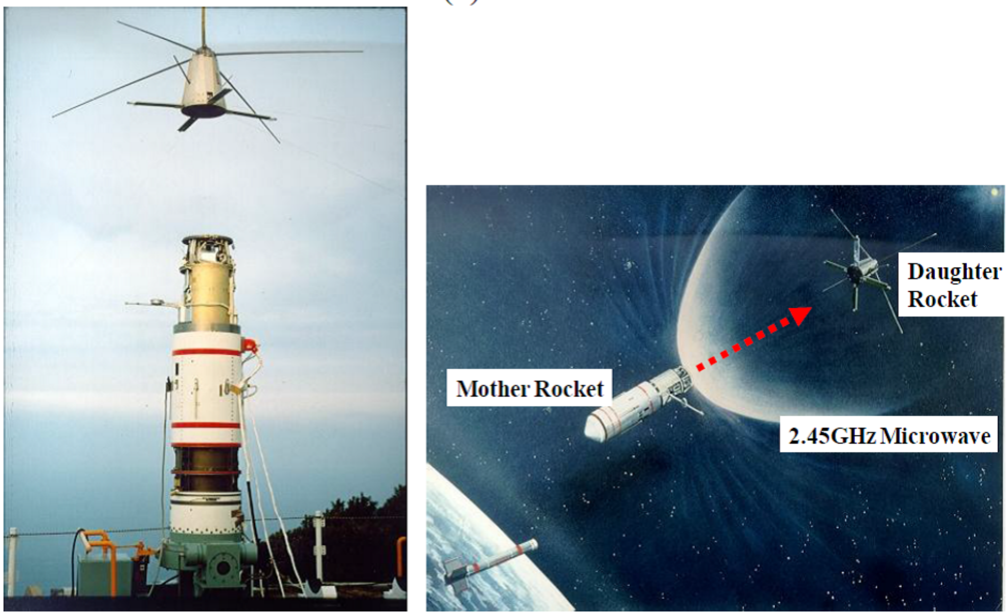

Figure 1.2: The first rocket experiment by H. Matsumoto in Japan in 1983, called the MINIX project. (a) Photo of mother and daughter rockets. (b) Photo of the experiment. These experiments were focused on the nonlinear interaction between intense microwaves and ionospheric plasmas and directed towards SSPS applications [8].

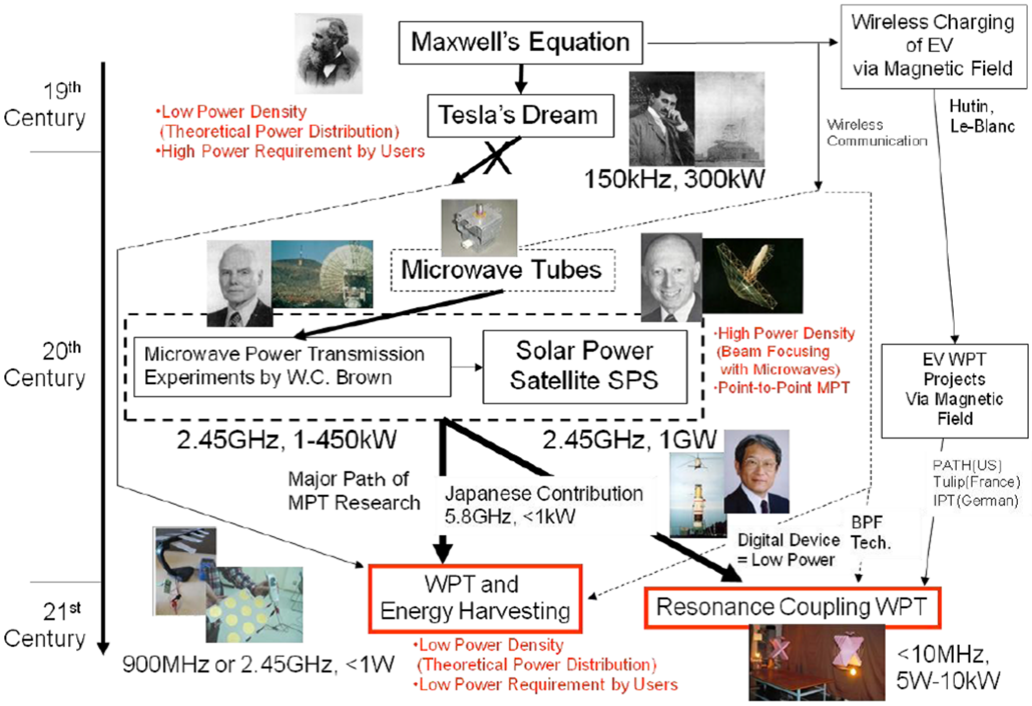

Figure 1.3: Historical summary of WPT from Maxwell's equation to RF harvesting technologies of recent years [10].

Table 1.1: Comparison of three WPT technologies [24].

	Radio wave or microwave	Resonance	Inductive coupling
Field	Electromagnetic (EM)	Resonance (Electric, Magnetic or EM)	Magnetic
Method	Antennas	Resonators	Coils
Efficiency	Low to high	High	High
Distance	Short to long	Medium	Short
Power	Low to high	High	High
Safety	EM	Under discussion (Evanescent)	Magnetic
Regulation	Radio wave or microwave	Under discussion	Under discussion

Nowadays, the common form of WPT is mainly carried out by three ways as follows: by radio waves or microwaves [12]-[15] based on wireless communication technologies and system design; by inductive coupling or be named as inductive power transmission [16]-[19]; by electric, magnetic or electromagnetic resonant coupling [20]-[23]. All of those WPT technologies are based on Maxwell's equations in theory but there are some differences in their applications. The characteristics of those WPT technologies are summarized in Table 1.1 [24].

1.2 Microwave Power Transmission

Microwave Power Transmission (MPT) is one type of WPT that mainly focuses on the frequency of 2.45 GHz, 5.8 GHz of ISM (Industry-Science-Medical) band. Based on the beam control technologies and high power transmission, the biggest advantage of MPT is that it offers the possibility of long-distance power transmission with a high efficiency [25]. Recently, with transmission power from micro-watt level to kilo-watt level, the MPT technologies have been used in various applications. According to the distance of power transmission, applications of MPT can be roughly classified into space-to-space, space-to-ground and ground-to-ground power transmission. Examples of potential space-to-space applications include MPT for a Mars observation airplane [26] and wireless sensors in the spacecraft [27]. A well-known space-to-ground application is SSPS [28]-[31]. The SSPS consists of mainly three segments: solar energy collectors to convert the solar energy into DC (direct current) electricity; DC-to-microwave converters; and a large antenna array to beam down the microwave power to the ground. The first solar collector can be either photo-voltaic cells or solar thermal turbines. The second segment, DC-to-microwave converters, can be either a microwave tube system or a semiconductor system or the combination of both. The third segment is a gigantic antenna array. The SPS is designed as a huge solar power satellite in geostationary orbit, 36,000 km above the Earth's surface, where there is no cloud cover and no night throughout the year. Since microwave energy is almost not absorbed by air, cloud or rain, SSPS is possible to obtain approximately ten times the solar power than that on the ground. As a stable and CO_2-free green energy source, SSPS is expected to be a main power supply in the future during the late 20^{th} century. However, the development of SSPS has been delayed due to the large cost involved and the need to improve the underlying technologies.

Simultaneously, various ground-to-ground applications have been studied such as MPT for wireless LAN devices [32][33], ZigBee devices [34], sensors in car engine compartment [35], electric vehicles [36], a micro-robot in a pipe [37], small DC motors [38][39], implanted medical devices [40] and so on. Most of those MPT applications involve continuous-wave(CW) power transmission, with the exceptions of ZigBee and wireless LAN devices, which use an intermittent microwave to avoid interference between communication and power transmission [34]. Furthermore, some systems that use only ultra low power can run on energy harvested from ambient RF wave and microwave radiation [41]-[43]. Radio frequency energy exists around us such as TV signals, wireless radio networks, cell phone signals and wireless LAN signals. By using a rectifying circuit linked to a receiving antenna, this free flowing RF energy can be captured and converted into usable DC voltage for electronic applications.

1.3 Objectives

1.3.1 Structure of MPT System

However, because of the low overall efficiency of DC-RF-DC conversion and high cost involved, there are few commercial applications of MPT at present. Figure 1.4 shows a common MPT system, which usually includes a microwave generator, transmitting antennas, receiving antennas, rectifying circuits, a power management and a powered device. Here, an RF power transmission system transmits microwave incident on a receiving antenna (or array). After rectification and management, a DC power can afford to a powered device. In MPT system, the overall efficiency of DC-RF-DC conversion can be separated into three stages. The first stage is the DC-to-RF conversion that refers microwave generation and amplification. The second stage is the RF-to-RF transmission that means the antenna efficiency and the microwave transmission efficiency which are decided by the beam control of the antenna array, the transmission power and the number of antenna elements. The third stage is the RF-to-DC conversion that refers RF rectification and power management. The efficiency of the third stage is decided by the rectifying circuit and power management circuit. This thesis will mainly discuss the third stage.

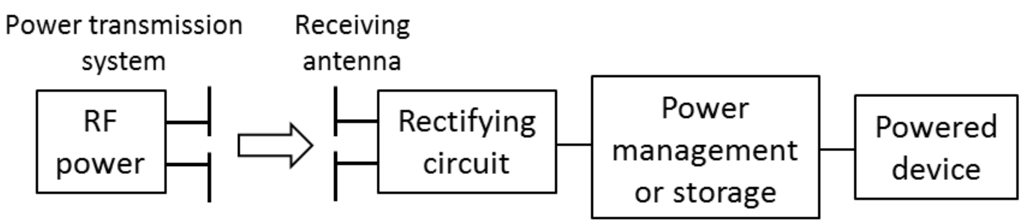

Figure 1.4: Block diagram of a MPT system. An RF power transmission system transmits microwave incident on a receiving antenna (array). After rectification and management, the DC power can afford to power an electrical device.

1.3.2 Overview of Rectenna Studies

The rectifying circuit , as a necessary component of a rectenna, is a very important element for the third stage of MPT system and significantly affects the overall efficiency of the whole MPT system. The single shunt rectifying circuit is the most common style of rectifying circuit as referred to in Appendix A. The RF-to-DC conversion efficiency of a rectenna depends on the input power and the connected load [44]. As shown in Fig. 1.5, the efficiency of a rectenna is mainly affected by the following three factors. First, the V_{j} (junction potential) effect: The efficiency is low in the low-power region because the voltage applied across the diode is less than or comparable to the forward drop voltage of the diode. Second, the higher harmonics effect: The efficiency increases as the power increases and levels off with the generation of strong higher order harmonics which reduces the proportion of energy that gets converted to DC. Third, the B_{V} (breakdown voltage) effect: The efficiency sharply decreases as the voltage applied across the diode exceeds the breakdown voltage of the diode. It means a rectenna exhibits a maximum efficiency for an optimal output load and lower efficiency for other loads. A maximum efficiency level corresponds to tradeoffs among those three factors of threshold voltage, harmonic generation, and reverse breakdown effects. In most researches on MPT, the load characteristics of the device being powered are matched with the optimal load for the rectenna. Many researches of rectennas at different frequencies have been reported in the literature. This thesis only focuses on the MPT using 2.45 GHz microwave. Table 1.2 lists the overview of relatively high-efficiency rectennas or rectifiers for 2.45 GHz. Until now, the MPT technologies have been developed over fifty years. Most researchers have focused primarily on improving the peak efficiency of rectenna which has reached up to 90 % in recent years [45]. This high efficiency is very close to the efficiency of power transmission by wires. Therefore, it is time to consider a rectenna as a power source for our living.

The efficiency as shown in Table 1.2 is the peak efficiency at a suitable load resistance which is referred as optimal load. However, for the different devices with different load characteristics, it is necessary to use different rectennas with different optimal loads. In other words, the relationship between rectennas and users is 1:1 mode. Furthermore, devices such as a battery, ZigBee sensor nodes and DC motors exhibit variable load characteristics that depend on the operating conditions. These devices will work at very low efficiency or even can not work when they are changed from one operating condition to another because of impedance mismatch. For example, it has been reported that by matching the optimal load of a rectenna array with the load of a DC motor, MPT was successfully used to drive the motor at 3000 rpm, with an efficiency from the antenna array to the motor input port of 50 % [38]. However, if the receiving power of rectenna

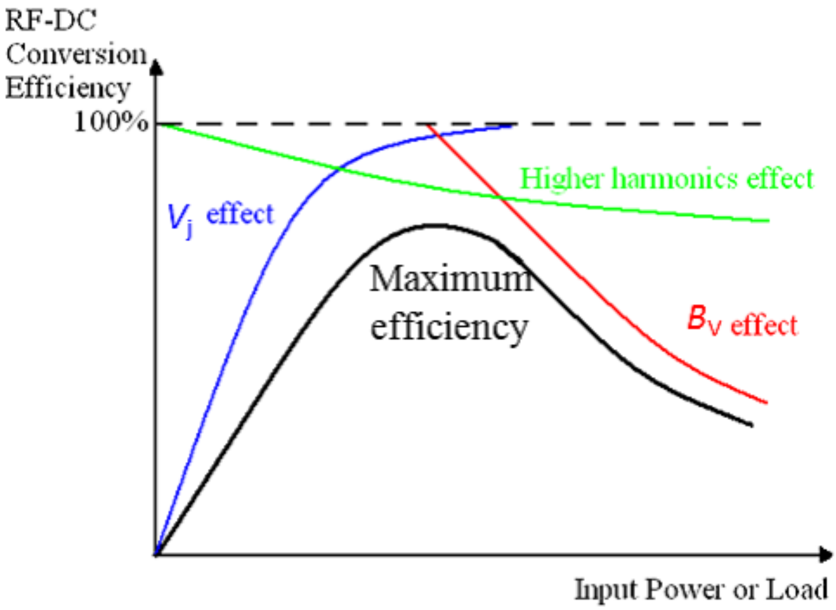

Figure 1.5: Efficiency characteristics of a general rectenna. The efficiency strongly depends on the input power or the load resistance [44].

array is changed because of some obstacles in the microwave transmission route, the efficiency would decrease due to impedance mismatch. Then the rotational speed of the DC motor can not maintain at 3000 rpm. Likewise, an airplane of MILAX (with a rectenna array) droved by a DC motor could not fly as far enough in the experiment [39]. This thesis proposes a flexible rectenna which can exhibit a high efficiency for different load characteristics of users. As shown in Fig. 1.6, the relationship between the flexible rectenna and users is 1:N mode. In this case, the flexible rectenna just seems to be a DC power source for various electronic applications.

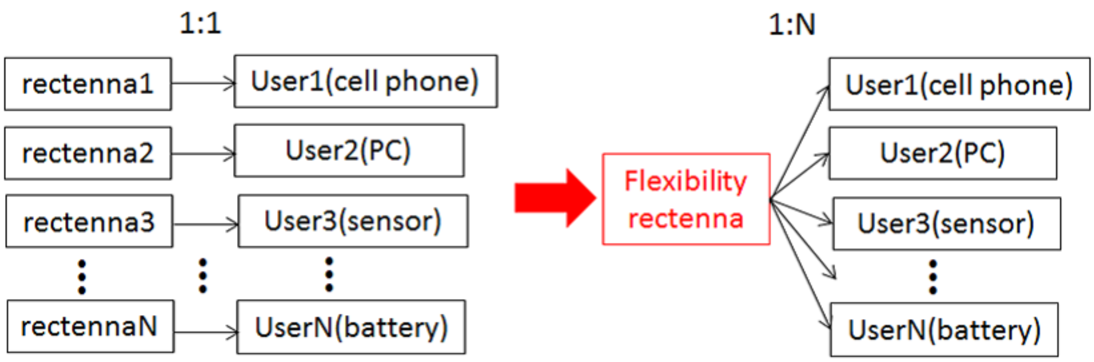

Figure 1.6: Comparison of a general rectenna and a flexible rectenna. A general rectenna for users is 1:1 mode. A flexible rectenna for users is 1:N mode.

In fact, the efficiency depends on the connected load resistance that is also a problem in other forms of WPT systems such as inductive coupling [18] and

Table 1.2: Overview of high-efficiency rectennas or rectifiers for 2.45 GHz microwave with input power levels from mW to W.

Reference	Year	Input power	HF diode	Peak efficiency
[45]	2011	8 W	unknown	90 %
[15]	1996	6.2 W	MA46135-32	81 %
[46]	2008	300 mW	HSMS282c	78 %
[47]	2014	158 mW	HSMS282c	82.3 %
[13]	2002	90 mW	MA4E1317	84.4 %
this work	2013	80 mW	HSMS286F	82.5 %
[48]	2008	32 mW	HSMS2860	75 %
[49]	2010	10 mW	HSMS2860	83 %
[50]	2004	10 mW	HSMS2820	77.8 %

resonance power transmission [22]. The resistance conversion DC-DC converter proposed in this thesis can also be used for impedance matching in other forms of WPT system.

1.4 Thesis Outline

This thesis consists of 6 chapters which mainly focus on the designing and experiment of both rectifying circuits and a resistance conversion DC-DC converter, and the application of MPT for driving a DC motor with a dynamic resistance characteristic. The thesis is organized as follows:

Chapter 1 introduces the development of WPT and the objectives of this thesis.

Chapter 2 utilizes a common pulse-width modulation (PWM) controlled boost converter to play an impedance matching role for a rectifying circuit in the simulation using advanced design system (ADS) simulator. We firstly give an overview of efficiency improvement methods of rectennas and a comparison of impedance matching methods in WPT studies. As a DC-DC converter improves the efficiency of the rectenna from the viewpoint of the DC output, it is easy to design and is independent of the operating frequency. Therefore, a simulation model of an RF-DC-DC circuit which consists of a rectifying circuit and a common boost converter is built. The simulation results indicate that the boost converter can prevent the reverse voltage applied on the rectifying diode from exceeding the breakdown voltage and then the rectifying circuit can keep acting at the peak efficiency point. However, this common boost converter just compresses a wide load range into a narrow load range which is not enough for an impedance matching requirement of the rectenna.

Chapter 3 analyzes the input/output resistance conversion relationships of three basic DC-DC converter topologies in continuous conduction mode (CCM) and discontinuous conduction mode (DCM). Among those six DC-DC converters, the input resistance of the DCM buck-boost converter is independent of the input voltage and the load resistance. Therefore, we design an externally-powered RF-DC-DC circuit which consists of a negative output voltage rectifying circuit and an inverting DCM buck-boost converter. Where the input resistance of the buck-boost converter is close to the optimal load of the rectifying circuit and the buck-boost converter requires an extra DC power source. Finally, the experiment on the externally-powered RF-DC-DC circuit is conducted.

Chapter 4 designs a self-powered RF-DC-DC circuit consisting of a positive output voltage rectifying circuit and a non-inverting DCM buck-boost converter. We firstly design a positive output voltage rectifying circuit with a relatively high peak efficiency. Then the DCM buck-boost converter in Chapter 3 is improved to be a non-inverting self-powered DCM buck-boost converter. Furthermore, the input resistance of the improved buck-boost converter is designed to be equal to the optimal load of the rectifying circuit. Finally, the experiment on the improved buck-boost converter and the self-powered RF-DC-DC circuit are conducted.

Chapter 5 conducts experiments on driving a low-power DC motor with continuous-wave (CW) power transmission and pulsed-wave power transmission. A compact power-receiving device, consisting of a rectenna array and a simplified buck-boost converter, is used for driving a dynamic resistance characteristic of a DC motor in MPT experiments. Firstly, we design a patch antenna as the power receiving antenna. Then we design two small rectifying circuits with different optimal load resistances. Moreover, two types of improved buck-boost converters, with the control-pulse circuit supplied by the input voltage or the output voltage, are also designed. With the combination of those antennas, two rectifying circuits and two buck-boost converters, there are four combinations of power-receiving devices. Using these four power-receiving devices, MPT experiments on driving a low-power DC motor in both CW and pulsed-wave are conducted.

Finally, Chapter 6 gives a summary and the contributions of this thesis and some directions for future work of MPT area.

Chapter 2

DC-DC Converter for Impedance Matching Application

2.1 Introduction

This chapter firstly gives an overview of efficiency improvement methods and summarizes the impedance matching applications in WPT researches. As a DC-DC converter deals with the DC output of the rectenna, it is easy to design and it plays a resistance conversion role independent of the operating frequency of the rectenna. Therefore, a common PWM controlled boost converter used for impedance matching application in rectifying circuit is investigated. We build a simulation model of an RF-DC-DC circuit which consists of a single shunt rectifying circuit and a PWM controlled boost converter using the simulator of ADS. Through the harmonic balance (HB) analyzing in ADS, the overall efficiency of the RF-DC-DC circuit can keep constant in a wide load range. More importantly, the reason for the constant overall efficiency of the RF-DC-DC circuit is clearly explained.

2.2 Overview of Impedance Matching Methods

The output of the receiving side of WPT is not directly suited to a power supply for circuits because of variations in power and voltage over the load resistance. Accordingly, a power management circuit, which should be able to adapt its input to the receiving side of WPT and its output to the load, is usually required. Therefore, in order to obtain a necessary DC voltage with high conversion efficiency, there are mainly three solutions reported in the literature. The first method is an active control method which focuses on the active element of the rectifier such as diodes and MOSFET in applications of the RF energy harvesting with an ultra-low RF power input. For example, Gate controlled diodes (GCD) which can achieve the near zero turn-on voltage [51] and Self-$\mathrm{V_{th}}$-Cancellation (SVC) CMOS where the threshold voltage of the MOSFET is cancelled by applying gate bias voltage generated from the output voltage of the rectifier itself [52]. This method intends to improve the V_{j} effect as shown in Fig. 1.5. The second method proposes a resistance compression networks (RCNs) in the rectifying circuit to reduce the sensitivity of the rectifying circuit versus variations of loads or input powers [53]-[56]. This method can compress a wide load range into a narrow load range in some degree, and the RCNs heavily depends on the operating frequency of the rectifying circuit. The third method uses a DC-DC converter connected to the output of the rectifying circuit for resistance conversion [22][23][43], which focuses on improving the B_{V} effect as shown in Fig. 1.5. The previous two methods implement solutions at the microwave circuit itself so that their effects are limited by the operating frequency of the rectenna. Their biggest advantage is that the overall efficiency almost do not decrease. The third method adds a DC-DC converter to the DC output of the rectifying circuit which implements solutions on the DC circuit so that it is independent of the operating frequency of the rectifying circuit but the overall efficiency would decrease because of the loss of the DC-DC converter.

Table 2.1 gives a comparison among examples of DC-DC converters, RCNs used in WPT system. Reference [22] used a common buck converter in continuous conduction mode (CCM) for impedance matching in magnetic resonant coupling system. The resistance relationships between the input side and the load resistance of three DC-DC converter topologies, such as buck converter, boost converter and buck-boost converter, were discussed. However, the summarized resistance relationships in [22] did not divide into the continuous conduction mode case and the discontinuous conduction mode (DCM) case. Similarly, in magnetic resonant coupling system, reference [23] utilized a microcontroller in the boost-buck converter to obtain a constant input resistance converter. Therefore, the system of [23] could maintain a constant efficiency in a wider load range than the one of [22]. In [43], it presented a microcontroller-based boost converter with online power stage efficiency optimization and maximum power point tracking in sub-milliwatt levels of

Table 2.1: Comparison of impedance matching methods used in WPT system.

Ref.	Application	Method	Eff. vs. P_{RF}	Eff. vs. R_{L}
[22]	resonant 13.56 MHz	buck converter in CCM	no discussion	constant from 4.7 to 30 Ω (1:7)
[23]	resonant 13.56 MHz	boost-buck converter	no discussion	constant from 100 to 1000 Ω (1:10)
[43]	RF harvesting 1.96 GHz	boost converter in CRM, DCM	constant from 0.2 to 1 mW (1:5)	no discussion
[56]	RF harvesting 915 MHz, 2.45 GHz	RCNs	low sensitivity	constant from 200 to 1000 Ω (1:5)
[57]	MPT 1.94 GHz, 2.45 GHz	no impedance matching	heavily depend	heavily depend
this work	MPT 2.45 GHz	buck-boost converter in DCM	constant from 30 to 140 mW (1:4.7)	constant from 0.2 to 10 kΩ (1:50)

RF power transmission. It also realized an efficient application of harvesting RF power from a nearby cellular tower with the input power range from 10 μW to 1 mW. In [56], the design of the rectifier was based on the concept of dual-band RCNs as the impedance matching network of the circuit. The 915 MHz/2.45 GHz rectifiers exhibit a low sensitivity at different loads and input powers. Reference [57] summarized some rectennas in different incident power levels and in different frequency, where the rectenna obtained a peak efficiency of 57 % with the power density of 25-200 μW/cm^2 at 2.45 GHz. However, the efficiency was heavily dependent on the incident power and the load resistance since the rectenna did not use any impedance matching circuit. This work proposes an RF-DC-DC circuit consisting of a rectifying circuit and a DCM buck-boost converter. The overall efficiency of the RF-DC-DC circuit exhibits independent of the load and a low sensitivity at different input power variations, which is far superior than other studies. A rectifying circuit connected to a DC-DC converter is firstly referred to as an RF-DC-DC circuit in this work.

According to the examples reported in Table 2.1, it includes distributed-constant circuits and lumped-constant circuits according to different operating frequencies. Magnetic resonant coupling circuits and DC-DC converters are lumped-constant circuits. Rectifying circuits and RCNs are distributed-constant circuits. Therefore, the impedance matching methods reported in Table 2.1 can be segregated into following three major divisions. First, the main circuit is a distributed-constant circuit and the impedance matching circuit is also a distributed-constant circuit such as references [53]-[56]. In this method, the impedance matching circuit heavily depends on the operating frequency used in the main circuit. Second, the main circuit is a lumped-constant circuit and the impedance matching circuit is also a lumped-constant circuit such as references [22][23]. Third, the main circuit is a distributed-constant circuit while the impedance matching circuit is a lumped-constant circuit such as references [43] and this work. In the later two methods, the impedance matching circuit is a lumped-constant circuit which is independent of the operating frequency used in the main circuit.

2.3 Simulation of Rectifying Circuit

The rectenna is very important for converting RF power into DC power. A rectenna usually contains a receiving antenna, a low pass filter, a rectifying element, a DC pass filter and a load resistance [13][44]. The receiving antenna collects microwave incident power, and the low pass filter matches the antenna impedance to the impedance of the rectifying circuit and rejects higher order harmonics from radiating through the antenna. A high frequency diode placed in shunt across the transmission line is commonly used as a rectifying element. The DC pass filter shorts the RF energy and passes the DC power. Two topologies of DC pass filters, such as a λ /4 line plus a capacitor and a $\lambda/4$ line plus some open stubs, are discussed and compared in [58][59].

This section simulates a simple quarter-wave single shunt rectifier using Advanced Design System (ADS) software of Agilent. Figure 2.1 shows the simulated schematic circuit of the rectifier. TL2, TL3, TL4 are matching circuits. A 100 pF capacitor (C2) is used as a DC block which passes the microwave from input and blocks the DC from the output. The DC pass filter consists of a $\lambda/4$ line (TL1) and

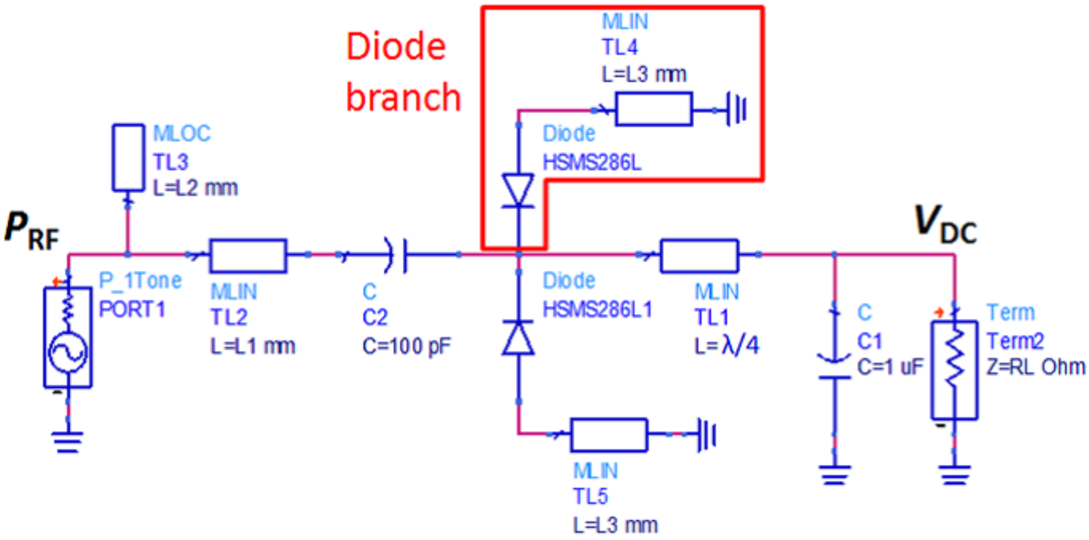

Figure 2.1: Circuit diagram of a simple quarter-wave single shunt rectifier.

Table 2.2: SPICE parameters of the HSMS2860 diode.

Parameter	Value	Unit
B_{V}	7	V
C_{j0}	0.18	pF
E_{g}	0.69	eV
I_{BV}	1E-5	A
I_{s}	5E-8	A
N	1.08	
R_{s}	6	Ω
P_{B}(VJ)	0.65	V
P_{T}(XTI)	2	
M	0.5	

a 1 μF capacitor (C1) which smoothes the DC voltage and reutilizes harmonics energy. The characteristic impedance of all lines is 50 Ω and the fundamental frequency of the input microwave is 2.45 GHz. The two symmetrical diode branches are inserted in the circuit. The RF-DC conversion efficiency is defined only by the diode rectifying efficiency excluding the reflection rate in some literature. Here, the RF-DC conversion efficiency $\eta_{\mathrm{rf-dc}}$ is defined as following, which includes the reflection.

$$\eta_{\mathrm{rf-dc}} = \frac{V_{\mathrm{DC}}^2}{P_{\mathrm{RF}} R_{\mathrm{L}}} \times 100\,\%, \tag{2.1}$$

where P_{RF}, V_{DC}, R_{L}, as shown in Fig. 2.1, are the input RF power, the DC output voltage and the load resistance, respectively.

As stated in Chapter 1.3.2, the RF-DC conversion efficiency mainly depends on the rectifying diodes. Therefore, it is important to select a suitable rectifying diode. Three diodes in different packages such as HSMS2860, HSMS2865 and HSMS286L of Avago HSMS286x series diode [60] are compared in the simulation. Table 2.2 shows the SPICE parameters of HSMS2860 and Fig. 2.2 shows the packages of three diodes. Using this three diodes in one diode branch or two diode branches, there are total 5 different rectifiers as shown in Table 2.3. These five rectifiers are simulated with the same input power and the comparison of maximum efficiency is shown in Fig. 2.3. The red point shows the maximum efficiency of five rectifiers on the matching state at the optimal load. The efficiency is increasing from 1D to 6D because the total diode loss is decreasing. The reason is that lower series resistance of parallel arranged diodes results in decreasing of diode's normal resistance losses. Therefore, the rectifier with two HSMS286L diode branches is selected in the simulation.

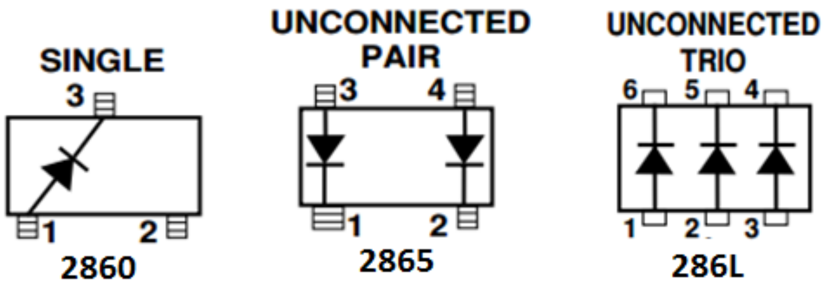

Figure 2.2: Top view of three rectifying diodes.

Then, using Harmonic Balance (HB) analysis of ADS, the rectifying circuit shown in Fig. 2.1 is simulated with the input power of 100 mW. Figure 2.4 shows the simulation results. The maximum RF-DC conversion efficiency is 83.4 % at an optimal load of 95 Ω and the reflection, the diode loss are 0.8 %, 14.7 %, respectively. At the range of load resistance from 50 to 125 Ω, the efficiency is over 70 % but it is strictly decreasing as the load resistance is greater than the optimal load. This is because the diode loss sharply increases as the reverse voltage applied on the diode is over the breakdown voltage. It is clearly seen from the Fig. 2.5 that the maximum voltage applied on the diode is greater than 7 V when the

Table 2.3: Five different simulated rectifiers: combination of three diodes in one diode branch or two diode branches.

Diode No.	Branch No.	Diode
1D	1	2860
2D	1	2865
3D	1	286L
4D	2	2865
6D	2	286L

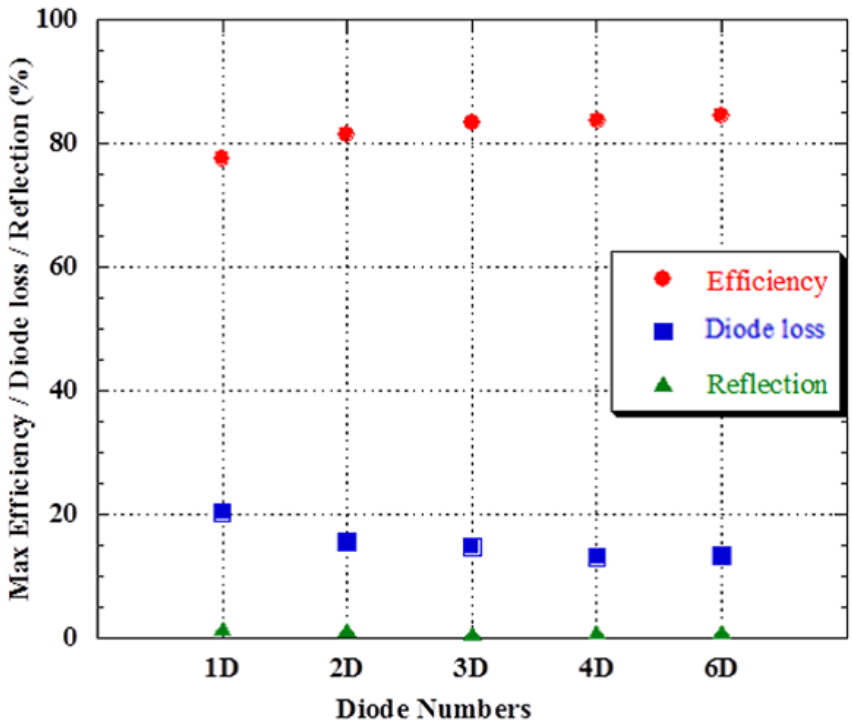

Figure 2.3: Maximum efficiency, diode loss and reflection comparison of five rectifiers.

load resistance is over the optimal load of 95 Ω. The output voltage of rectifier (V_{out}) is 2.8 V at the optimal load of 95 Ω.

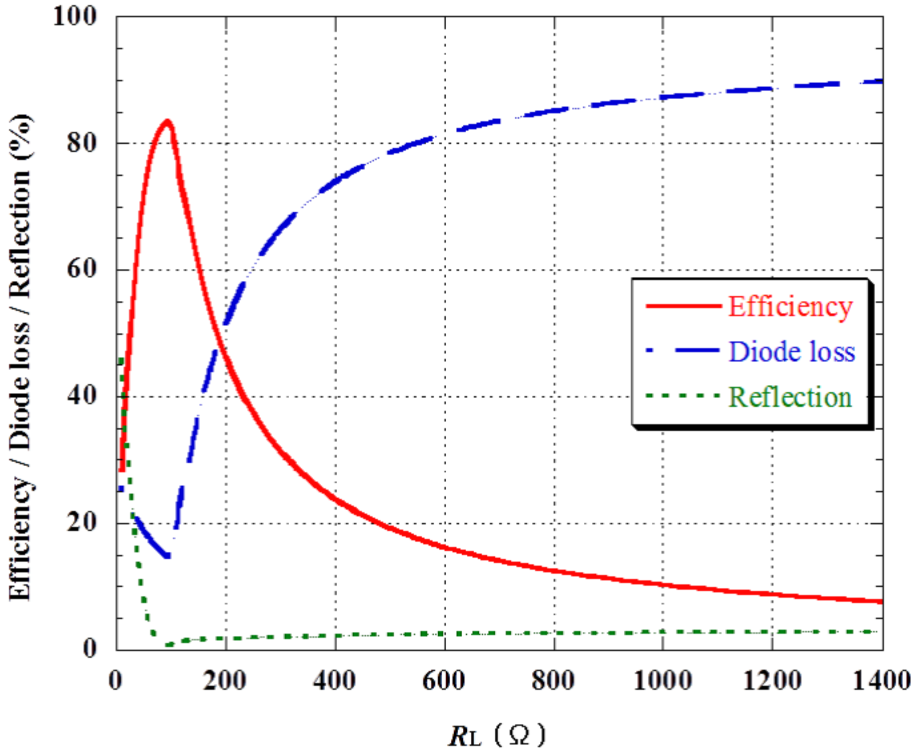

Figure 2.4: Efficiency, diode loss, reflection vs. load resistance of the 6D rectifier (two HSMS286L diode branches).

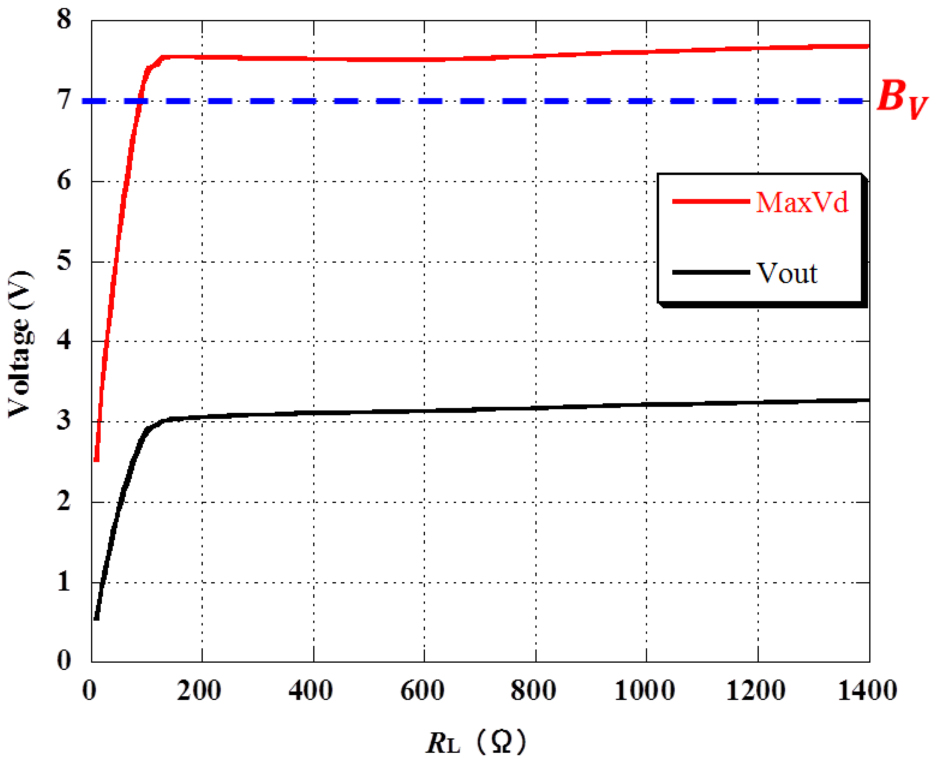

Figure 2.5: Maximum voltage applied on the rectifying diode (MaxV_d), output voltage of the rectifier(V_{out}).

2.4 DC-DC Converter Simulation Using ADS

2.4.1 Common DC-DC Converter

Common DC-DC converters are electronic devices usually used whenever we want to change DC electrical power efficiently from one voltage level to another. They are employed in many applications such as computers, office equipments, spacecraft power systems and telecommunications equipments [62]. The basic components of the DC-DC converter can be rearranged to form a buck converter, a boost converter, or a buck-boost converter. The buck converter has a linear control characteristic, and the output voltage is less than or equal to the input voltage. The boost converter is capable of producing an output voltage with a magnitude that is greater than that of the input voltage. The buck-boost converter can either increase or decrease the magnitude of the voltage, but the polarity is inverted. So, with a negative input voltage, the buck-boost converter can produce a positive output voltage of any magnitude.

Most DC converters use MOSFET devices as switching devices because of their very low on-resistance and zero gate-current. When the gate of the MOSFET is off, practically speaking, there is no current, and when the MOSFET is on, there is almost no voltage drop across the drain and the source. Hence, the ideal MOSFET dissipates no power, and the ideal DC-DC converter exhibits 100 % efficiency. In practice, using actual MOSFETs, diodes, and capacitors, DC-DC converter efficiencies of 80 % to 95 % are typically obtained [63]. Additionally, MOSFET probably operates at a high switching frequency which brings about the smaller and lighter transformers, inductors and capacitors. Generally, the converter is used to manage the output voltage with pulse-width modulation (PWM) control [64] or pulse-frequency modulation (PFM) control [65] or PWM/PFM switchable control which uses PFM for low load impedance and automatically switches to PWM control for large load impedance [66].

2.4.2 PWM Controlled Boost Converter

A boost converter is widely applied in energy harvesting systems since the power is very low in an ambient RF environment [61]. In this chapter, a feedback PWM controlled boost converter is used and the schematic circuit is shown in Fig. 2.6.

Table 2.4: Simulation parameters of a PWM controlled boost converter: V_{in} is the input voltage, f_{sw} is the switching frequency of PWM controller.

Parameter	Value	Unit
V_{in}	2.8	V
f_{sw}	1.8	MHz
L	10	μH
C	10	μF
R_1	1	kΩ
R_2	0.5	kΩ

The voltage difference between the feedback node (V_{fb}) and the reference (V_{ref}) is called the error voltage (V_{error}). The PWM wave, generated by comparing the error voltage to the sawtooth wave (V_{saw}), controls the gate of the MOSFET. Table 2.4 shows the simulation parameters. An MBR0520L diode which has a low junction potential voltage of 0.38 V and a high breakdown voltage of 20 V is used. The circuit is simulated by HB analysis of ADS and Fig. 2.7 shows the efficiency, MOSFET loss (P_{mos}), diode loss (P_{d}) versus the load resistance. The efficiency is over 84 % as the load is varying from 370 to 1300 Ω. The maximum efficiency is 89.1 % with the P_{mos} of 5.9 % and the P_{d} of 5 %.

Here, the input resistance of the DC-DC converter (R_{in}) is defined as Eq. (2.2) where the V_{in}, I_{inave} are the input voltage and the average of input current, respectively. Figure 2.8 shows the simulated results of R_{in} which are compressed in the range of 80 to 105 Ω with the load range from 370 to 1300 Ω.

$$R_{\mathrm{in}} = \frac{V_{\mathrm{in}}}{I_{\mathrm{inave}}}. \tag{2.2}$$

2.5 RF-DC-DC Circuit

The RF-DC-DC circuit is a combination of RF-DC rectifier and the boost converter as mentioned above. Fig. 2.9 shows the block diagram of the RF-DC-DC circuit where the boost converter is connected to the RF-DC rectifier. Therefore, the

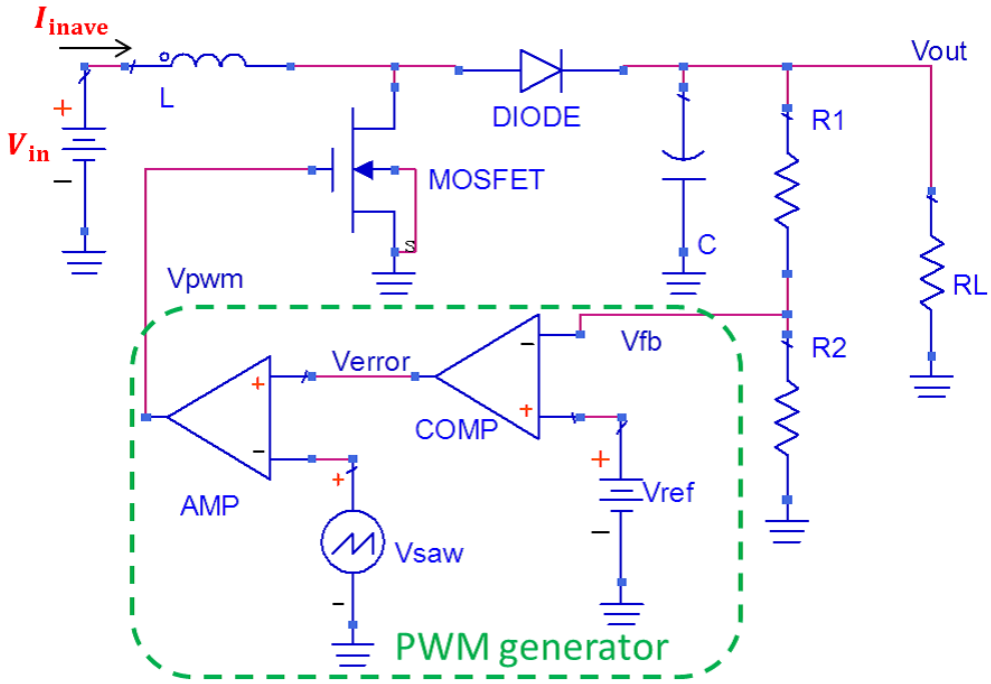

Figure 2.6: Circuit diagram of the simulated DC-DC converter: a PWM controlled boost converter.

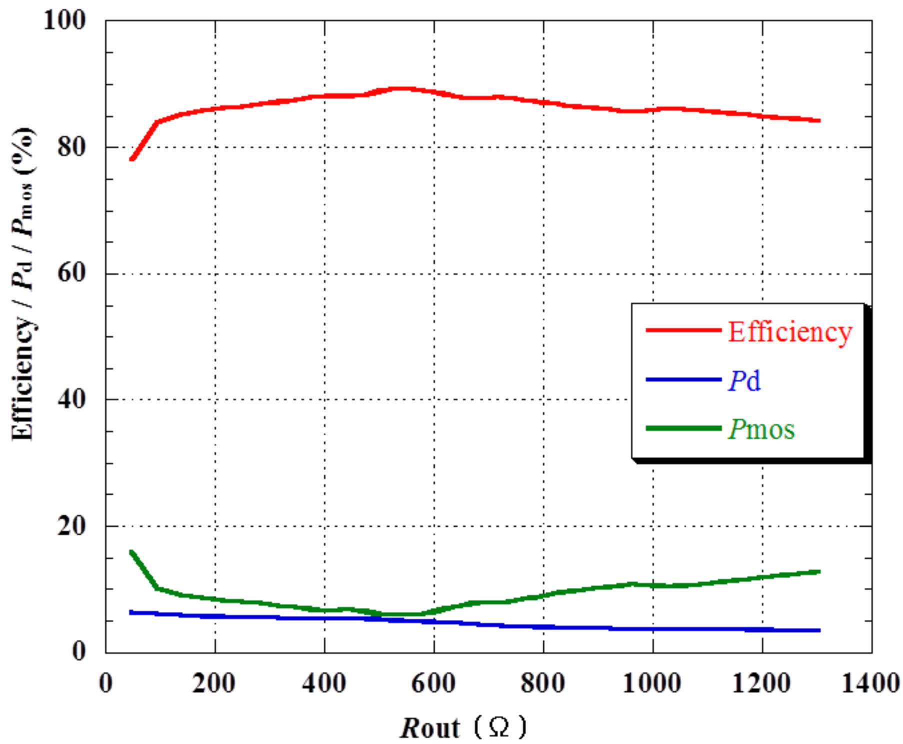

Figure 2.7: Simulation results of the boost converter such as Efficiency, MOSFET loss (P_{mos}), diode loss (P_{d}) vs. load resistance.

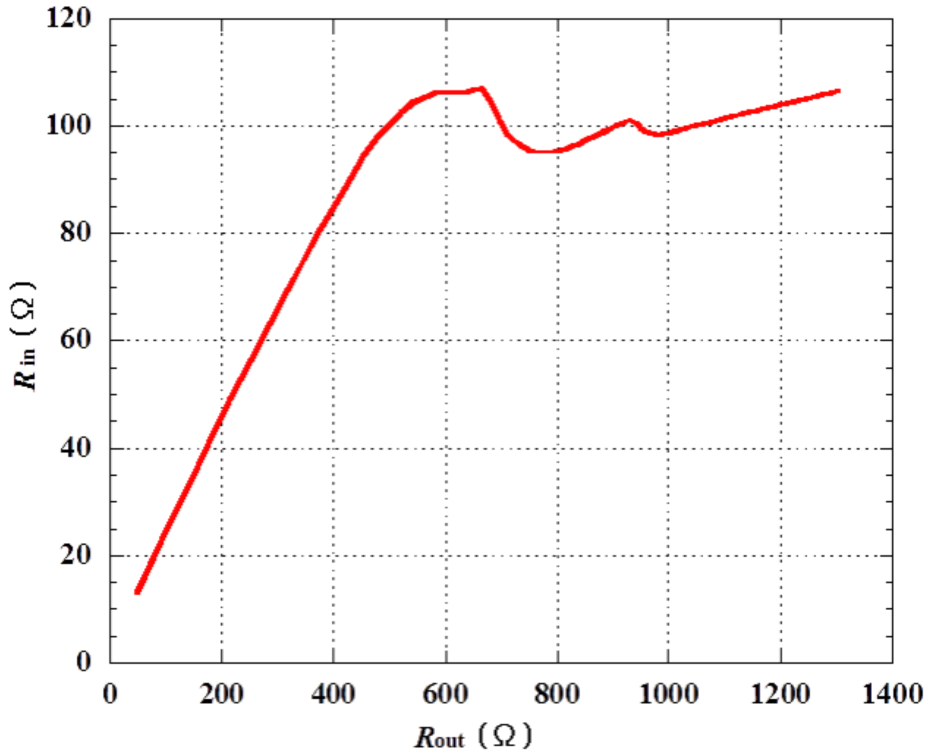

Figure 2.8: Simulation results of the boost converter such as the input resistance (R_{in}) vs. load resistance.

overall efficiency of the RF-DC-DC circuit η_{all} should satisfy following equation.

$$\eta_{\text{all}} = \eta_{\text{rf-dc}} \cdot \eta_{\text{dc-dc}}, \tag{2.3}$$

where $\eta_{\text{dc-dc}}$ is the efficiency of the boost converter.

The relationships between efficiency and load are shown in Table 2.5. As the input resistance R_{in} of the boost converter is matching with the output impedance of rectifier, the overall efficiency of the combined RF-DC-DC circuit is expected to be over 67 %.

Using HB analysis in ADS at two fundamental frequencies of 2.45 GHz and 1.8 MHz to simulate the RF-DC-DC circuit which is shown in Fig. 2.10. The input microwave power is also 100 mW which is the same as the RF-DC rectifier. Figure 2.11 shows the efficiency comparison of the RF-DC-DC circuit and the RF-DC rectifier. Comparing to a narrow range of 50 to 125 Ω of the RF-DC rectifier, the overall efficiency of the RF-DC-DC circuit is almost constant greater than 70 % at the load range of 370 to 1300 Ω. Figure 2.12 shows the impedance comparison which indicates that the Z_{out} of the RF-DC-DC circuit is almost the

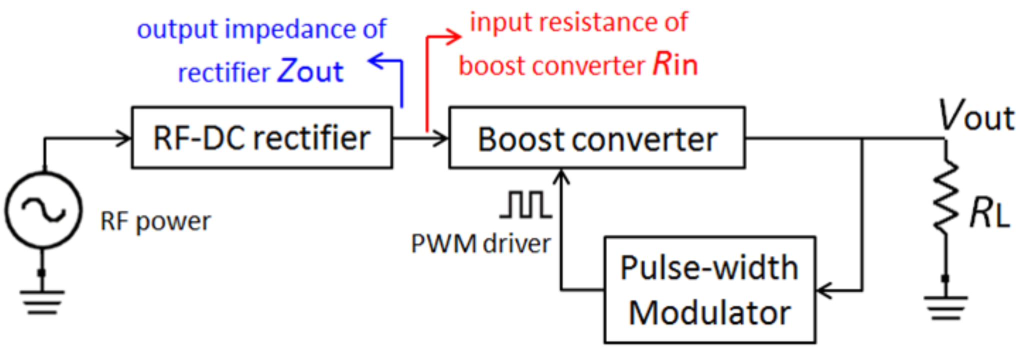

Figure 2.9: Block diagram of the RF-DC-DC circuit: the boost converter is connected to the RF-DC rectifier.

Table 2.5: Efficiency and load relationships of the RF-DC rectifier and boost converter.

	R_{out}	R_{in}	Efficiency
RF-DC rectifier	70-105 Ω		80-83.4 %
boost converter	370-1300 Ω	80-105 Ω	84-89 %
RF-DC-DC circuit	370-1300 Ω		predicted value 67 %

same as the R_{in} of the boost converter. Therefore, the simulation results of the RF-DC-DC circuit agree well with that of the two circuits simulated separately. A comparison of the maximum reverse voltage on the rectifying diode (V_{d}) of the two circuits is shown in Fig. 2.13. It is clear that V_{d} of the RF-DC-DC circuit is constant under 7 V (breakdown voltage) while V_{d} of the RF-DC rectifier is over 7 V when the load resistance is bigger than the optimal load. This results mean that the boost converter limits the maximum reverse voltage of the rectifying diode to prevent the conversion efficiency of the RF-DC rectifier from sharply decreasing.

Finally, the output voltage of the RF-DC-DC circuit is increasing as the load increases which is shown in Fig. 2.14. Here, the output voltage is different with the constant output voltage of the conventional PWM controlled boost converter. According to Figs. 2.13 and 2.14, a constant overall efficiency of the RF-DC-DC circuit can be explained as follows. In the RF-DC-DC circuit, the output voltage of the rectifier (when it is connected with the converter) is almost constant even though the load is changed, which leads to the maximum voltage applied on the diode being constant and under the breakdown voltage. As a result, the efficiency of the rectifier (when it is connected with the converter) is almost constant which leads to a constant overall efficiency of the RF-DC-DC circuit even though the load is changed. In contrast, the output voltage of the rectifier (when it is not connected with the converter) is increasing as the load is increased, which leads to the maximum voltage applied on the diode increasing up to over the breakdown voltage and the increase of diode losses. Consequently, the efficiency of the rectifier (when it is not connected with the converter) decreases at a high load resistance.

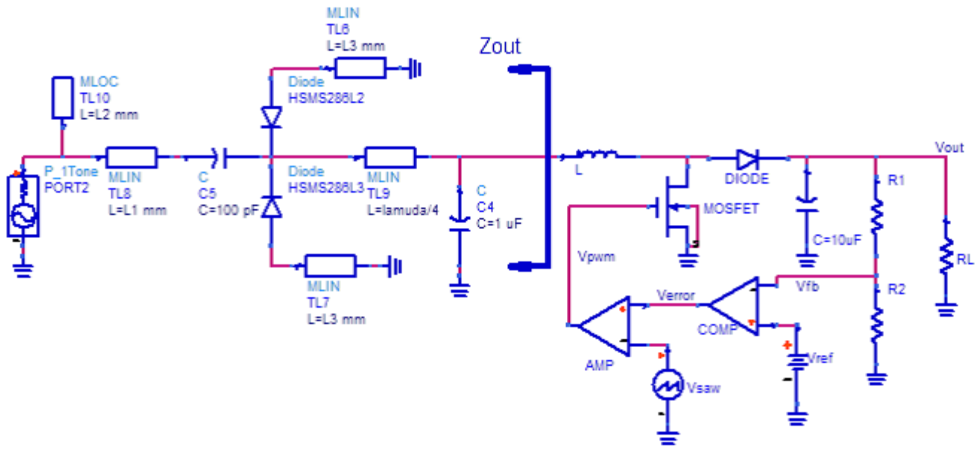

Figure 2.10: Circuit diagram of the RF-DC-DC. Simulate it with two fundamental frequencies of 2.45 GHz and 1.8 MHz using HB analysis in ADS.

2.6 Summary

Firstly, we give an overview of efficiency improvement methods in rectenna researches and a comparison of impedance matching methods in WPT studies. The DC-DC converter addresses the DC output of the rectifying circuit and improves the B_{v} effect in the efficiency-load characteristics. More importantly, the DC-DC converter as an impedance matching application which is independent of the operating frequency of the rectenna. Therefore, a PWM controlled boost converter is used to improve the efficiency-load characteristics of the rectifying circuit. Using HB analysis of ADS, we build a model of RF-DC-DC circuit which consists of the single shunt rectifying circuit and the PWM controlled boost converter. The RF-DC-DC circuit obtains a steady high overall efficiency (over 70 %) at the load

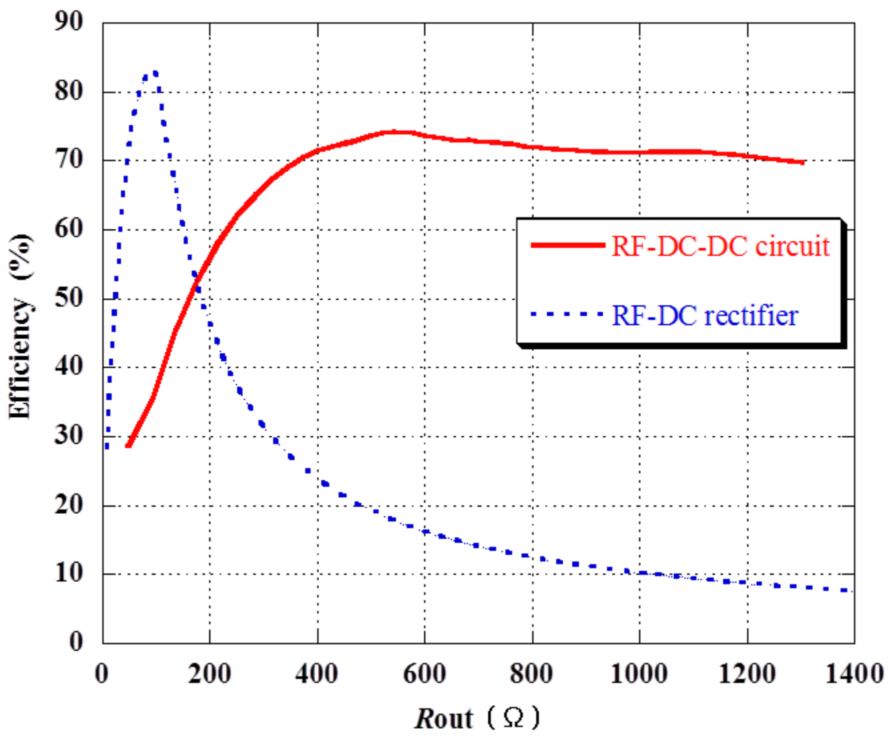

Figure 2.11: Efficiency comparison of the RF-DC-DC circuit and general rectifier.

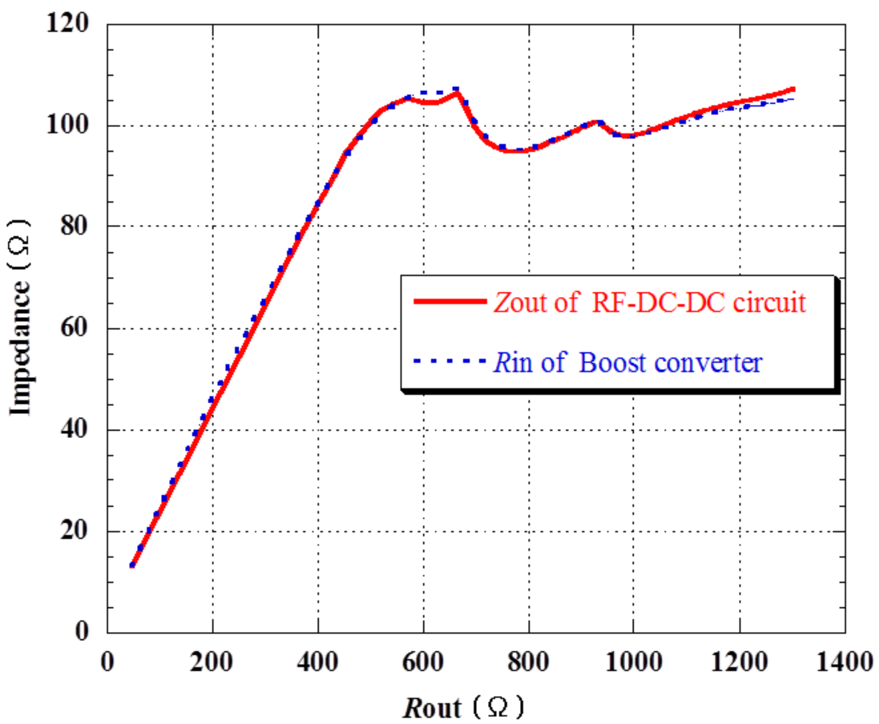

Figure 2.12: Impedance comparison: Z_{out} of the RF-DC-DC circuit is almost the same as R_{in} of the boost converter.

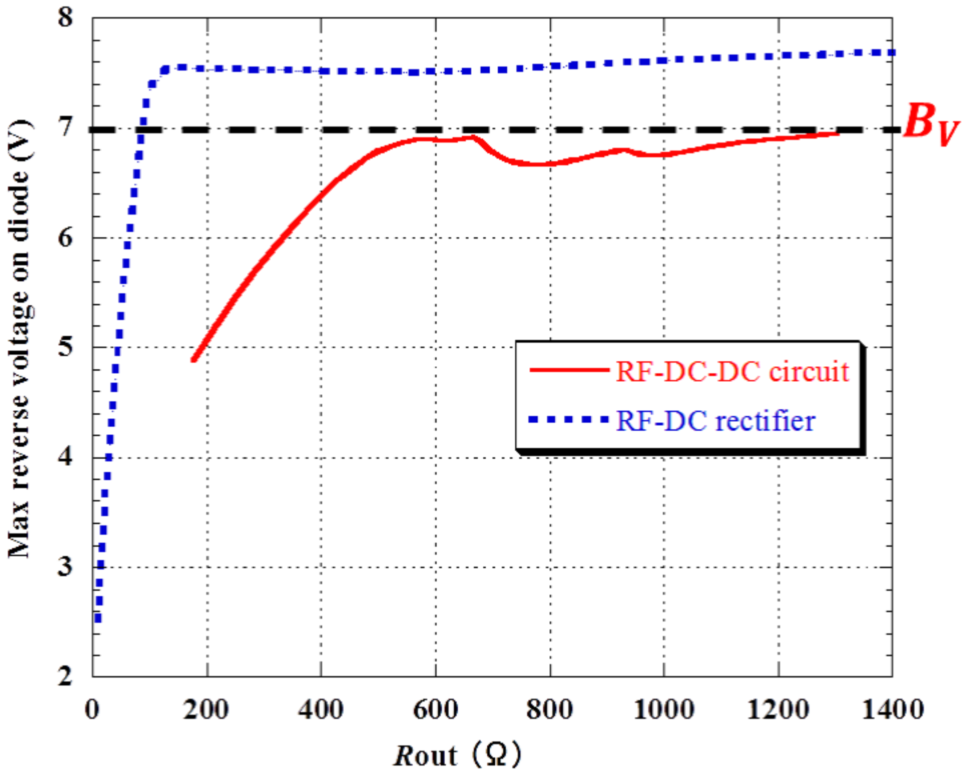

Figure 2.13: Maximum reverse voltage on the rectifying diode (MaxV_d) comparison: MaxV_d of the RF-DC-DC circuit is under breakdown voltage (7 V).

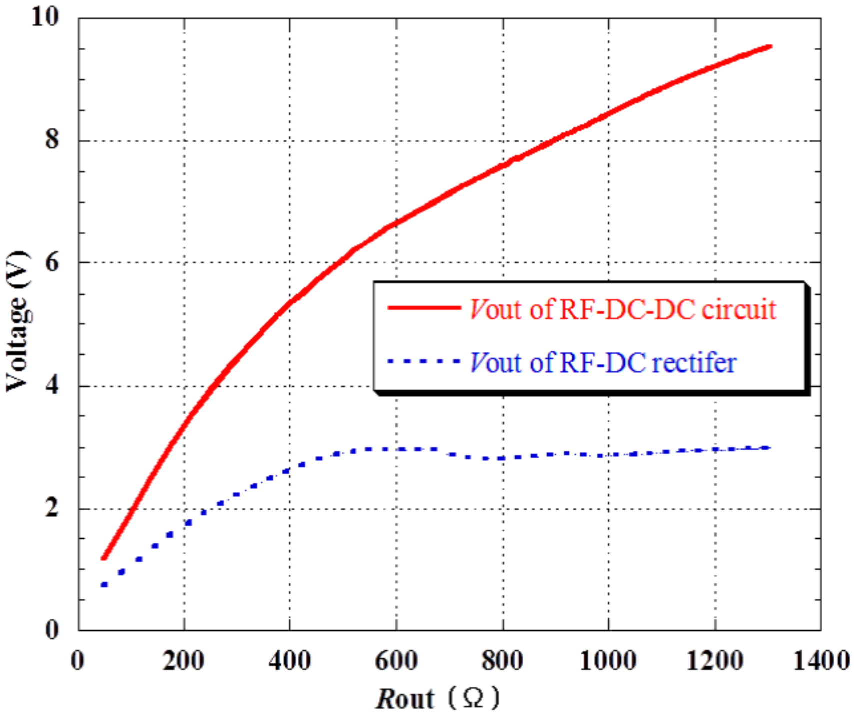

Figure 2.14: Output voltage of the RF-DC-DC circuit and the voltage at the output port of RF-DC rectifier.

range of 370 to 1300 Ω, where the load range is wider than the RF-DC rectifier at the same efficiency level. Additionally, that the boost converter is connected to the RF-DC rectifier can limit the maximum reverse voltage applied on the rectifying diode under breakdown voltage at this load range. The simulation results clearly explain the reason why a DC-DC converter has an effect on impedance matching for RF-DC rectifier. Therefore, an RF-DC-DC circuit is verified to be available for improving efficiency-load relationships of the rectenna in this chapter. However, the simulated PWM controlled boost converter just compresses a wide output load range into a narrow input resistance range in some degree. It is insufficiency for impedance matching for a flexible rectenna. Therefore, based on the simulation results of this chapter, a much more effective DC-DC converter is proposed and discussed in the next chapter.

Chapter 3

Externally-powered RF-DC-DC Circuit

3.1 Introduction

Last chapter demonstrates that a DC-DC converter is useful for impedance matching of a rectifying circuit based on simulation. In this chapter, to select a suitable DC-DC converter for impedance matching of the rectenna, the three basic topologies DC-DC converters such as buck converter, boost converter, buck-boost converter in CCM and DCM are discussed. The CCM is defined by continuous inductor current which is greater than zero over the entire switching period. The DCM is defined by discontinuous inductor current which equals to zero during a portion of the switching period. Hence, the energy stored in the inductor is zero at the beginning and at the end of each switching period. The CCM is preferred for high efficiency and good utilization of semiconductor switches and passive components. The DCM may be used in applications with special control requirements because the dynamic order of the converter is reduced. It is uncommon to mix these two operating modes because of different control algorithms [67].

Both CCM and DCM are discussed for three basic topologies DC-DC converters in this chapter. Unlike the usual discussion on DC-DC converter, this chapter will analysis the relationships between input resistance and load resistance instead of input/output voltages. Comparing those DC-DC converters, an inverting buck-boost converter in DCM, which exhibits constant input resistance, is selected. The control-pulse circuit of this buck-boost converter requires an extra DC power source. Additionally, to match the polarity of the input voltage and the output voltage, a negative output voltage rectifier is designed. Then, an externally-powered RF-DC-DC circuit consisting of the rectifier and the buck-boost converter is proposed. Finally, experiments on the externally-powered RF-DC-DC converter are conducted.

3.2 DC-DC Converter in CCM and DCM

3.2.1 DC-DC Converter in CCM

A DC-DC converter operating in CCM or DCM depends on the characteristics of the inductor current. In the case of the CCM, the inductor current is continuous and never falls to zero. Figure 3.1 shows the operating waveform of the inductor (I_{L}) in CCM at the steady condition. The I_{LP} is the peak inductor current and I_{LV} is the minimum inductor current which is greater than zero. Figure 3.2 shows the schematic circuits of three basic topologies DC-DC converters which consist of capacitors, an inductor, an N-channel MOSFET (N-MOS), and a diode. T_{on}, T_{off}, T are the on-state time, off-state time and the period, respectively. D is the duty-on ratio of the control-pulse. Then it yields:

$$D = \frac{T_{\mathrm{on}}}{T} = \frac{T_{\mathrm{on}}}{T_{\mathrm{on}} + T_{\mathrm{off}}}. \tag{3.1}$$

As we know, the relationship between the inductance L, the inductor voltage (V_{L}) and the inductor current (I_{L}) satisfies the following formula:

$$V_{\mathrm{L}} = L\frac{\Delta I_{\mathrm{L}}}{\Delta t}. \tag{3.2}$$

Moreover, ΔI_{Lon}, ΔI_{Loff} are the current variation of the inductor at on-state and off-state, respectively. As the overall current variation of the inductor should be zero when the converter operates at steady-state. Then it means:

$$\Delta I_{\mathrm{Lon}} + \Delta I_{\mathrm{Loff}} = 0. \tag{3.3}$$

A). Buck converter

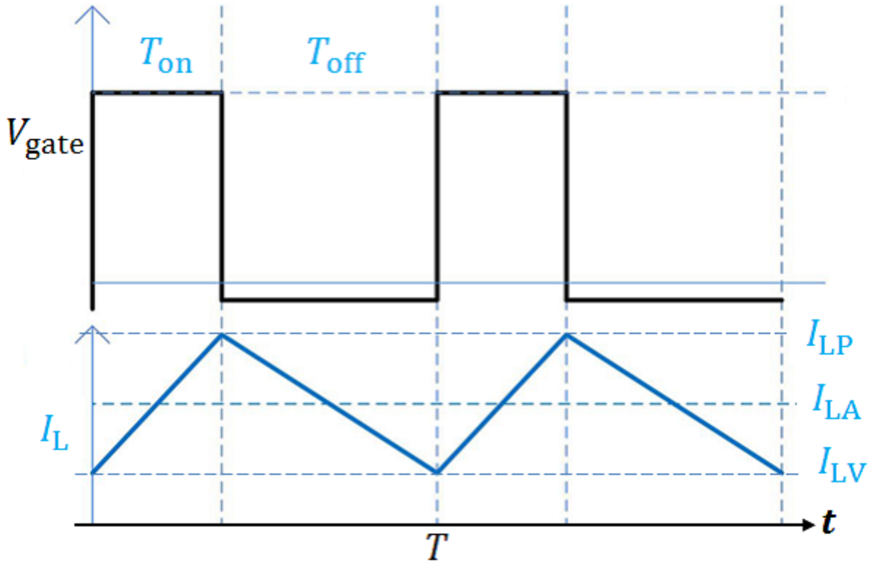

Figure 3.1: Operating waveforms of the inductor current (I_{L}) and gate control voltage (V_{gate}) for a DC-DC converter in CCM.

As can be seen from the Fig. 3.2(a), when the gate voltage V_{gate} is at high level, N-MOS lets the current flow through drain to source then the current flows through the inductor to the load. At this on-state, the inductor current is increasing to the peak value I_{LP} and no current flows through the diode since it is reverse-biased by the voltage. Then the inductor voltage at on-state (V_{Lon}) can be written as:

$$V_{\text{Lon}} = V_{\text{in}} - V_{\text{o}}. \tag{3.4}$$

Using Eqs. (3.2) and (3.4), the current variation of the inductor ΔI_{Lon} can be calculated as:

$$\Delta I_{\text{Lon}} = \frac{V_{\text{in}} - V_{\text{o}}}{L} DT. \tag{3.5}$$

When the gate voltage V_{gate} is at low level (or zero), N-MOS does not let the current flow through drain to source, then the current stored in the inductor flows through the load and diode. At this off-state, the inductor current is decreasing to the valley value I_{LV} and the current flows through diode as it is forward-biased. Then the inductor voltage at off-state (V_{Loff}) can be written as:

$$V_{\text{Loff}} = -V_{\text{o}}. \tag{3.6}$$

Similarly, using Eqs. (3.2) and (3.6), the current variation of the inductor ΔI_{Loff} can be calculated as:

$$\Delta I_{\text{Loff}} = -\frac{V_{\text{o}}}{L}(1 - D)T. \tag{3.7}$$

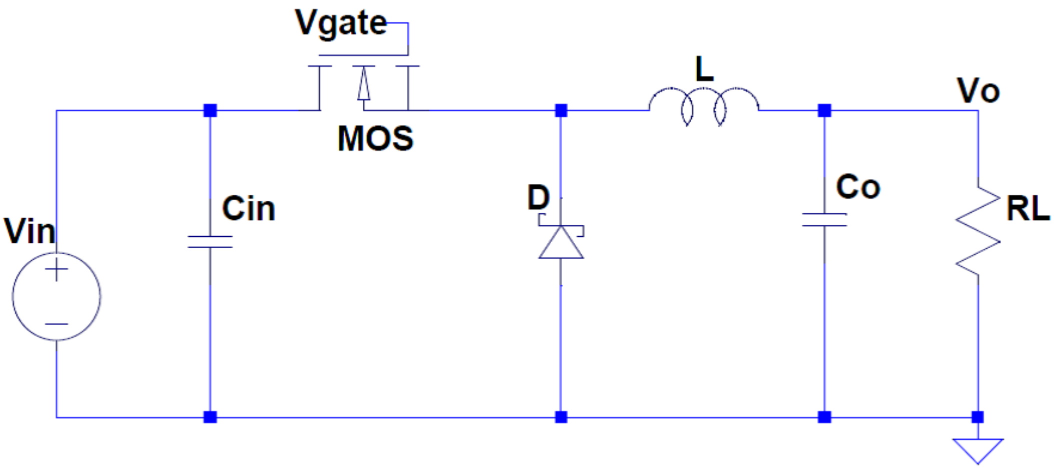

(a)

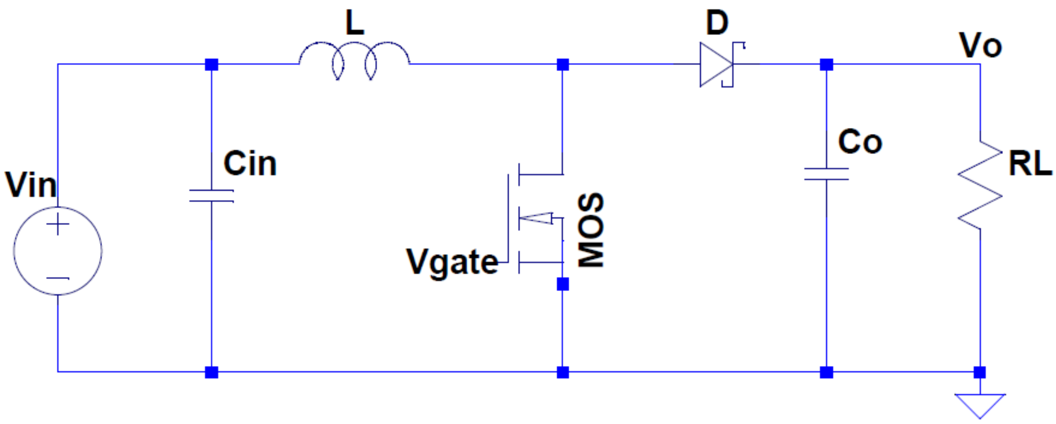

(b)

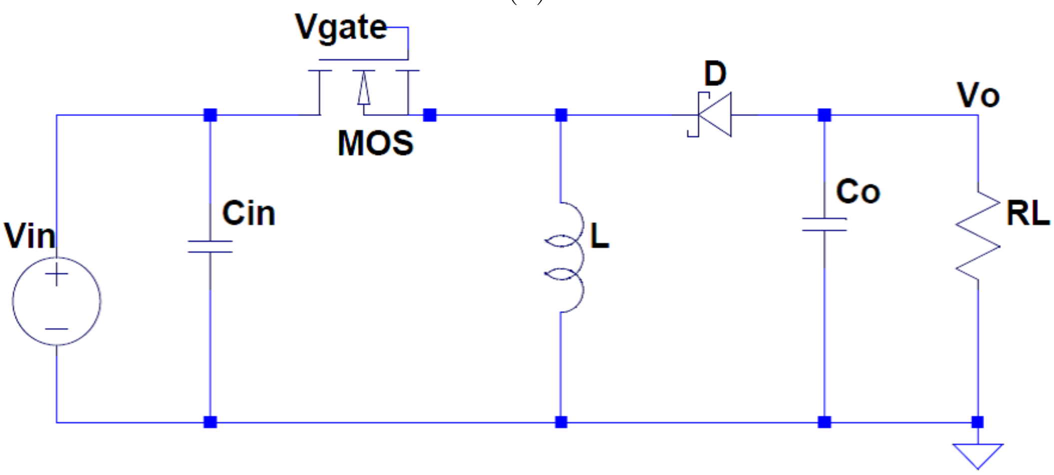

(c)

Figure 3.2: Circuit diagram of three basic topologies DC-DC converters. (a) Buck converter. (b) Boost converter. (c) Buck-boost converter.

Based on Eqs. (3.3), (3.5) and (3.7), it yields:

$$V_o = DV_{in}. \tag{3.8}$$

R_{in} is the average input resistance of the converter and R_L is the load resistance. P_{in}, P_o are the input power and output power, respectively. Then:

$$P_{in} = \frac{V_{in}^2}{R_{in}}, \tag{3.9}$$

$$P_o = \frac{V_o^2}{R_L}. \tag{3.10}$$

Assuming it is an ideal converter, the input power P_{in} should equal the output power P_o. Then it means:

$$\frac{V_{in}^2}{R_{in}} = \frac{V_o^2}{R_L}. \tag{3.11}$$

According to Eqs. (3.8) and (3.11), R_{in} can be written as:

$$R_{in} = \frac{1}{D^2} R_L. \tag{3.12}$$

As $D < 1$, then, $R_{in} > R_L$ for the buck converter.

B). Boost converter

Similarly, as shown in Fig. 3.2(b), the current flows through the inductor to the ground then the diode and load are shorted at on-state. The inductor current is increasing linearly to the peak value I_{LP}. At off-state, the current flows through the inductor and diode to the load. Then, the inductor current is decreasing to the valley value I_{LV}. This yields following equations.

$$V_o = \frac{1}{1-D} V_{in}, \tag{3.13}$$

$$R_{in} = (1-D)^2 R_L. \tag{3.14}$$

Hence, as for boost converter, $R_{in} < R_L$.

C). Buck-boost converter

As shown in Fig. 3.2(c), the current flows through the inductor to the ground at on-state. The inductor current is increasing linearly to the peak value I_{LP}. At off-state, the current flows through the inductor to the load and diode. Then, the inductor current is decreasing to the valley value I_{LV}. The polarity of the output voltage V_{o} is negative because the converter inverts the polarity of input and output voltages. This gives following equations.

$$V_{\mathrm{o}} = -\frac{D}{1-D}V_{\mathrm{in}}, \tag{3.15}$$

$$R_{\mathrm{in}} = (\frac{1}{D} - 1)^2 R_{\mathrm{L}}. \tag{3.16}$$

Hence, as for buck-boost converter, $0 < R_{\mathrm{in}} < \infty$. It can be smaller than R_{L} or bigger than R_{L}.

Therefore, we summarize the relationships of input/output resistances and input/output voltages for these three basic topologies DC-DC converters in CCM in Table 3.1.

Table 3.1: Input/output resistance and voltage relationships of three basic topologies DC-DC converters in CCM.

Topology	Voltage	Resistance	Variation of R_{in}
buck	$V_{\mathrm{o}} = DV_{\mathrm{in}}$	$R_{\mathrm{in}} = \frac{1}{D^2}R_{\mathrm{L}}$	$R_{\mathrm{L}} < R_{\mathrm{in}} < \infty$
boost	$V_{\mathrm{o}} = \frac{1}{1-D}V_{\mathrm{in}}$	$R_{\mathrm{in}} = (1-D)^2 R_{\mathrm{L}}$	$0 < R_{\mathrm{in}} < R_{\mathrm{L}}$
buck-boost	$V_{\mathrm{o}} = -\frac{D}{1-D}V_{\mathrm{in}}$	$R_{\mathrm{in}} = (\frac{1}{D} - 1)^2 R_{\mathrm{L}}$	$0 < R_{\mathrm{in}} < \infty$

3.2.2 DC-DC Converter in DCM

In some cases, the amount of energy required by the load is small enough to be transferred in a time not the whole commutation period. In this case, the DC-DC converter operates in DCM, where the current through the inductor falls to zero during a part of the period. Figure 3.3 shows the operating waveform of the inductor (I_{L}) in DCM at the steady condition. There are three states according to three time intervals. 0 - $t1$ is the on-state that the inductor current is increasing linearly; $t1$ - $t2$ is the off-state that the inductor current is decreasing linearly; $t2$ - T is the zero-state that the inductor current is zero. Those time intervals satisfy following equations:

$$t1 = DT, \tag{3.17}$$

$$t2 - t1 = \delta T. \tag{3.18}$$

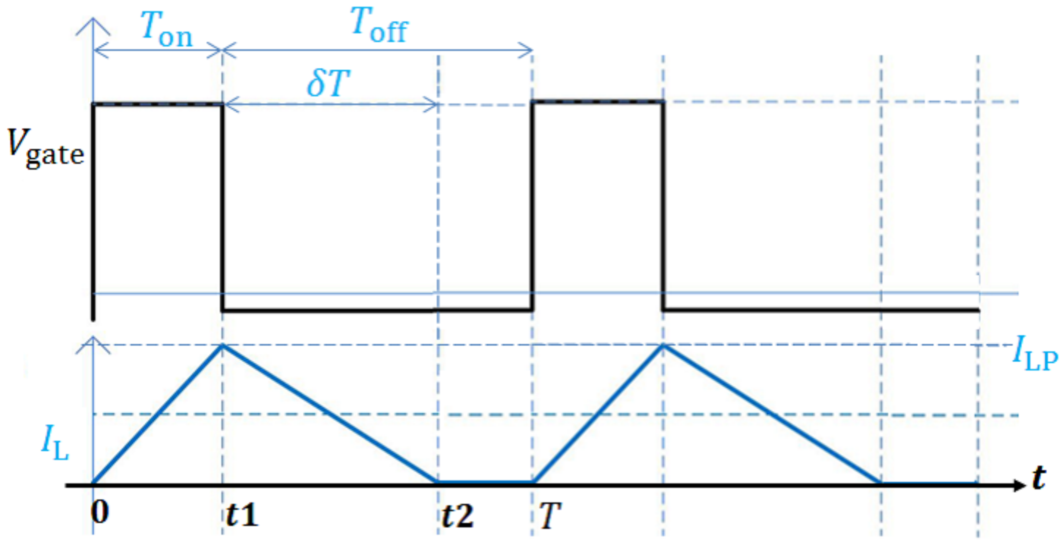

Figure 3.3: Operating waveforms of the inductor current (I_{L}) and gate control voltage (V_{gate}) for a DC-DC converter in DCM.

The only difference with the CCM is that the inductor is completely discharged at the end of the commutation cycle. Although slight, the difference has a strong effect on the output voltage equation and the input resistance equation.

A). Buck-boost converter

Referring to the Fig. 3.2(c), the current flows through the N-MOS to the inductor at on-state which makes the input voltage (V_{in}) appear across the inductor. The inductor current is increasing from 0 to the peak value I_{LP}. Considering Eqs. (3.2) and (3.17), inductor current variation at on-state ΔI_{Lon} can be written as following:

$$\Delta I_{\mathrm{Lon}} = \frac{DT}{L} V_{\mathrm{in}}. \tag{3.19}$$

At the off-state, the current flows through the inductor to the load and diode until the inductor current falls to zero through δT period. Assuming zero voltage drop across the diode, the output voltage (V_{o}) appears across the inductor. Then the inductor current variation at off-state ΔI_{Lon} is given by:

$$\Delta I_{\mathrm{Loff}} = \frac{\delta T}{L} V_{\mathrm{o}}. \tag{3.20}$$

Applying Eqs. (3.19) and (3.20) to Eq. (3.3) leads to the following:

$$\delta = -D\frac{V_{\text{in}}}{V_{\text{o}}}. \tag{3.21}$$

At the zero-state, the inductor current maintains zero and there is no current flowing to the load which seems that the converter falls into sleeping interval.

As analyzed above, no current flows to the diode and load during the on-state. The output current (I_{o}) is equal to the average of the diode current. During the off-state, the diode current is equal to the inductor current. Therefore, I_{o} can be written as following:

$$I_{\text{o}} = \delta\frac{I_{\text{LP}}}{2}. \tag{3.22}$$

Based on Eqs. (3.19), (3.21) and (3.22), V_{o} is obtained as following:

$$V_{\text{o}} = -\frac{D^2T}{2LI_{\text{o}}}V_{\text{in}}^2. \tag{3.23}$$

Compared to Eq. (3.15), the relationships of the input/output voltage for DCM are much more complicated than that in CCM.

Additionally, considering $P_{\text{o}} = |V_{\text{o}}I_{\text{o}}|$, Eq. (3.23) can be rewritten as following:

$$P_{\text{o}} = \frac{D^2T}{2L}V_{\text{in}}^2. \tag{3.24}$$

Assuming it is an ideal DC-DC converter, then $P_{\text{in}} = P_{\text{o}}$ is formed. Combining Eqs. (3.9) and (3.24), it is obvious that:

$$R_{\text{in}} = \frac{2L}{D^2T}. \tag{3.25}$$

If f_{sw} is the frequency of the V_{gate}, then, $f_{\text{sw}} = \frac{1}{T}$. Hence, Eq. (3.25) can be rewritten as following:

$$R_{\text{in}} = \frac{2Lf_{\text{sw}}}{D^2}. \tag{3.26}$$

As seen from Eq. (3.26), the input resistance R_{in} is independent of the input voltage V_{in} and the load resistance R_{L} with respect to the buck-boost converter in DCM. The input resistance R_{in} is only decided by the inductance L, switching frequency f_{sw} and the duty-on ratio D.

B). Buck converter

For the same reason, the variation of the inductor current should be zero among the on-state and off-state. Then δ can be given by following:

$$\delta = D\frac{V_{\mathrm{in}} - V_{\mathrm{o}}}{V_{\mathrm{o}}}. \tag{3.27}$$

The current always flows through the inductor and load both at on-state and off-state as shown in Fig. 3.2(a). Therefore, the output current I_{o} should be equal to the average of the inductor current I_{L}.

$$I_{\mathrm{o}} = \frac{1}{2}(D+\delta)I_{\mathrm{LP}}. \tag{3.28}$$

Applying Eqs. (3.5) and (3.27) to Eq. (3.28) leads to the following:

$$V_{\mathrm{o}} = \frac{1}{\frac{2LI_{\mathrm{o}}}{D^2T} + V_{\mathrm{in}}}V_{\mathrm{in}}^2. \tag{3.29}$$

Similarly, Eq. (3.29) can be rewritten as

$$R_{\mathrm{in}} = \frac{2Lf_{\mathrm{sw}}}{D^2}\frac{1}{1-\frac{V_{\mathrm{o}}}{V_{\mathrm{in}}}}. \tag{3.30}$$

Therefore, the input resistance R_{in} is complicated and depended on the proportion of output and input voltages.

C). Boost converter

Similarly, as for boost converter, the V_{o} and R_{in} also can be expressed as following:

$$V_{\mathrm{o}} = (\frac{D^2T}{2LI_{\mathrm{o}}}V_{\mathrm{in}} + 1)V_{\mathrm{in}}, \tag{3.31}$$

$$R_{\mathrm{in}} = \frac{2Lf_{\mathrm{sw}}}{D^2}(1-\frac{V_{\mathrm{in}}}{V_{\mathrm{o}}}). \tag{3.32}$$

Finally, we summarize the relationships of the input/output resistances and input/output voltages for these three basic topologies DC-DC converters in DCM as shown in Table 3.2. Referring to the Table 3.1, R_{in} of three topologies DC-DC converters in CCM are all relative to the load resistance R_{L}. In the DCM case, R_{in} of buck and boost converters are both relative to the proportion of V_{in} and V_{o}. However, the R_{in} of the buck-boost converter is independent of V_{in}, V_{o} and R_{L}. If the inductance L, switching frequency f_{sw}, duty-on ratio D are decided, the R_{in} of the buck-boost converter can be calculated and it will be constant. Therefore,

Table 3.2: Input/output resistance and voltage relationships of three basic topologies DC-DC converters in DCM.

Topology	Voltage	Resistance	Variation of R_{in}
buck	$V_{\text{o}} = \frac{1}{\frac{2LI_{\text{o}}}{D^2T}+V_{\text{in}}} V_{\text{in}}^2$	$R_{\text{in}} = \frac{2Lf_{\text{sw}}}{D^2}\frac{1}{1-\frac{V_{\text{o}}}{V_{\text{in}}}}$	depends on $\frac{V_{\text{o}}}{V_{\text{in}}}$
boost	$V_{\text{o}} = (\frac{D^2T}{2LI_{\text{o}}}V_{\text{in}} + 1)V_{\text{in}}$	$R_{\text{in}} = \frac{2Lf_{\text{sw}}}{D^2}(1 - \frac{V_{\text{in}}}{V_{\text{o}}})$	depends on $\frac{V_{\text{o}}}{V_{\text{in}}}$
buck-boost	$V_{\text{o}} = -\frac{D^2T}{2LI_{\text{o}}}V_{\text{in}}^2$	$R_{\text{in}} = \frac{2Lf_{\text{sw}}}{D^2}$	independent of V_{in} and R_{L}

a buck-boost converter operated in DCM is chosen for impedance matching in the rectenna circuit.

3.3 Externally-powered DCM Buck-boost Converter

3.3.1 Input Resistance R_{in}

The buck-boost converter in DCM exhibits constant input resistance despite the load resistance as mentioned above. However, it inverts the polarity of input and output voltages. Therefore, we design an inverting DCM buck-boost converter which inputs a negative voltage to get a positive output voltage. The proposed inverting DCM buck-boost converter is shown in Fig. 3.4(a) where the control-pulse circuit consists of a 5 V power source, a low-frequency (LH) oscillator, a high-frequency (LH) oscillator and a MOSFET gate driver. The LF and HF oscillators respectively generate the LF, HF pulse waves which are combined into the gate control pulse V_{gate}. Through the gate driver, the V_{gate} controls the N-MOS's gate on or off. Here, the input port of the converter is expected to be connected to the output of the rectenna (or rectifier). Figure 3.4(b) shows the operating waveform of the proposed converter where I_{in}, I_{L}, I_{D} are input current, inductor current, diode current, respectively, and V_{gate}, V_{h}, V_{ι} are gate control pulse wave, HF pulse wave, LF pulse wave, respectively. An additional 5 V power source powers the LF oscillator and gate driver, and the HF oscillator is powered by the LF oscillator. It means that the V_{gate} is as same as the V_{h} when the V_{ι} is on while the V_{gate} is off when the V_{ι} is off. As seen from the waveform, there is no current flowing though the circuit at the off-state of the LF oscillator. It seems that the LF oscillator compels the circuit to be sleep state at an interval then the current becomes discontinuous.

The operating condition can be classified into two states such as a work-state and a sleep-state. The work-state is when the LH pulse is on. At work-state, there are three operating states as same as mentioned in Chapter 3.2.2. The sleep-state is when the LH pulse is off. At sleep-state, there is no current flowing through the circuit. As shown in Fig. 3.4(b), the input current is equal to the inductor current only at the on-state. If I_{inave} is the average input current, then:

$$I_{\text{inave}} = \frac{I_{\text{LP}} D_{\text{h}} D_{\iota}}{2}, \tag{3.33}$$

where D_{h}, D_{ι} are the high, low frequency pulse duty-on ratio. Referring to Eq. (3.19), the peak inductor current I_{LP} can be written as following:

$$I_{\text{LP}} = \frac{V_{\text{in}} D_{\text{h}} T_{\text{h}}}{L}, \tag{3.34}$$

where the T_{h} is the period of the HF pulse. Furthermore, input power P_{in} satisfies the following equation:

$$P_{\text{in}} = V_{\text{in}} I_{\text{inave}}. \tag{3.35}$$

Combining Eqs. (3.9), (3.33), (3.34) and (3.35), the input resistance R_{in} is given as follows:

$$R_{\text{in}} = \frac{2L}{D_{\text{h}}^2 D_{\iota} T_{\text{h}}}. \tag{3.36}$$

Let f_{h} represent the frequency of the HF pulse, applying $T_{\text{h}} = \frac{1}{f_{\text{h}}}$ to Eq. (3.36) leads to the following:

$$R_{\text{in}} = \frac{2L f_{\text{h}}}{D_{\text{h}}^2 D_{\iota}}. \tag{3.37}$$

Hence, the R_{in} of the proposed inverting DCM buck-boost converter is decided by the inductance L , low, high frequency pulse duty-on ratio D_{ι}, D_{h} and the high frequency f_{h}.

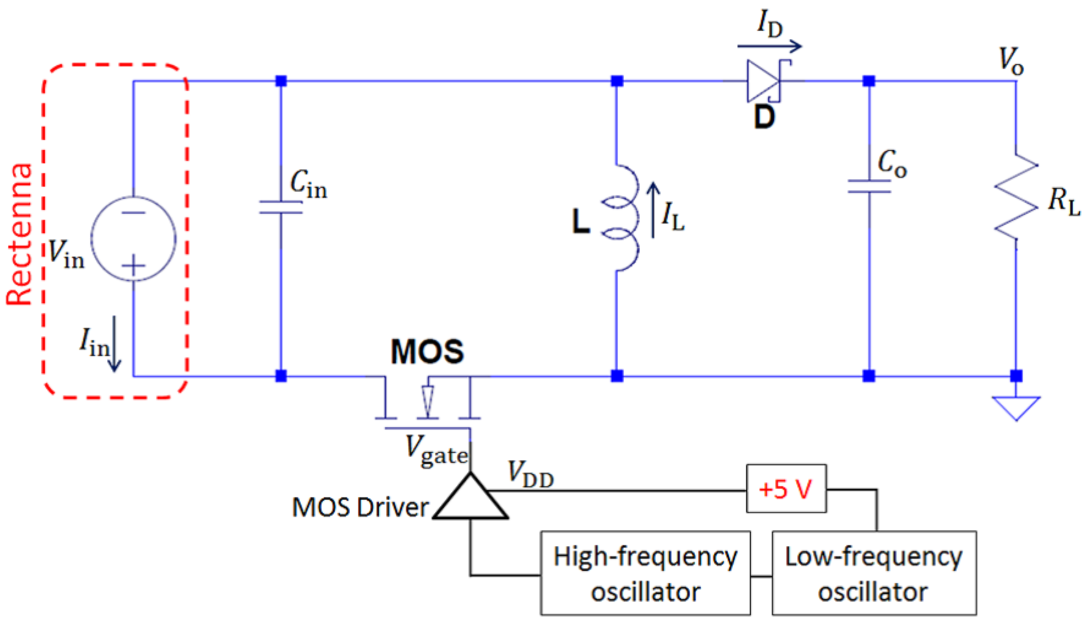

(a)

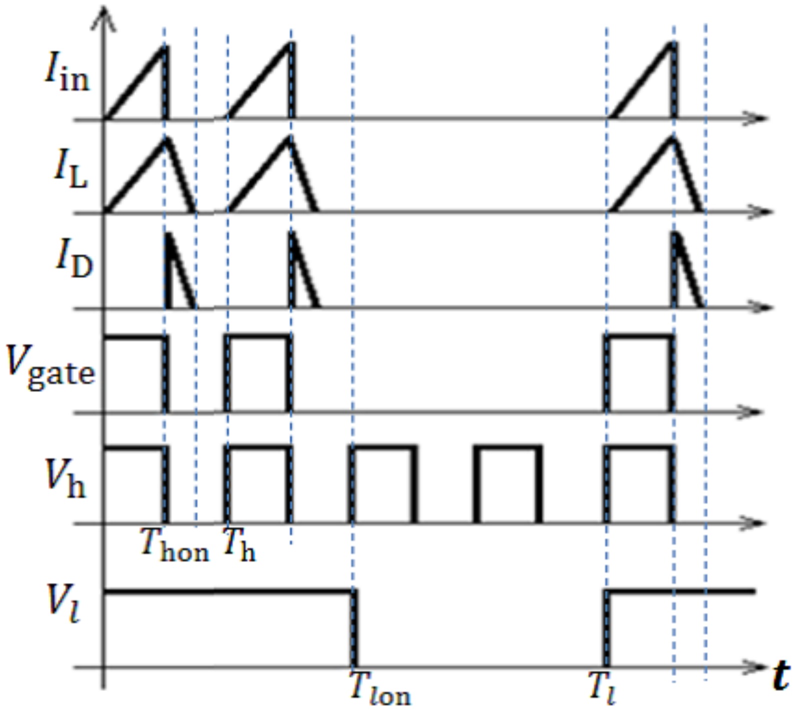

(b)

Figure 3.4: Inverting DCM buck-boost converter. An extra +5 V power source is required for the control-pulse circuit. Input a negative voltage to obtain a positive output voltage. (a) Structure. (b) Operating waveforms.

Table 3.3: Components of the proposed inverting DCM buck-boost converter.

Component	Maker	Part NO.	Description
High-frequency oscillator	Linear Technology	LTC6900	$I_{\mathrm{SS}} = 0.5$ mA ($f = 3$ MHz); $V_{\mathrm{SSmin}} = 2.7$ V
Low-frequency oscillator	Linear Technology	LTC6992	I_{SS}= 115 μA ($f = 100$ Hz); $V_{\mathrm{SSmin}} = 2.25$ V
N-MOS	Fairchild	FDS6298	$V_{\mathrm{DSS}} = 30$ V; $R_{\mathrm{DS(on)}} = 12$ mΩ ($V_{\mathrm{GS}} = 4.5$ V)
Schottky Diode	Toshiba	CRS01	$V_{\mathrm{RRM}} = 30$ V; V_{FM}= 0.36 V
MOSFET Driver	Microchip	TC1427	$V_{\mathrm{DDmin}} = 4.5$ V
Inductor	Panasonic	ELC18B102L	$L = 1$ mH; $R_{\mathrm{dc}} = 0.39$ Ω; I_{dc} = 1.1 A
Capacitor	Rubycon	Electrolytic Capacitors	$C_{\mathrm{in}} = 47$ μF ($V_{\mathrm{rated}} = 10$ V); $C_{\mathrm{o}} = 100$ μF ($V_{\mathrm{rated}} = 50$ V)

3.3.2 Simulation and Experimental Results

In this buck-boost converter, set $L = 1$ mH, $D_{\mathrm{h}} = 0.5$, $D_{\iota} = 0.6$, and $f_{\mathrm{h}} = 10$ kHz, so that the input resistance of the converter R_{in} becomes 133 Ω, as calculated using Eq. (3.37). Table 3.3 lists the components used in the buck-boost converter, and Fig. 3.5 shows a photograph of the buck-boost converter, which uses dielectric substrate as a printed circuit board (PCB).

In order to verify the theory as mentioned above, we simulate the converter by LTspice and conduct an experiment on it. The structure of the experiment circuit is shown in Fig. 3.6, where a negative voltage supplied by a DC power source is the input voltage. A +5 V power source supplies the power for the control-pulse circuit. An ammeter and a voltmeter measure the input current and the output voltage, respectively. We measure the efficiency and the input resistance of the converter with an input voltage from 0.8 to 5 V, where the input power is from 5 to 187 mW. Figure 3.7 shows the simulation and experimental results for input

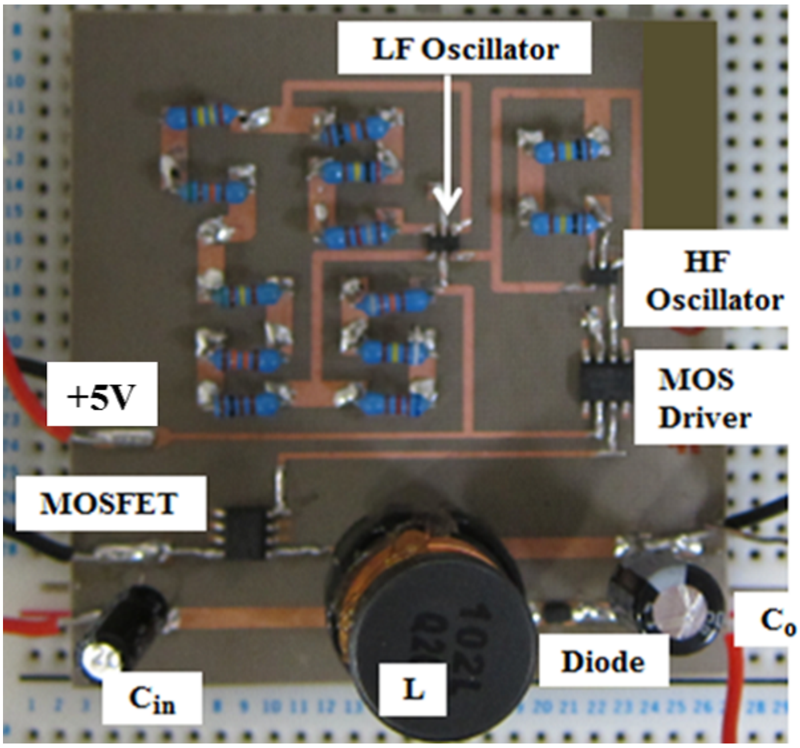

Figure 3.5: Photograph of the inverting DCM buck-boost converter.

resistance $R_{\rm in}$ versus the load resistance $R_{\rm L}$ from 100 to 5000 Ω for the input voltage of 1.2 and 3 V. According to Fig. 3.7, the simulation results almost agree well with the theory of 133 Ω. The experimental $R_{\rm in}$ is near the calculated value of 133 Ω, but it is slightly lower for a low load resistance when the $R_{\rm L}$ is smaller than 400 Ω. This is because the inductor current becomes continuous at the beginning of the switching-on period of the MOSFET at a low load resistance. However, the equation of the input resistance (Eq. (3.37)) is calculated as a discontinuous conduction mode. Thus, the measured input current is slightly larger than the calculated value. Consequently, the input resistance is smaller than the calculated value. Figure 3.8 shows the $R_{\rm in}$ versus the input power from 2 to 187 mW for the load resistance of 1000 Ω. According to Fig. 3.8, the experimental $R_{\rm in}$ almost agrees with the simulation results, and it is varying in the range of 123 to 133 Ω as the input power is changing from 5 to 187 mW. Therefore, according to Figs. 3.7 and 3.8, as expected, the designed buck-boost converter has constant input resistance despite the load resistance and the input power.

Furthermore, the efficiency of the converter is also measured. Here, the efficiency does not include the power dissipated by the control circuit. Similarly, Figure 3.9 shows the measured efficiency of the converter for load resistances from 100 to 5000 Ω for the input voltage of 1.2 and 3 V, where the input power are 12

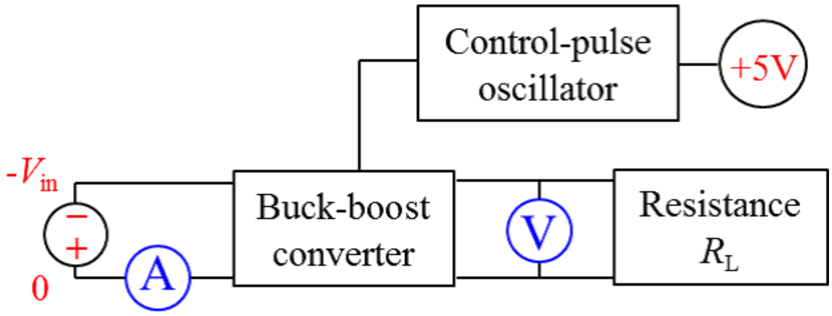

Figure 3.6: Measurement setup of the externally-powered buck-boost converter. An extra +5 V power source is required.

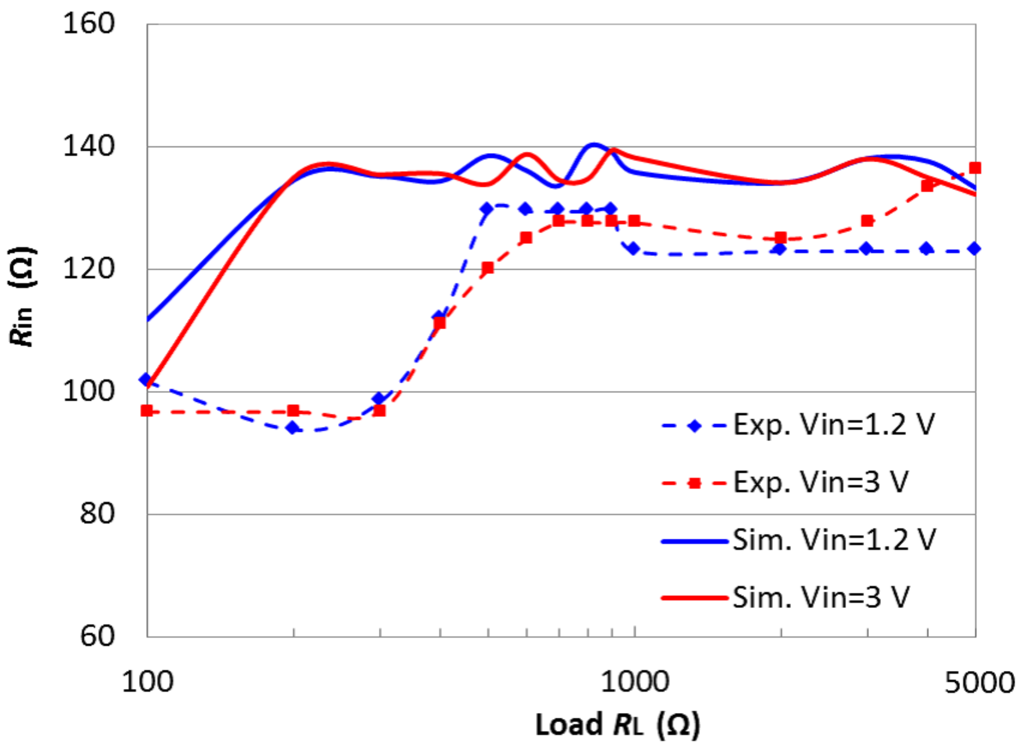

Figure 3.7: Simulation and experimental results of the input resistance R_{in} vs. load resistance for an input voltage of 1.2 or 3 V.

and 70 mW, respectively. The efficiency is almost greater than 80 % for a wide range of loads from 200 to 5000 Ω at the input voltage of 3 V. The efficiency is a little low at load resistance of 100 Ω because the load resistance is smaller than the input resistance and the input voltage is reduced by the converter. At this moment, the converter works as a buck converter, where the output voltage is lower than the input voltage. The efficiency decreases under a large load resistance because the output current is shunted by the output capacitor. The current flowing through the output capacitor will increase as the load resistance is increased. Figure 3.10 shows the measured efficiency of the converter for input power from

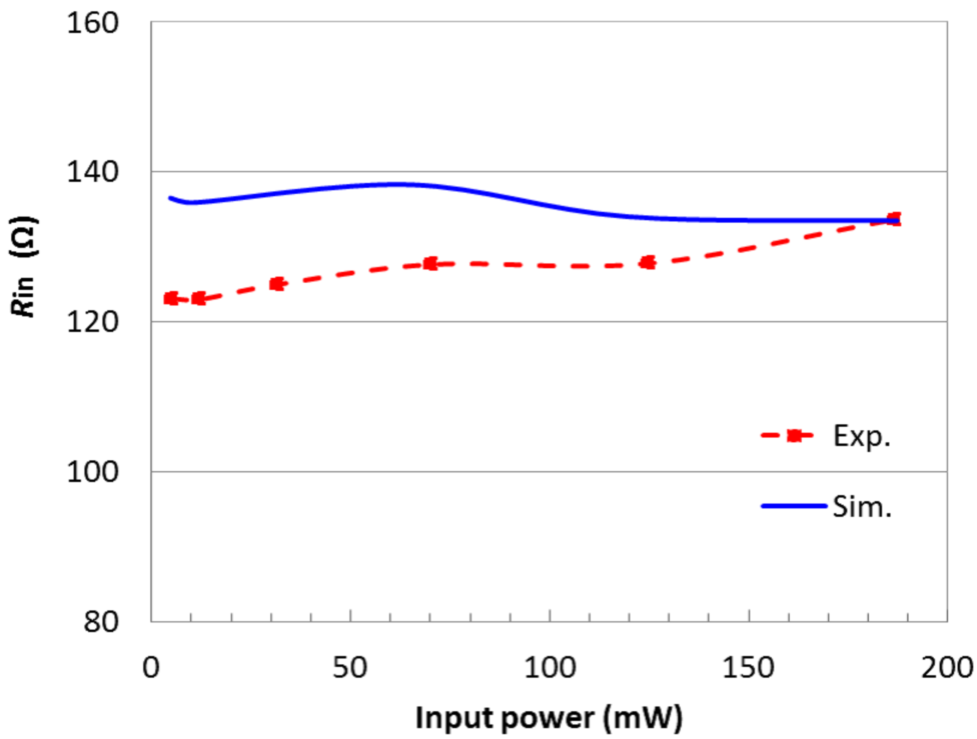

Figure 3.8: Simulation and experimental results of the input resistance R_{in} vs. input power for a fixed load resistance of 1000 Ω.

5 to 187 mW for a fixed load resistance of 1000 Ω. The efficiency is increasing lightly as the input power is increasing. In this case, the measured efficiency is greater than 85 % for this wide range of input powers. Additionally, since ideal capacitors and wires are used in the simulation, the measured efficiency is almost 5 % lower than the simulation results which both can be seen from Figs. 3.9 and 3.10.

3.4 Rectifying Circuit with Negative Output Voltage

As mentioned in Chapter 2.3, there are two types of dc pass filters such as a $\lambda/4$ line plus a capacitor [58] and a $\lambda/4$ line plus some open stubs in single shunt rectifier. The authors obtained a higher experimental efficiency using open stubs instead of capacitor [59]. We also utilize a $\lambda/4$ line plus four open stubs as a dc pass filter as shown in Fig. 3.11(a). The impedance of the dc pass filter Z_{dc}, opposite to the class-F^{-1} mode [68], presents zero for even harmonics and

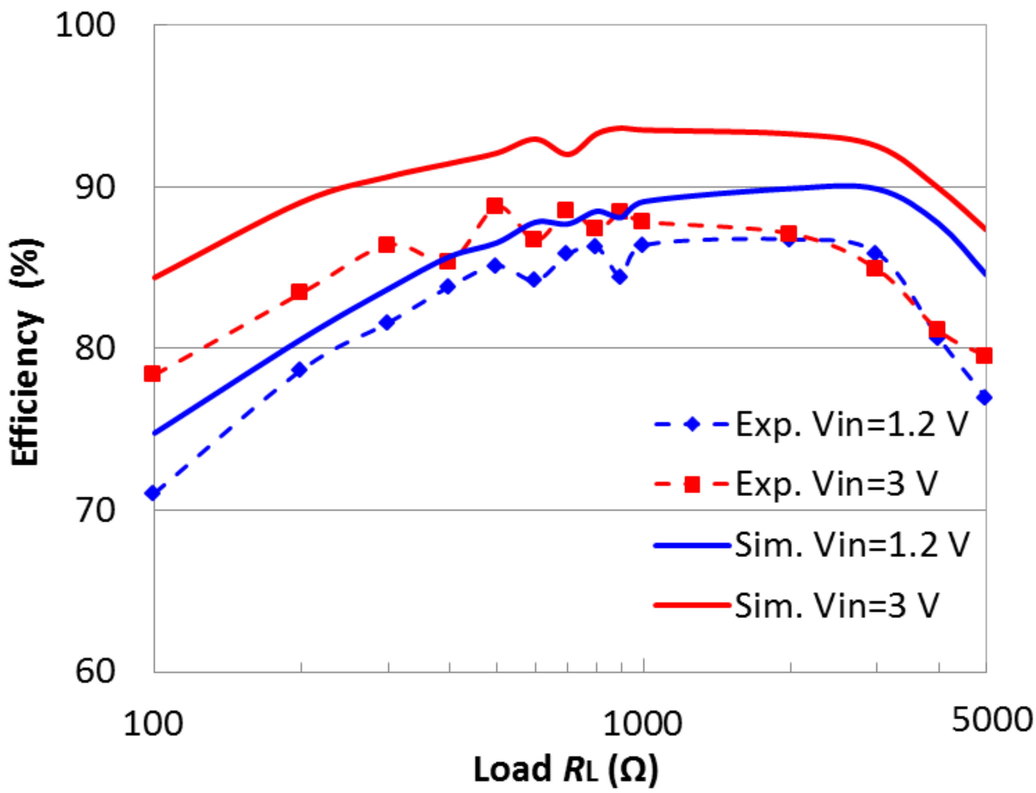

Figure 3.9: Simulation and experimental results of the efficiency vs. load resistance for an input voltage of 1.2 or 3 V.

infinity for odd harmonics. In other words, all even harmonics are terminated in short circuits and all odd harmonics are terminated in open circuits. The set of harmonic terminations is the same as for a class-F amplifier [69], thus this rectifier is referred to as a class-F rectifier. In fact, the impedance of the dc pass filter, consisted of a $\lambda/4$ line and a capacitor in shunt, also presents a class-F characteristic which is analyzed in [59]. Due to the parasitic components of a real capacitor, the combination of a $\lambda/4$ line and a capacitor can not satisfy the demand of the dc pass filter characteristic for high harmonica frequencies.

The designed buck-boost converter inverts the polarity of the input voltage and the output voltage, which is described in Chapter 3.3. Hence, unlike other rectifiers, we reverse the polarity of the diode in order to obtain a negative output voltage from the rectifier. There is a little discussion and comparison about the diode topologies in single, two-diode package and two anti-parallel diodes in [57] which indicates that two-diode rectifier would result in higher efficiency for high power levels. Additionally, the rectifier using two-diode parallel HSMS2865 or three-diode parallel HSMS286L obtained a higher efficiency in simulation results

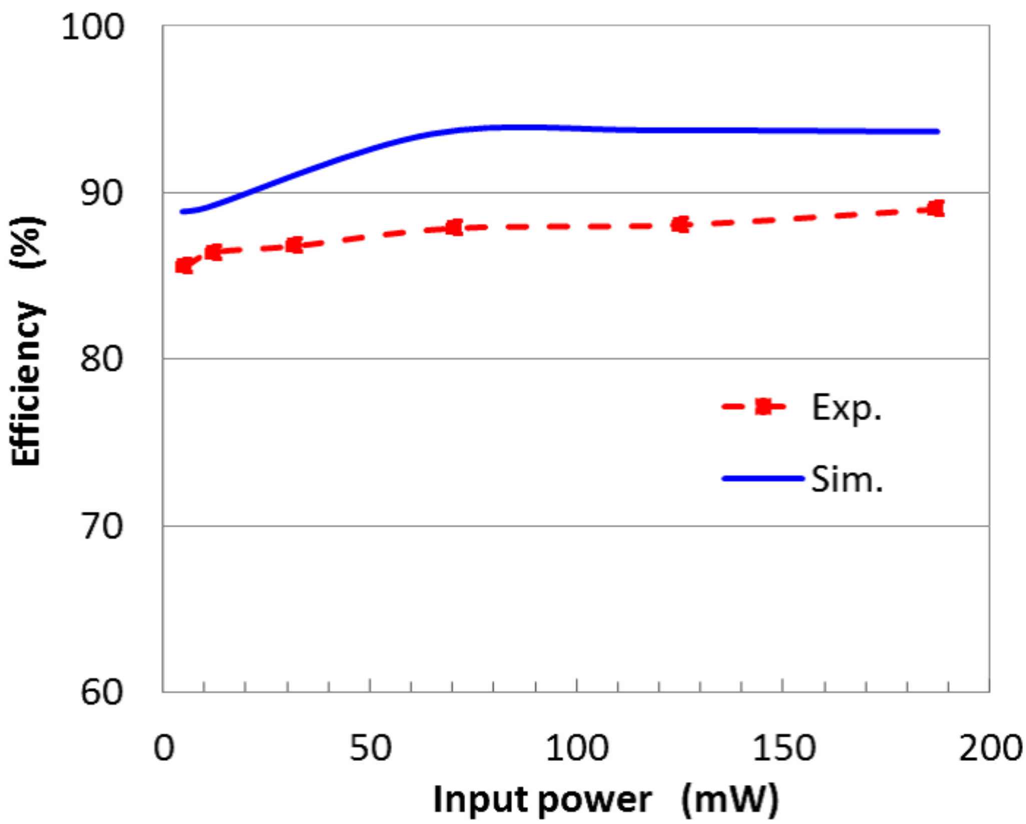

Figure 3.10: Simulation and experimental results of the efficiency vs. input power for a fixed load resistance of 1000 Ω.

in Chapter 2.3. However, as seen from Fig. 2.2, the physical size of HSMS2865 (4 pins) and HSMS286L (6 pins) are too wide to limit the characteristic impedance of the connected microstrip line. Therefore, considering the physical size and the parallel diodes, we choose two HSMS286F as a rectifying diode. HSMS286F diode, consisting of two HSMS2860 diodes mounted into a single surface mount package, has 3 pins because of a common cathode pin. Table 3.4 lists the components used in the rectifier and Fig. 3.11(b) shows the photograph of the designed rectifier.

We first simulate the rectifying circuit using ADS2011. We optimize the whole rectifying circuit to gain the highest efficiency not just considering the impedance matching with the diodes but also reducing the dissipation power of diodes in the simulation. Then, we fabricate it and test it with 2.45 GHz microwave power. The simulation and experimental results of the rectifier circuit are shown in Fig. 3.12.

Figure 3.12(a) shows the RF-DC conversion efficiency versus load resistances ranging from 50 to 1000 Ω, which represents a typical efficiency characteristic of

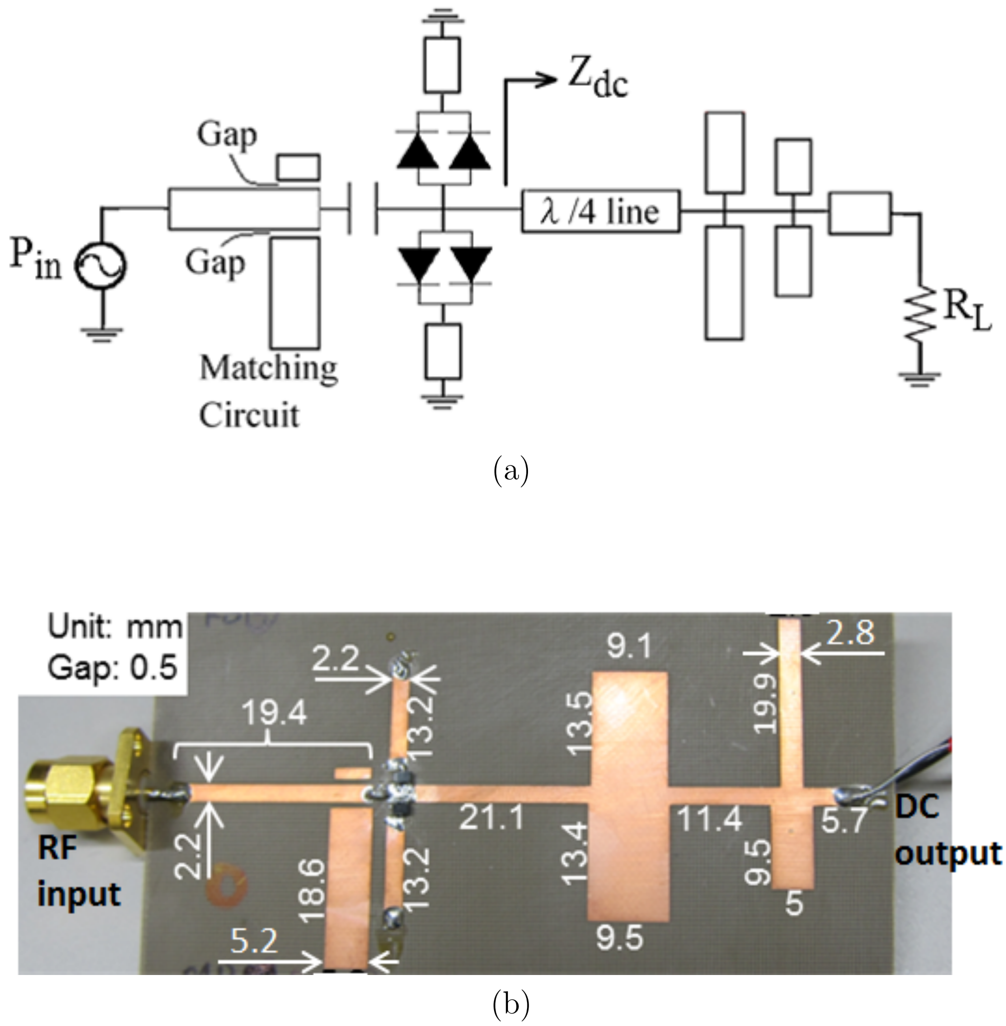

Figure 3.11: Proposed negative output voltage rectifier. (a) Structure. (b) Photograph.

the rectifying circuit. The two solid curves are simulation results and the dot curve is the experimental results. Sim.1 gets the maximum simulation efficiency of 82.5 % at the input power of 69 mW. However, the maximum experimental efficiency is 79.2 % at input power of 82 mW as shown in Exp. curve. Then, when we set the input power as 82 mW in simulation, the maximum efficiency of 81.8 % is obtained (Sim.2 curve). The detailed results of these three curves are summarized in Table 3.5. We obtain the maximum efficiency of 79.2 % at an optimal load of 160 Ω. In particular, the measured efficiency difference between an optimal load of 160 and 1000 Ω is approximately 53 %, which clearly indicates that the efficiency of the rectifier depends on the load resistance.

Figure 3.12(b) shows the simulation and experimental efficiency versus the

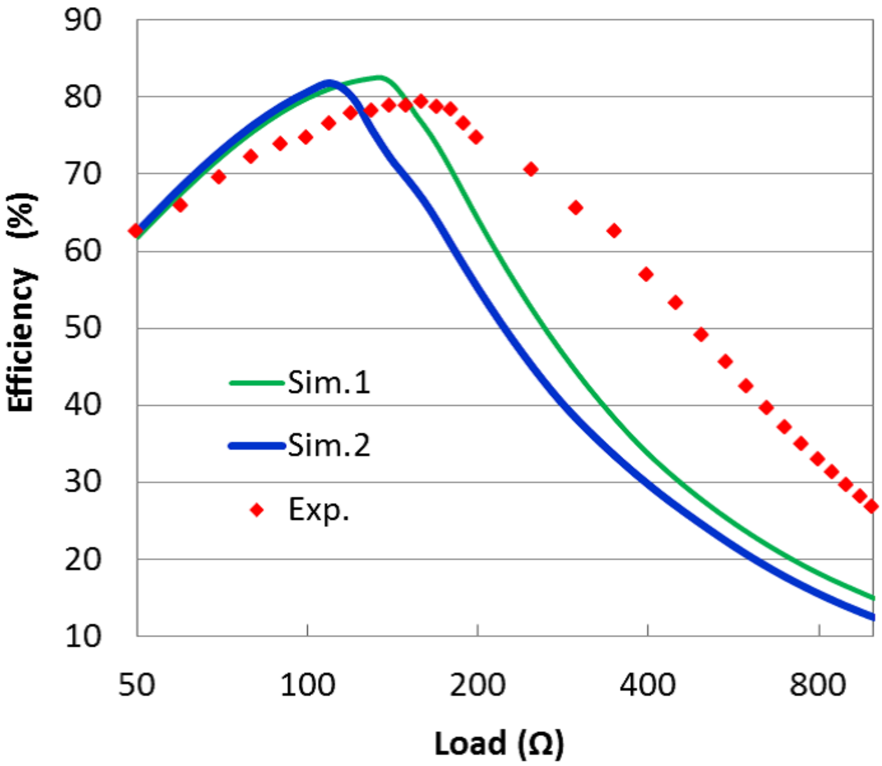

(a)

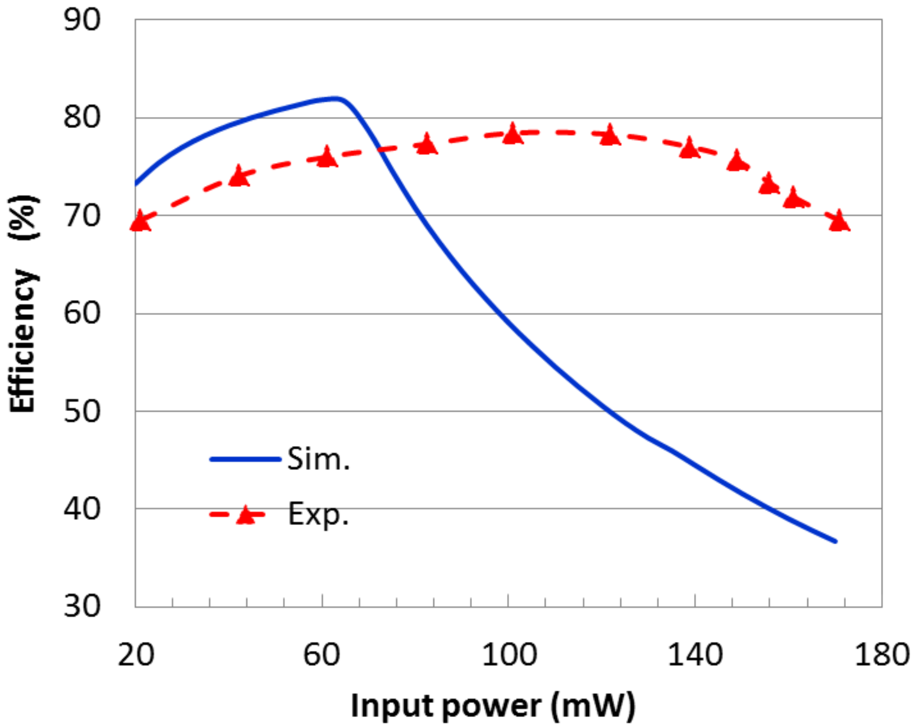

(b)

Figure 3.12: Simulation and experimental results of the proposed negative output voltage rectifier. (a) Efficiency vs. load resistance for a constant input power of 82 mW. (b) Efficiency vs. input power for a constant load of 150 Ω.

Table 3.4: Components of the negative output voltage rectifier.

Component	Maker	Part NO.	Description
DC block capacitor	Murata	GRM1882C1-H331JA01D	$C = 330$ pF; $V_{\text{rated}} = 50$ V
HF diode	Avago	HSMS286F	Refer to Table 2.2
Dielectric substrate	Nippon pillar	NPC-F260	$\varepsilon_{\text{r}} = 2.53$; $\tan\delta = 0.0018$; $t = 18$ μm; H = 0.8 mm

Table 3.5: Comparison of simulation and experimental results of the rectifier.

	Input power	Efficiency	Reflection	Optimal load
Sim.1	69 mW	82.5 %	1.6 %	135 Ω
Exp.	82 mW	79.2 %	4.9 %	160 Ω
Sim.2	82 mW	81.8 %	3.4 %	110 Ω

input power ranging from 20 to 170 mW at the load of 150 Ω. The efficiency is changing with the input power while the maximum difference in efficiency is only 10 % for this range of input powers. In simulation, the maximum efficiency is obtained at the input power of 60 mW, while the efficiency drops rapidly with the input power exceeding 60 mW because the reverse voltage is over the breakdown voltage of the diode. However, in experiment, the efficiency gets much higher even though the input power increases far over 60 mW. A similar phenomena can be seen from Fig. 3.12(a), the experimental efficiency is higher than the simulation one when the load resistance exceeds the optimal load. This is because the real breakdown voltage is higher than the value (7 V) given by the SPICE parameters. A high precision HF diode model is required in ADS simulation.

Table 3.6: Efficiency and load relationships of the rectifier and buck-boost converter in experimental results.

	R_{L}	R_{in}	Efficiency
RF-DC rectifier	130 Ω		78 %
buck-boost converter	400-5000 Ω	130 Ω	80 %
RF-DC-DC circuit	400-5000 Ω		predicted value 62 %

3.5 Experiment on Externally-powered RF-DC-DC Circuit

The experiment on the RF-DC-DC circuit consisted of the rectifier and the buck-boost converter designed above is conducted. Figure 3.13(a) is the experimental architecture for measuring the efficiency of the RF-DC-DC circuit and Fig. 3.13(b) is the experiment photograph. The microwave power is first regulated by the RF-DC rectifier, and the DC output voltage of the RF-DC rectifier is again regulated by the buck-boost converter. The input resistance of the DC-DC converter seen from the left side is also the output impedance of the rectifier. Summarize the efficiency and load relation of the rectifier and the buck-boost converter designed above in Table 3.6. The designed R_{in} of the converter is 133 Ω which is slightly different with the optimal load (160 Ω) of the rectifier, while the efficiency of the rectifier at 133 Ω is only 1.2 percentage points lower than that at the optimal load. Thus, as expected, the buck-boost converter can track the maximum efficiency of the rectifier and the overall efficiency of the RF-DC-DC circuit is expected to be steady and over 62 %.

Following Fig. 3.13(a), we use a 2.45 GHz microwave power generated from a signal generator. Power sensor A measures the input power of the rectifier. Through the circulator, power sensor B measures the reflection power at the input point of the DC block. Here, we use a DC block to prevent the DC voltage from passing through the rectifier, which also can prevent the positive output pole of the rectifier from being grounded, because the positive input pole of the buck-boost converter is not allowed to become grounded. Referring to Fig. 3.4, if the

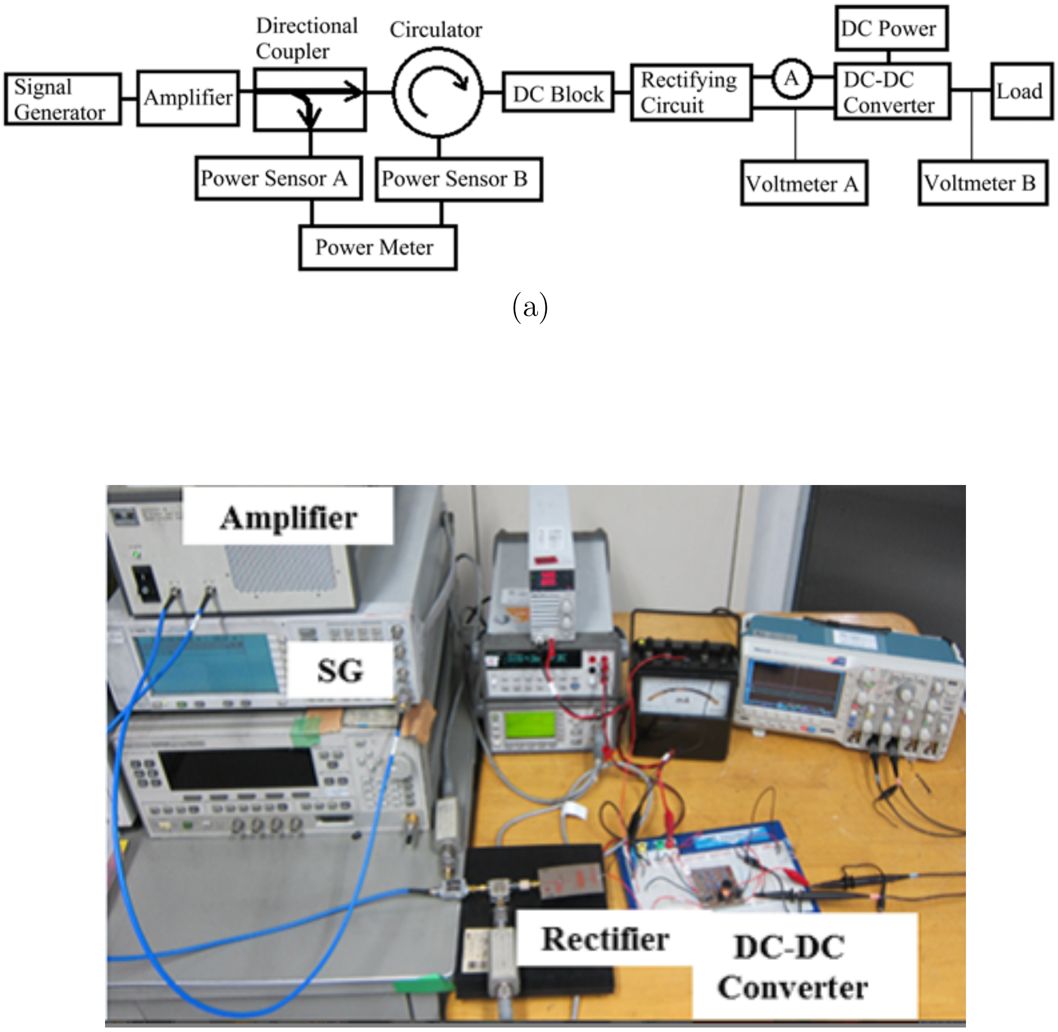

(a)

(b)

Figure 3.13: Experimental setup for measuring the efficiency of the RF-DC-DC circuit. (a) Block diagram. (b) Experiment photograph.

positive input pole of the converter is grounded, the MOSFET will be shorted and the converter can not act as a buck-boost converter. An ammeter is used to measure the input current of the converter, and voltmeters A and B are used to measure the output voltage of the rectifier and the output voltage of the converter, respectively. We use DC power for the control circuit to supply voltage to the LF oscillator and the gate driver in the experiment. Before reporting the experimental results, the tracking efficiency η_{track} is defined as follows:

$$\eta_{\text{track}} = \frac{\eta'_{\text{rf-dc}}}{\eta_{\max(\text{rf-dc})}} \times 100\,\%, \tag{3.38}$$

where $\eta'_{\mathrm{rf-dc}}$ is the conversion efficiency of the RF-DC rectifying circuit when it is connected to the buck-boost converter, and $\eta_{\mathrm{max(rf-dc)}}$ is the maximum conversion efficiency of the RF-DC rectifying circuit at the optimal load without a buck-boost converter.

Figure 3.14 shows the measured efficiency versus the load resistance from 100 to 5000 Ω and an input power from 20 to 100 mW. Figure 3.14(a) compares the efficiency of the RF-DC-DC circuit with the rectifying circuit described in Chapter 3.4 under the input power of 82 mW. The blue curve, RF-DC (with converter), is the efficiency of only the rectifying circuit when it is connected to the buck-boost converter. The black curve, RF-DC (without converter), is the efficiency of the rectifying circuit alone when it is not connected to the buck-boost converter. The black curve decreases dramatically when the load exceeds the optimal load and the efficiency is only 26 % at the load of 1000 Ω. In comparison, the conversion efficiency of the rectifying circuit connected with the converter is almost steady at 75 %, which is near the maximum power point of the rectifying circuit, even though the load resistance is changed from 100 to 5000 Ω. Furthermore, as expected, the overall efficiency of the RF-DC-DC circuit is over 60 % in a wide range of load resistances from 100 to 5000 Ω, as indicated by the red curve. Compared to the rectifying circuit without a converter, the overall efficiency is lower than that when the load is below 300 Ω. However, the overall efficiency is much higher than that when the load exceeds 300 Ω. Under the large load resistance, the overall efficiency decreases slightly because the efficiency of the buck-boost converter decreases as the load increases.

Figure 3.14(b) shows the overall efficiency versus the input power changing from 20 to 100 mW at the load resistance of 1000 Ω. Note that the variation of the overall efficiency is small and the overall efficiency is over 55 % in this power range.

Additionally, we also check the tracking efficiency and the input resistance R_{in} of the buck-boost converter when it is utilized in the RF-DC-DC circuit as shown in Fig. 3.15. Figure 3.15(a) shows that the tracking efficiency η_{track} remains over 92 % over the entire range of loads from 100 to 5000 Ω and the input resistance R_{in} is approximately near to the designed value of 133 Ω. The coherent variation trend of two curves can be seen from Fig. 3.15(a). This is because the $\eta'_{\mathrm{rf-dc}}$ is increasing when the R_{in} is close to 133 Ω, which leads to η_{track} increasing according to Eq. (3.38). Similarly, Fig. 3.15(b) presents η_{track} and R_{in} with input power ranging

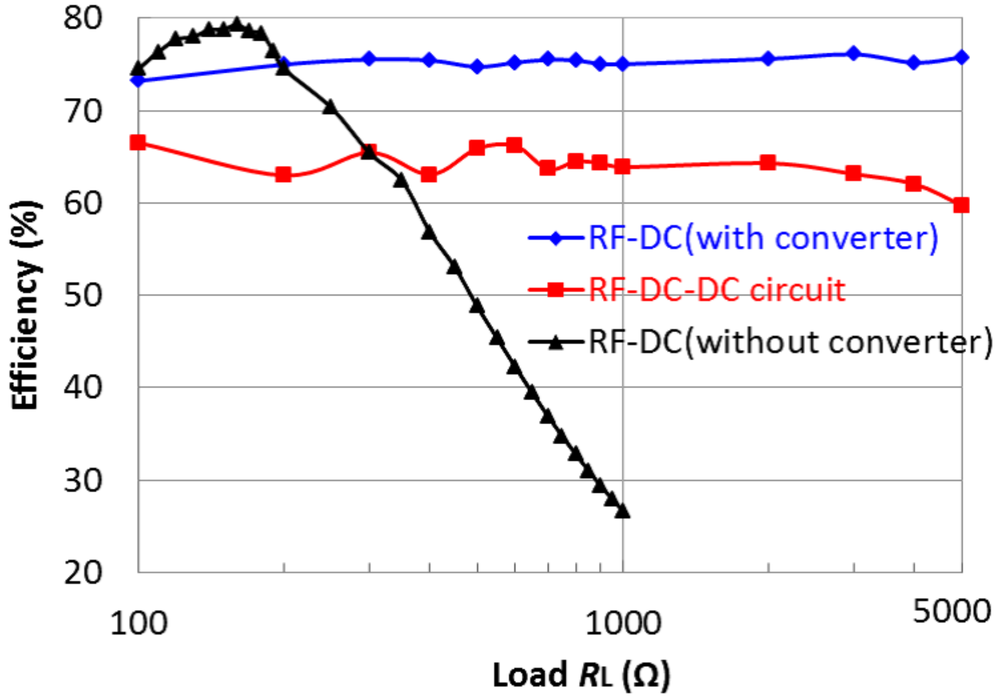

(a)

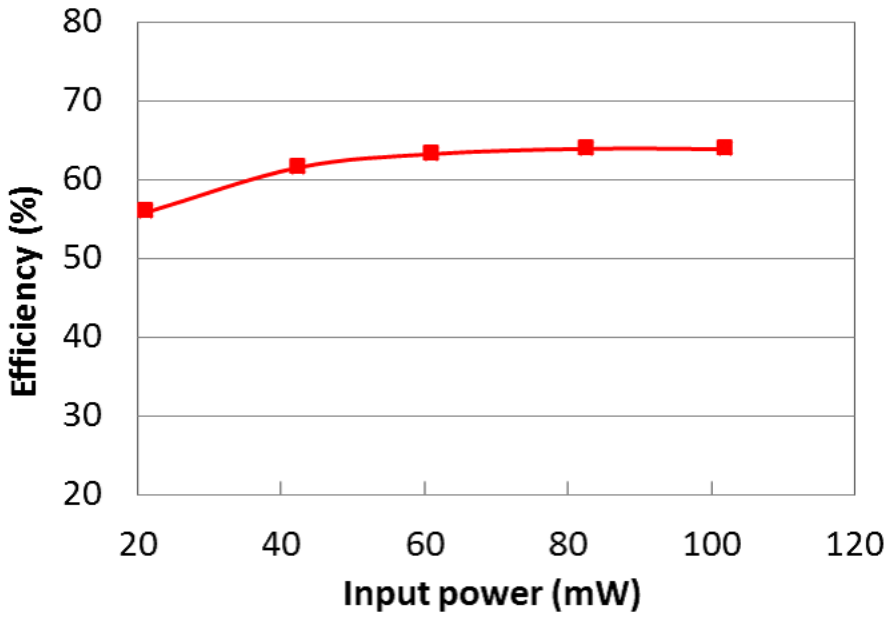

(b)

Figure 3.14: Measured overall efficiency of the RF-DC-DC circuit. (a) Efficiency comparison of the RF-DC-DC circuit and the general rectifier for a constant input power of 82 mW. (b) Overall efficiency vs. input power for a constant load of 1000 Ω.

from 20 to 100 mW at the load resistance of 1000 Ω. Note that the tracking efficiency is slightly increasing as the input power increases. The reason is as follows. The input resistance of the converter is close to the optimal load of the rectifier as the input power is increased, which leads to increase in the efficiency of the rectifier ($\eta^{'}_{\mathrm{rf-dc}}$). However, the maximum difference of the tracking efficiency is about 2 percentage points in this power range.

Figure 3.16 compares the output voltage versus load resistance at the input power of 82 mW. The red curve is the output voltage of the RF-DC-DC circuit, which is increasing as the load resistance increases. The black curve is the output voltage of the rectifier when it is not connected to the converter. Compared to it, the blue curve is the output voltage of the rectifier when it is connected to the converter, where the voltage is almost steady at 2.7 V. Note that the RF-DC-DC circuit obtains a higher output voltage than the usual rectifier at a same load resistance. Here, the relation of three voltage curves agree well with the simulation results reported in Fig. 2.14.

3.6 Summary

This chapter, firstly, from a new viewpoint, the input/output voltages and input/output resistances relationships of three basic topologies DC-DC converters are discussed. Unlike conventional application, the DC-DC converter is used in resistance conversion instead of voltage conversion. Based on the discussion results, a DCM inverting buck-boost converter, whose input resistance is independent of the load resistance or input power, is chosen for impedance matching in rectenna.

Secondly, we design a DCM inverting buck-boost converter which requires an extra DC power source for powering the control-pulse circuit. The buck-boost converter inputs a negative voltage to obtain a positive output voltage. More importantly, the input resistance of the buck-boost converter match the optimal load of the rectifying circuit to track the maximum efficiency point of the rectifying circuit. As expected, the measured input resistance of the buck-boost converter is approximately 133 Ω, despite the changes of the load resistance and input power. The measured efficiency of the converter exceeds 80 % for a wide range of loads or input powers. Next, we design a rectifying circuit with negative output voltage and peak experimental efficiency of 79.2 %.

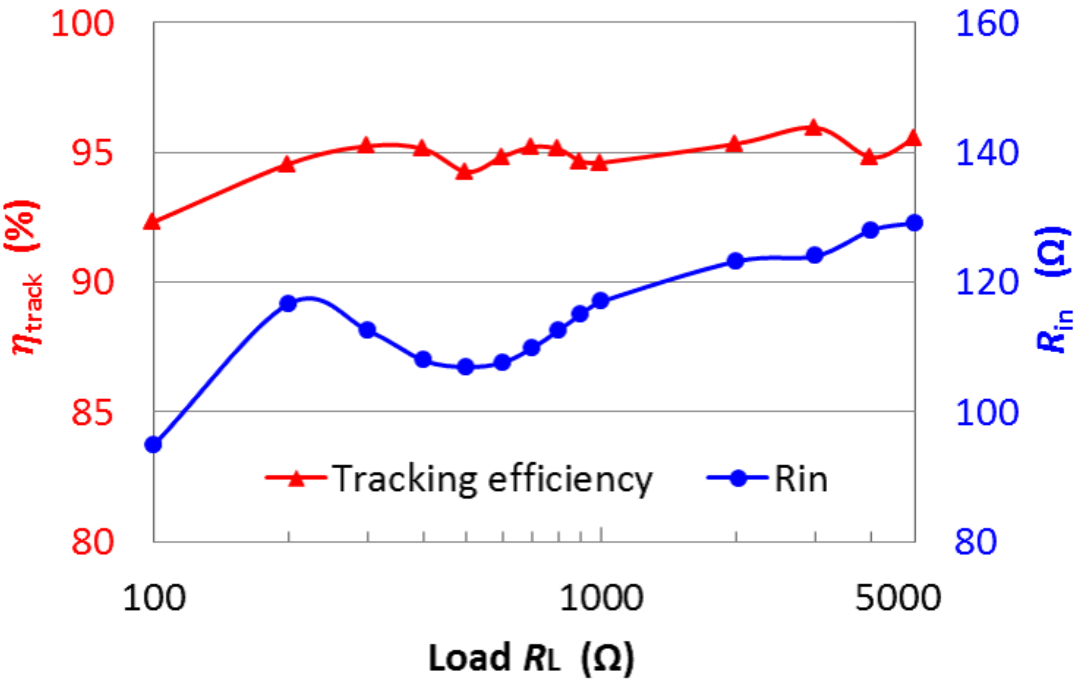

(a)

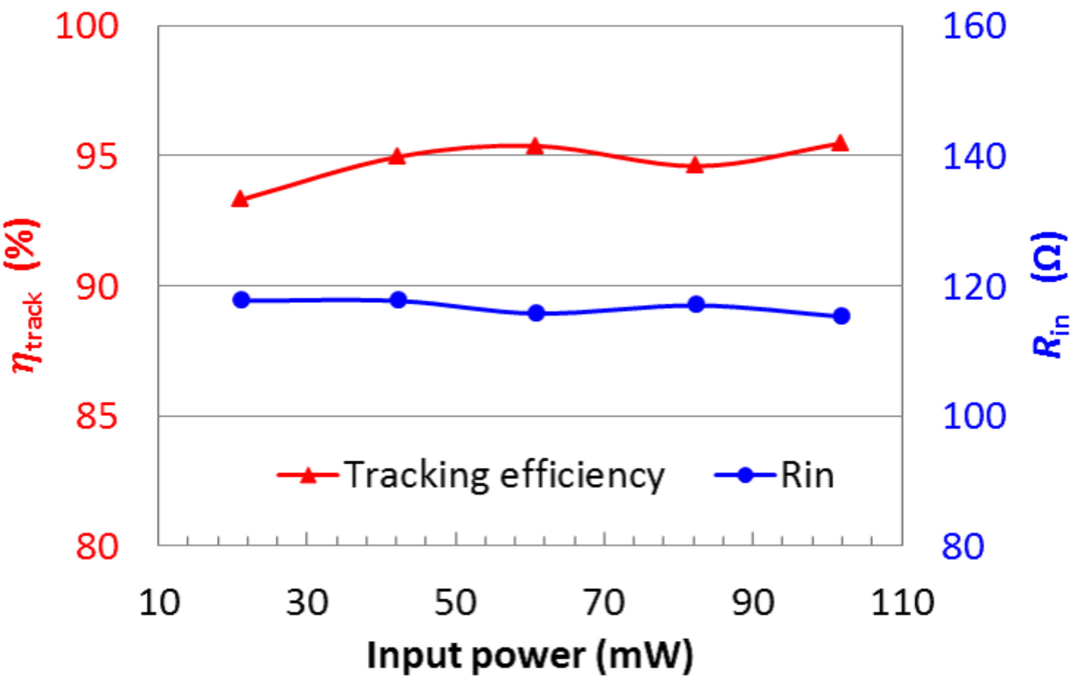

(b)

Figure 3.15: Measured tracking efficiency and input resistance R_{in}. (a) Tracking efficiency and R_{in} vs. load resistance. (b) Tracking efficiency and R_{in} vs. input power.

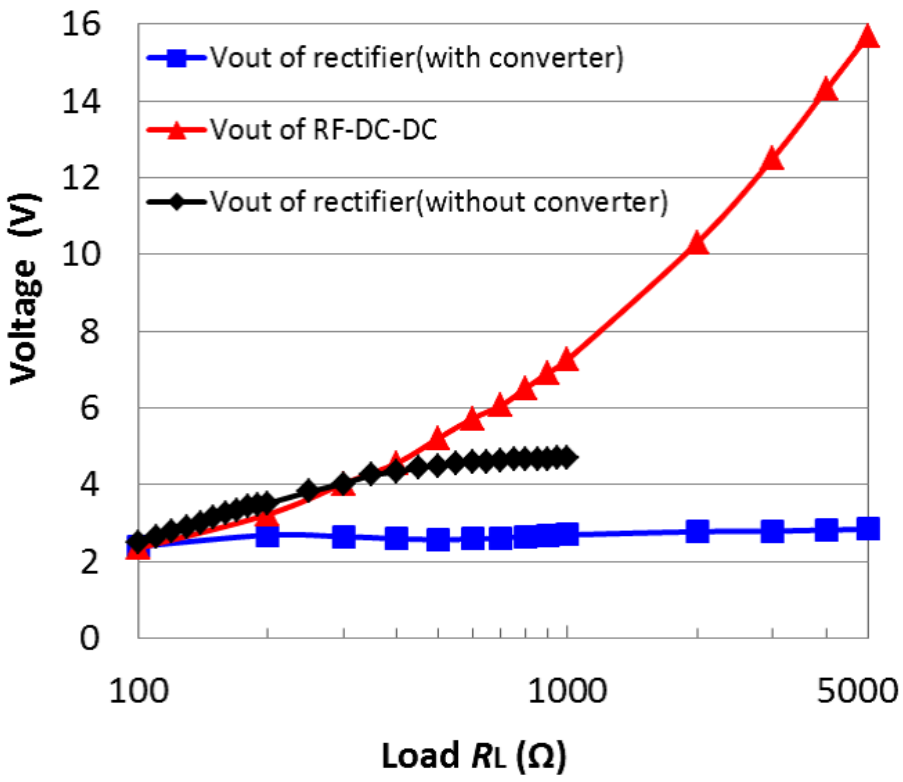

Figure 3.16: Measured output voltage vs. load resistance for a constant input power of 82 mW.

Finally, we verify that the proposed converter successfully tracks the maximum efficiency of the rectifying circuit. The conversion efficiency of the rectifier is approximately steady at 75 %, despite the load resistance varying from 100 to 5000 Ω for an input microwave power of 82 mW. This means that the maximum power tracking efficiency is over 94 %, compared to the maximum efficiency of 79.2 % at the optimal load. Additionally, the overall efficiency of the RF-DC-DC circuit is approximately steady over 60 %, despite the load resistance changing from 100 to 5000 Ω. According to the experimental results, the proposed RF-DC-DC circuit is an effective MPPT method to rectennas.

However, one big disadvantage is that the proposed buck-boost converter requires an additional DC power source for the control-pulse circuit which makes it hard for practical application. Additionally, owing to the loss of the buck-boost converter, the overall efficiency of the RF-DC-DC circuit is much lower than the maximum efficiency of the general rectifying circuit. Therefore, it is necessary to improve the efficiencies both of the rectifying circuit and the converter. Next chapter will give a solution about the problems above.

Chapter 4

Self-powered RF-DC-DC Circuit

4.1 Introduction

Based on the simulation and experiment results of previous discussions, a buck-boost converter in DCM is practicable for impedance matching in rectifying circuit. However, some critical issues such as the lower overall efficiency of the RF-DC-DC circuit and the requirement of an additional DC power source are need to be solved. Therefore, this chapter will solve the issues as mentioned above to improve the RF-DC-DC circuit. To improve the overall efficiency, we design a rectifying circuit with high peak efficiency. Furthermore, the input resistance of the buck-boost converter completely agrees with the optimal load of the rectifying circuit, which increases the tracking efficiency leading to a higher overall efficiency. To remove the additional DC power source, a non-inverting DCM buck-boost converter, whose control-pulse circuit is powered by the output of the rectifying circuit, is proposed. Similarly, an experiment on RF-DC-DC circuit is conducted to verify the advantages of the improved RF-DC-DC circuit.

4.2 High-efficiency Rectifying Circuit

As shown in Fig. 4.1, we also use a class-F rectifier with output filter consisted of a $\lambda/4$ line and four open stubs in this chapter. Compared with the rectifier in Chapter 3.4, the rectifier designed in this chapter has some differences as follows. First, with respect to the input filter, two open stubs are applied for impedance

Table 4.1: Efficiency and output voltage with different input powers for a fixed load of 190 Ω.

Input power (mW)	40	60	80	100
Efficiency (%)	80.2	81.9	82.5	81.4
Output voltage (V)	2.46	3.06	3.54	3.93

matching at the input port. Second, the DC blocking capacitor is removed because the equivalent series resistance of the capacitor causes some losses. Instead of a DC blocking capacitor in the rectifying circuit, a DC blocking element is used in the experimental equipment to block DC voltage from diodes. Third, the same rectifying diode of HSMS286F is used but the polarity of the diode is inverted to obtain a positive output voltage as usual. In simulation, we optimize the dimensions of each microstrip line to make a trade-off between reflection, diode loss, high harmonic loss and the efficiency until obtaining a high efficiency. Figure 4.1(a) shows the layout circuit and the size of the designed rectifier. We use the same dielectric substrate of NPC-F260 whose parameters are listed in Table 3.4. Figure 4.1(b) shows the photograph of the fabricated rectifier and the whole size of the circuit is approximately as same as the circuit in Chapter 3.4.

Similarly, the efficiency of the rectifying circuit is confirmed and the results are shown in Fig. 4.2. Figure 4.2(a) shows the experimental results of the efficiency versus the load resistance from 100 to 400 Ω for different input powers such as 40, 60, 80, 100 mW. It is obvious that the efficiency is varying with the load resistance. As seen from the figure, the optimal load is approximately steady at 190 Ω even slight smaller as the input power is increasing. At the load of 190 Ω, the peak efficiency and output voltage of each input power level are presented in Table 4.1. In these input power ranges, the peak efficiency is changing from 80.2 % to 82.5 %, where the variation is small. In addition, For a higher input power, the efficiency curve rises early and also drops rapidly with the increase of load resistance. This is because the higher input power gets a higher output voltage which causes the voltage applied on the diode exceeding the breakdown voltage.

Figure 4.2(b) shows the simulation and experimental results of the efficiency versus the input power varying from 20 to 120 mW when the load resistance is

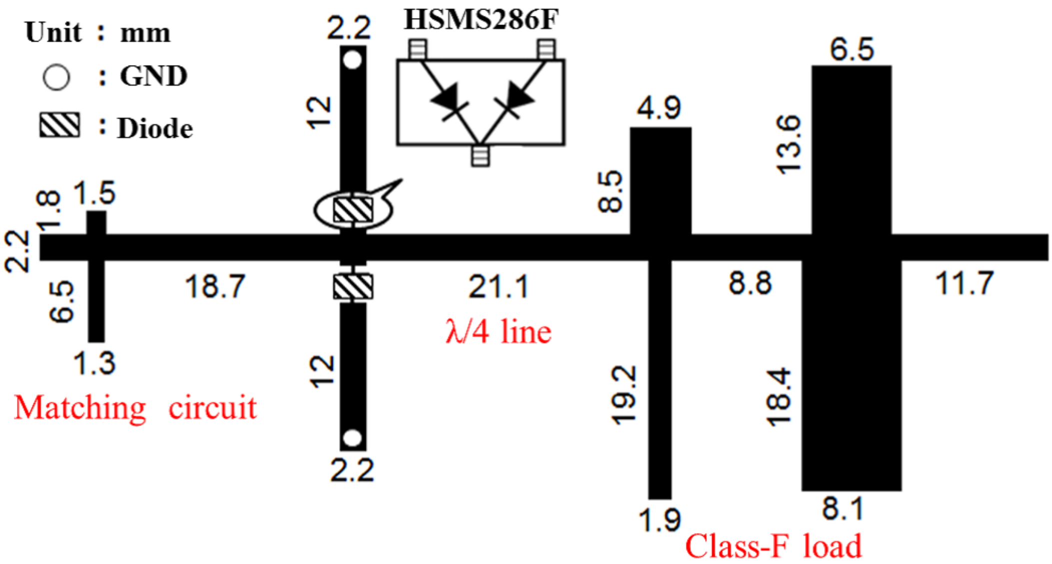

(a)

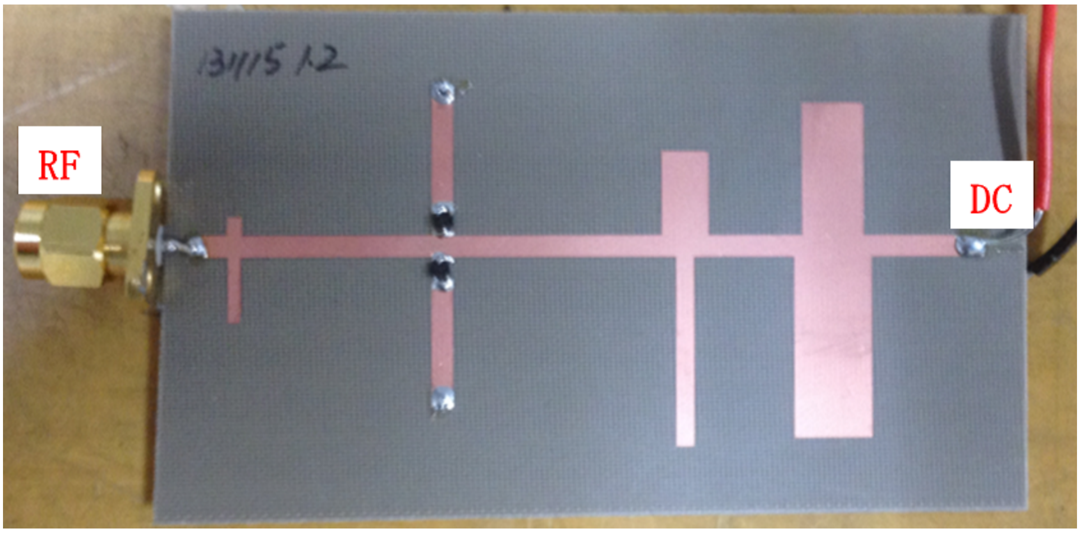

(b)

Figure 4.1: Proposed positive output voltage rectifier. (a) Structure and size. (b) Photograph.

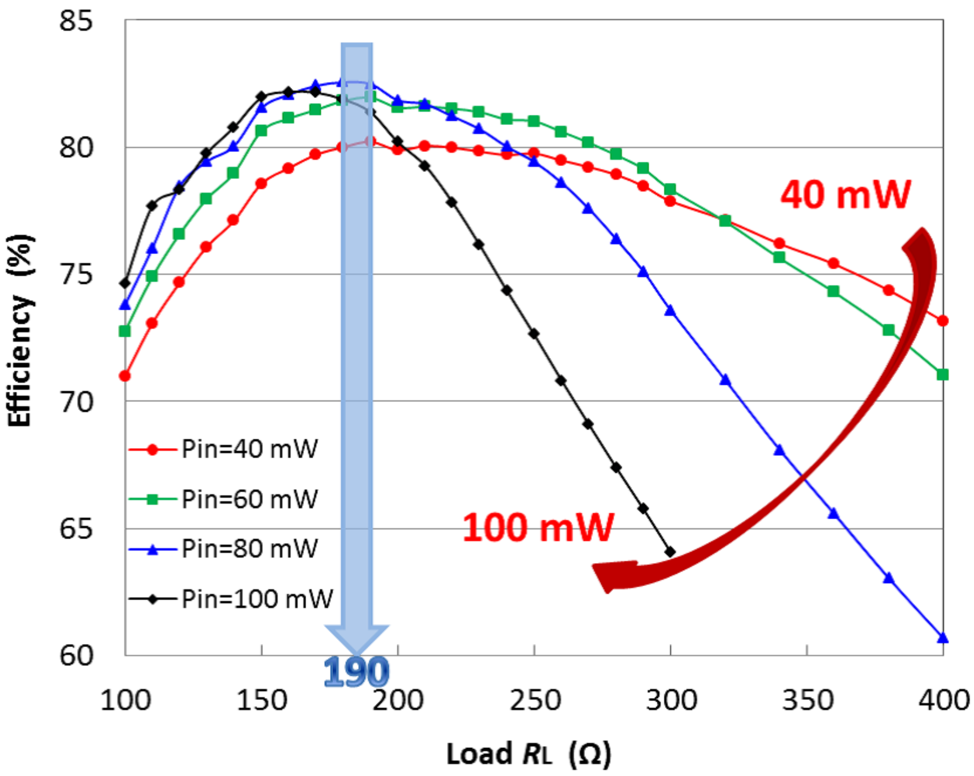

(a)

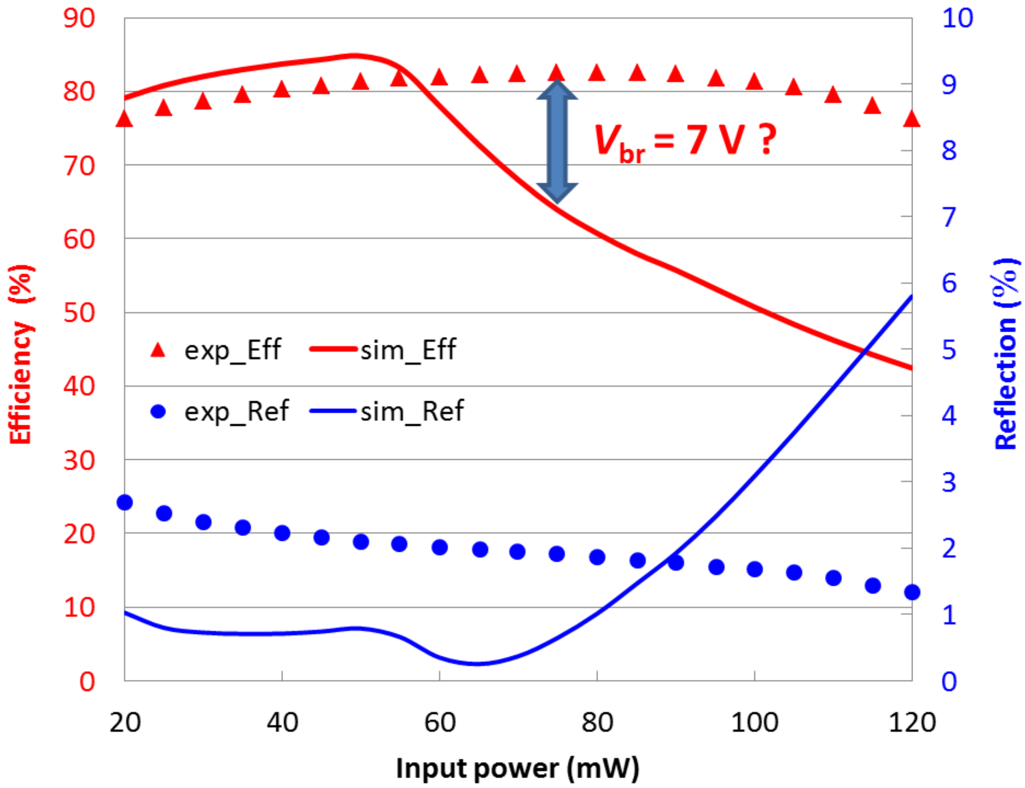

(b)

Figure 4.2: Simulation and experimental results of the high-efficiency rectifier. (a) Efficiency vs. load resistance. (b) Efficiency vs. input power.

fixed at 190 Ω. In the case of the simulation, maximum efficiency is 84.7 % at the input power of 50 mW. In the case of the experiment, maximum efficiency of 82.5 % is obtained at input power of 80 mW. The experiment results almost agree with the simulation when the input power is below 60 mW. However, they are greatly different with the simulation results when the input power is over 60 mW. There are some differences between simulation and experiment results as same as the rectifying circuit in Chapter 3.4. The diode model of di_hp_HSMS286F_20000301, which is a high frequency diode model in ADS library, is used in the simulation. This diode model uses the SPICE parameter where the breakdown voltage B_{V} is 7 V. The reverse current will reach the limitation value of I_{BV} when the reverse voltage reaches B_{V}, and it will increase when the reverse voltage exceeds the B_{V} until the reverse direction of the diode is completely conducted. In simulation, the impedance of the diode is greatly changed when the voltage applied on the diode exceeds the breakdown voltage. Hence, the reflection and diode losses increase rapidly which leads to a decrease in efficiency. However, in experiment, the real breakdown voltage of the diode is far over 7 V that the efficiency falls slowly as the diode loss is increasing even though the power exceeds the power value at peak efficiency point. There is an actual example that a diode with breakdown voltage of 9 V in SPICE parameter can bear a reverse voltage over 20 V in experiment [70].

4.3 Self-powered DCM Buck-boost Converter

4.3.1 Self-powered Non-inverting Buck-boost Converter

Compared to the externally-powered buck-boost converter in Chapter 3, this chapter proposes a self-powered non-inverting buck-boost converter as shown in Fig. 4.3. The main circuit also consists of capacitors, an inductor, an N-MOS and a diode whereas the diode and GND position are changed. Due to those changes, the converter affords a positive output voltage with a positive input voltage. The control-pulse circuit only includes two oscillators which are powered by the input voltage of the converter. Similarly, the operating waveform is as same as Fig. 3.4(b) while the current flowing direction is different. There are three state intervals when the LF oscillator is at work-state. The on-state is that the current flows through the inductor and N-MOS to the GND when the gate voltage is at high-level. The off-state is that the current flows through the inductor and diode to the load resistance when the gate voltage is at low-level. The zero-state is that no current flows through the circuit which is as same as the sleep-state of the LF oscillator.

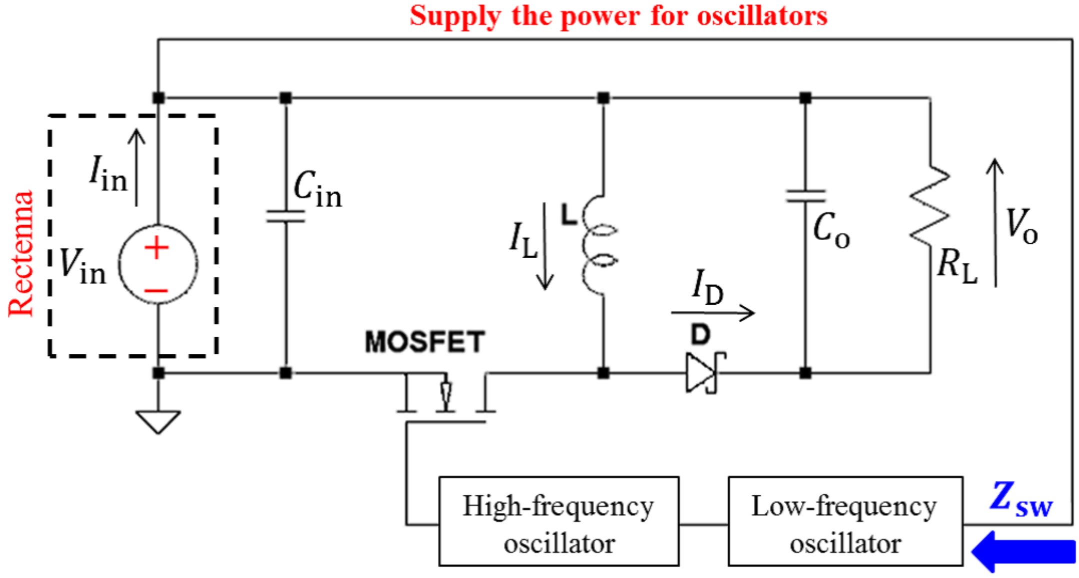

Figure 4.3: Block diagram of the self-powered non-inverting buck-boost converter.

Therefore, this buck-boost converter also operates at discontinuous conduction mode. Assuming R'_{in} to be input resistance of this converter, it is the combination of R_{in} (Eq. (3.37) mentioned in Chapter 3.3) and the impedance of the control-pulse circuit Z_{sw} in parallel as seen in Fig. 4.3. Hence, R'_{in} satisfies the following equation:

$$R'_{\text{in}} = \frac{R_{\text{in}}}{1 + \frac{R_{\text{in}}}{Z_{\text{sw}}}}. \tag{4.1}$$

To measure the impedance of the control-pulse circuit Z_{sw}, the simulation and experiment on the control-pulse circuit are conducted and Fig. 4.4 shows the schematic of the simulation circuit and the simulation waveform in LTspice. As same as the previous converter, LF and HF oscillators utilize LTC6992 and LTC6900, respectively. Figure 4.4(b) shows the operating waveforms such as LF pulse V_ι and the control pulse V_{gate} at the input voltage of 3 V. Figure 4.5 shows the measured waveforms of the control-pulse circuit at the supplied voltage of 3 V, where the high, low frequency are 10 kHz and 98 Hz, respectively. The amplitude of V_{h} and V_ι are both 3.96 V, which is almost equal to the supplied voltage of 3 V.

Figure 4.6(a) shows the simulation and experimental results of the impedance Z_{sw} which indicates that Z_{sw} is large enough to exceed 8 kΩ when the supplied voltage is over 3 V. This value also agrees with the calculated value of 8.5-14 kΩ, according to the data sheet of LTC6992 [71]. By the way, the power dissipation of the control-pulse circuit is also investigated as shown in Fig. 4.6(b), which indicates that the power consumption is small and increasing as the supplied voltage increases.

Practically, the input resistance of the buck-boost converter R'_{in} is designed close to 190 Ω which is the optimal load of the rectifying circuit in RF-DC-DC circuit. Compared with Z_{sw}, 190 Ω is small enough, which leads to following:

$$R'_{\mathrm{in}} \approx R_{\mathrm{in}}. \tag{4.2}$$

Therefore, Eq. (3.37) is also adapted to R'_{in}.

4.3.2 Parameters Selection

According to Eq. (3.37), the R_{in} is decided by the inductance, two pulse duty-on ratios and the high frequency. Furthermore, the designed rectifying circuit exhibits a peak efficiency at the load of 190 Ω. Hence, it is necessary to make R_{in} equal to 190 Ω with suitable value of four parameters. Figure 4.7 shows the schematic diagram of the HF oscillator LTC6900 and LF oscillator LTC6992. LTC6900 is a precision, low power oscillator that is easy-to-use and occupies very little PC board space. The oscillator frequency is programmed by a single external resistor (R_{SET}) as shown in Fig. 4.7(a). The three-state DIV input determines whether the master clock is divided by 1, 10 or 100 before driving the output, providing three frequency ranges spanning 1 kHz to 20 MHz. The oscillator can be easily programmed using the simple formula below [72]:

$$f_{\mathrm{h}} = \frac{10\mathrm{MHz}}{N}\frac{20\mathrm{k}\Omega}{R_{\mathrm{SET}}}, N = 1, 10, 100. \tag{4.3}$$

If we supply a 3 V voltage to pin 4 and assume R_{SET} as 200 kΩ, then, N becomes 100 and f_{h} can be calculated to be 10 kHz referring to Eq. (4.3). In

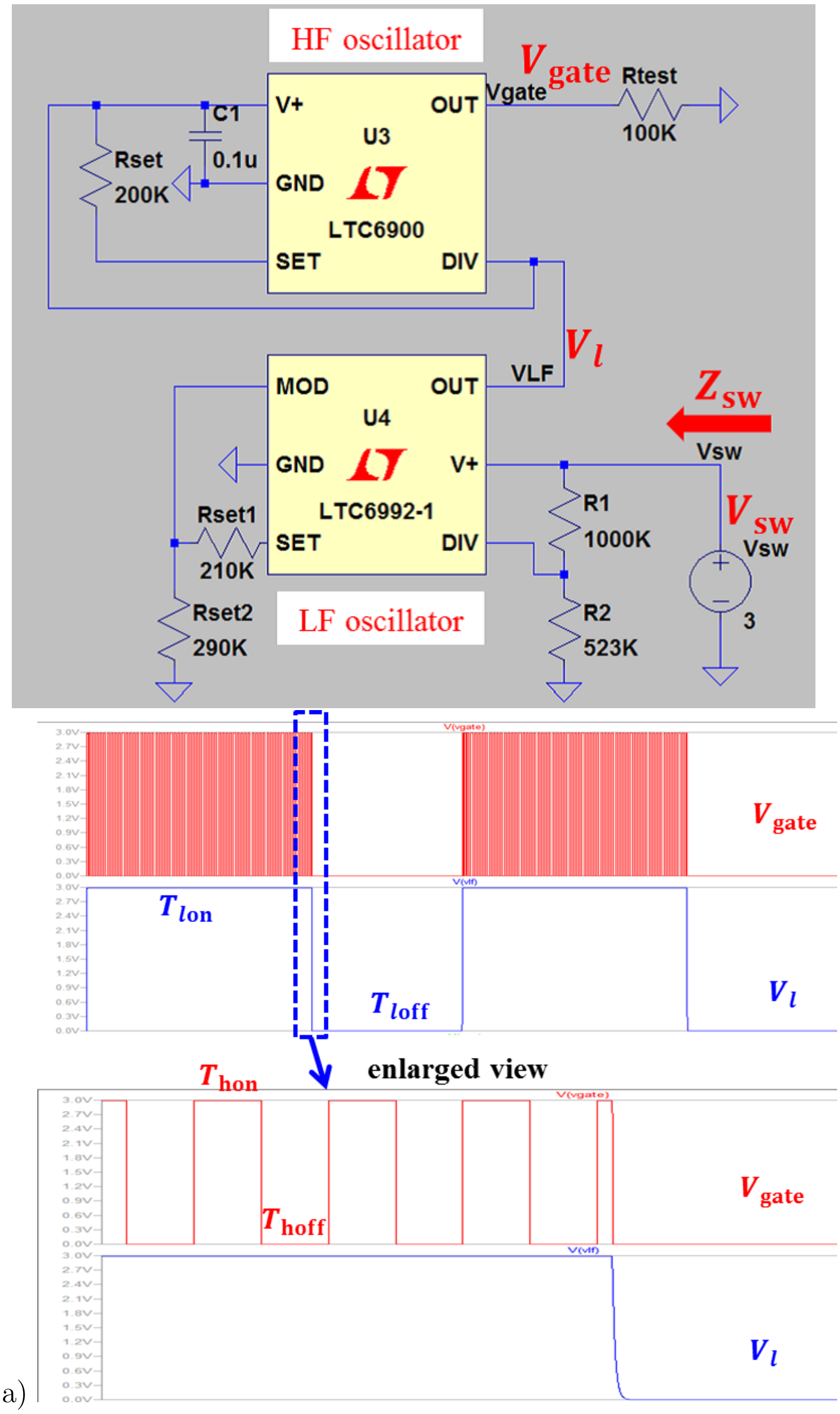

(a)

(b)

Figure 4.4: Control-pulse circuit of the buck-boost converter in simulation (LT-spice). (a) Simulation circuit: LTC6992 is the LF oscillator; LTC6900 is the HF oscillator. (b) Simulated waveforms.

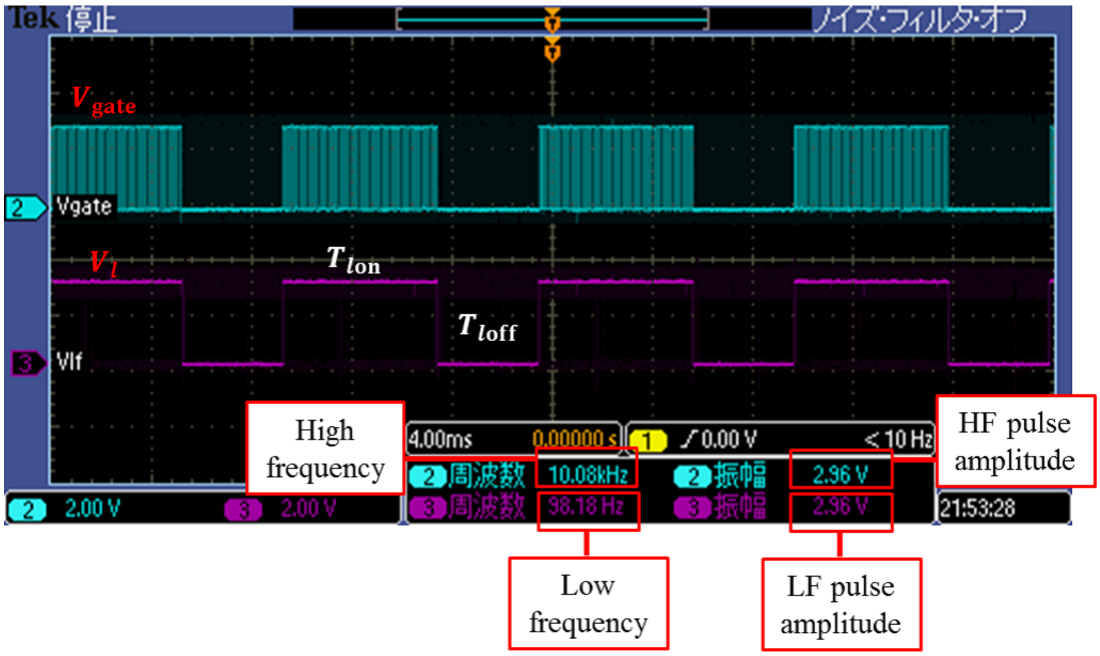

Figure 4.5: Measured waveforms of the control-pulse circuit.

addition, LTC6900 operates from a single 2.7 to 5.5 V supply and outputs a square pulse with the duty-on ratio of 0.5. Hence, D_h is 0.5.

The LF oscillator LTC6992 is a silicon oscillator with an easy-to-use analog voltage-controlled pulse width modulation (PWM) capability. The resistance, R_SET1 and R_SET2, program the LTC6992's internal master oscillator frequency. The output frequency is determined by this master oscillator and an internal frequency divider (N_DIV), programmable to eight settings from 1 to 16384. The divider ratio N_DIV that relates to R_1 and R_2 is set by a resistor divider attached to the DIV pin. With a single 2.25 to 5.5 V supply, the output frequency f_ι, exhibits wide from 3.81 Hz to 1 MHz, can be expressed as following [71]:

$$f_\iota = \frac{1\mathrm{MHz}}{N_\mathrm{DIV}} \frac{50\mathrm{k}\Omega}{R_\mathrm{SET1} + R_\mathrm{SET2}}, N_\mathrm{DIV} = 1, 4, 16....16384. \tag{4.4}$$

Here, the divider ratio N_DIV and $R_\mathrm{SET1} + R_\mathrm{SET1}$ are chosen to be 1024 and 530 kΩ, respectively. According to Eq. (4.4), f_ι becomes approximately 100 Hz. The LF f_ι does not effect R_in as seen from Eq. (3.37). Whereas the efficiency of the converter will decrease because switching loss is increased as f_ι rises. On the other hand, if f_ι is too low, gate-off time of the MOSFET gets longer which results in a big output capacitor to stabilize power supply to the load. Therefore, f_ι of 100 Hz is selected.

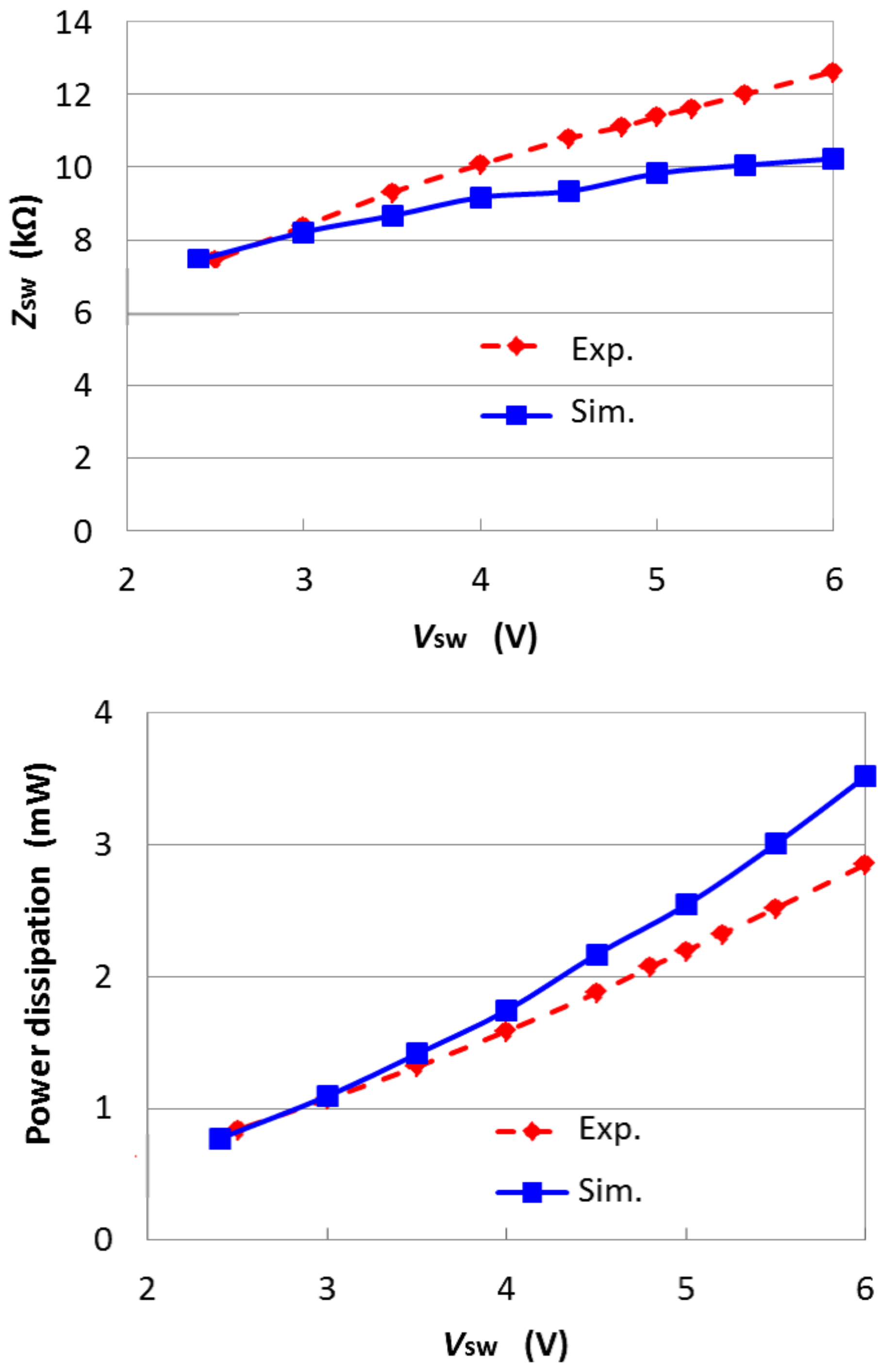

(a)

(b)

Figure 4.6: Simulation and experimental results of the control-pulse circuit. (a) Impedance Z_{sw}. (b) Power consumption.

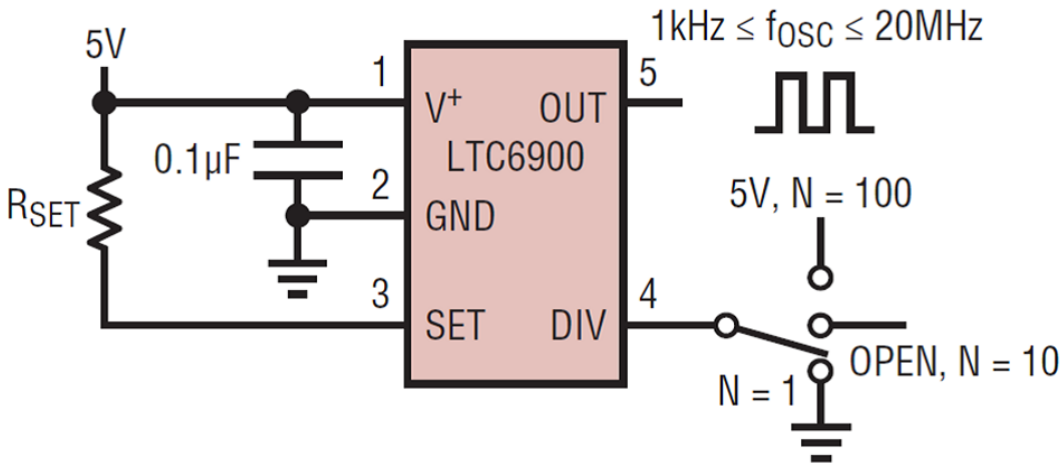

(a)

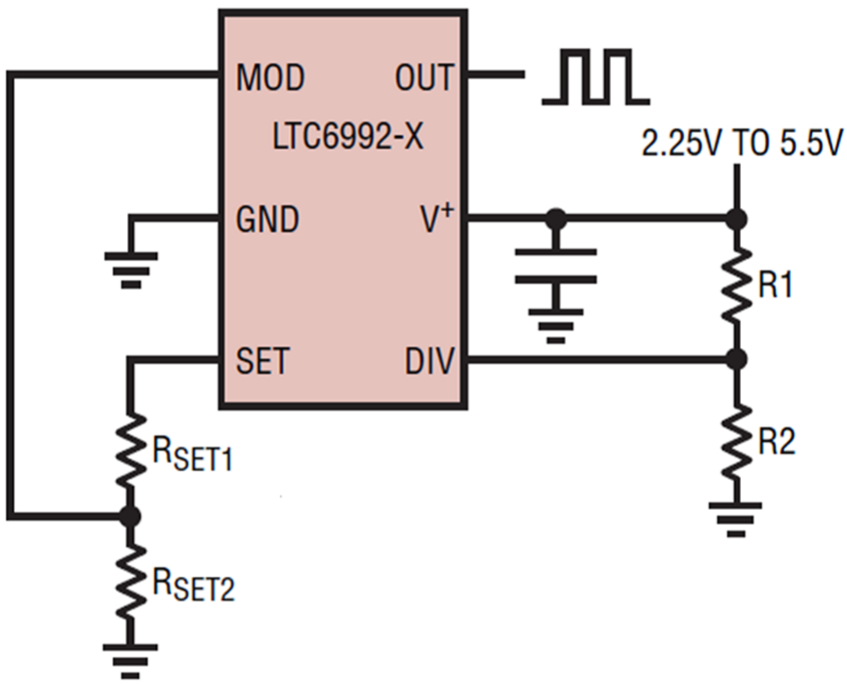

(b)

Figure 4.7: Block diagram of oscillators. (a) HF oscillator LTC6900 [72]. (b) LF oscillator LTC6992 [71].

Figure 4.7(b) shows a simple circuit for generating an arbitrary duty cycle at a fixed frequency. The LF duty-on ratio D_ι can operate wide from 0 % to 100 % and it can be expressed as below [71]:

$$D_\iota = \frac{5}{4}\frac{R_{\mathrm{SET2}}}{R_{\mathrm{SET1}} + R_{\mathrm{SET2}}} - \frac{1}{8}. \tag{4.5}$$

We use a variable resistance of 530 kΩ which is divided into two parts such as R_{SET1} and R_{SET2}. We assign R_{SET2} to be 234 kΩ, then, D_ι becomes approximately 0.427. Here, a variable resistor is used, then the proportion of R_{SET2} and R_{SET2} is adjustable to change D_ι. Consequently, the R_{in} is changeable. So far, the four parameters are decided as following: $f_{\mathrm{h}} = 10$ kHz, $D_{\mathrm{h}} = 0.5$, $D_\iota = 0.427$, and inductance L is chosen to be 1 mH. Applying these parameters into Eq. (3.37), R_{in} becomes 187 Ω, which is very close to the optimal load (190 Ω) of the rectifying circuit. It means that the input resistance of the new buck-boost converter is designed to equal the optimal load of the rectifying circuit in theoretical analysis.

With respect to the other components of the converter such as diode, N-MOS, inductor and capacitors are the same as the one outlined in Table 3.3, while the input capacitor $C_{\mathrm{in}} = 220$ μF ($V_{\mathrm{rated}} = 35$ V) is selected. The ripple of the voltage is small if the input voltage supplied from a DC power source. But the input voltage of the converter utilizes the output voltage of the rectifying circuit where the ripple is very big. In order to limit the input voltage ripple of the converter in RF-DC-DC circuit, a relatively high input capacitance is selected. Due to input voltage ripple, the efficiency varying ripple is much big in Figs. 3.14(a) and 3.15. Additionally, the MOSFET gate driver is removed in this new buck-boost converter. A MOSFET gate driver is usually applied to short switching time to minimize the switching loss for a large gate capacitance MOSFET. However, the N-MOS FDS6298 has been designed specifically to improve the overall efficiency of DC-DC converters using either synchronous or conventional switching PWM controllers. It has been optimized for low gate charge, low $R_{\mathrm{DC(on)}}$ and fast switching speed [73]. Note that the output of the HF oscillator directly drives the gate of the N-MOS in Fig. 4.3. Compared with the control-pulse circuit of the previous converter, the new one will dissipate less power because of no power consumption from gate diver.

4.3.3 Input Resistance Verification

With surface-mount device (SMD) resistors instead of axial-lead resistors, the new buck-boost converter mounts on a 3 cm × 3 cm PCB as shown in Fig. 4.8. Then, to verify the input resistance, simulate the circuit using LTspice and conduct an experiment using the measurement circuit as shown in Fig. 4.9(a) where does not need an extra DC power source. Figure 4.9(b) shows the operating waveform of V_{gate} at the input voltage of 3 V. Observe that the high frequency is 10 kHz, and the amplitude is 2.88 V which is a little smaller than the one measured in control-pulse circuit in Chapter 4.3.2. This is because the impedance of gate-source is not big enough to neglect the output impedance of the HF oscillator resulting in a drop of V_{gate}. However, this voltage drop is sufficiently small that does not affect driving the gate of the N-MOS.

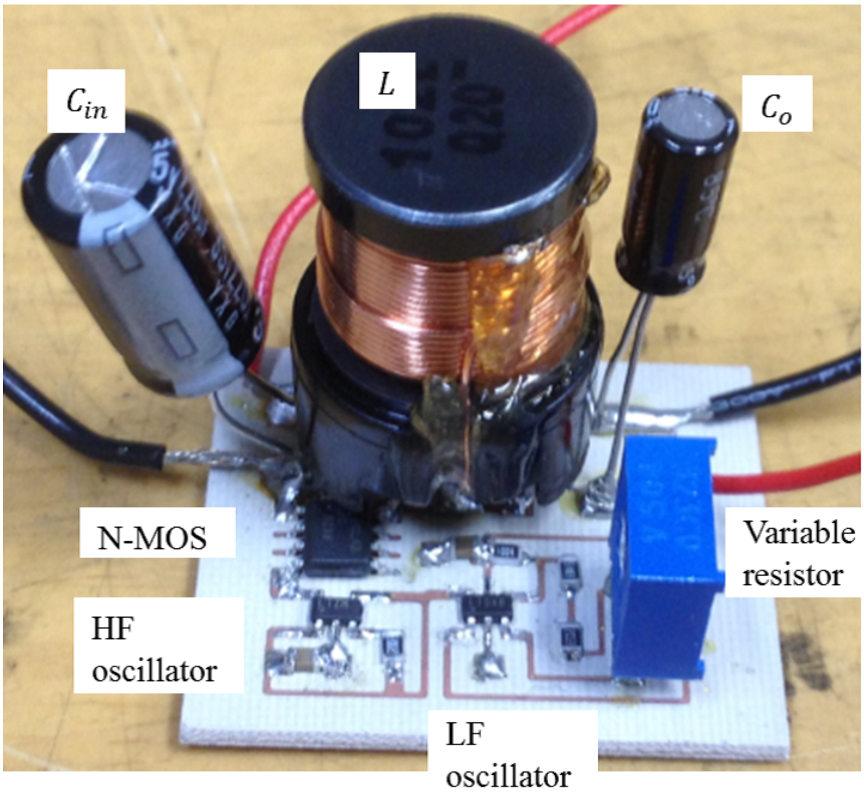

Figure 4.8: Photograph of the self-powered non-inverting buck-boost converter.

The simulation and experimental results of the self-powered buck-boost converter are shown in Fig. 4.10, where Sim_Eff and Exp_Eff represent the efficiency of the simulation and experimental, Sim_Rin and Exp_Rin represent the input resistance of the simulation and experimental, respectively. Figure 4.10(a), at a fixed input voltage of 3.5 V, shows the efficiency and the input resistance R'_{in}

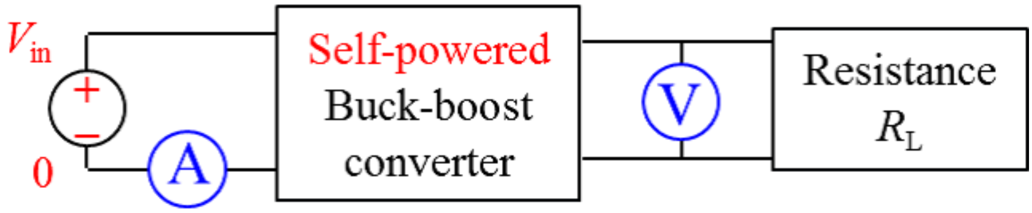

(a)

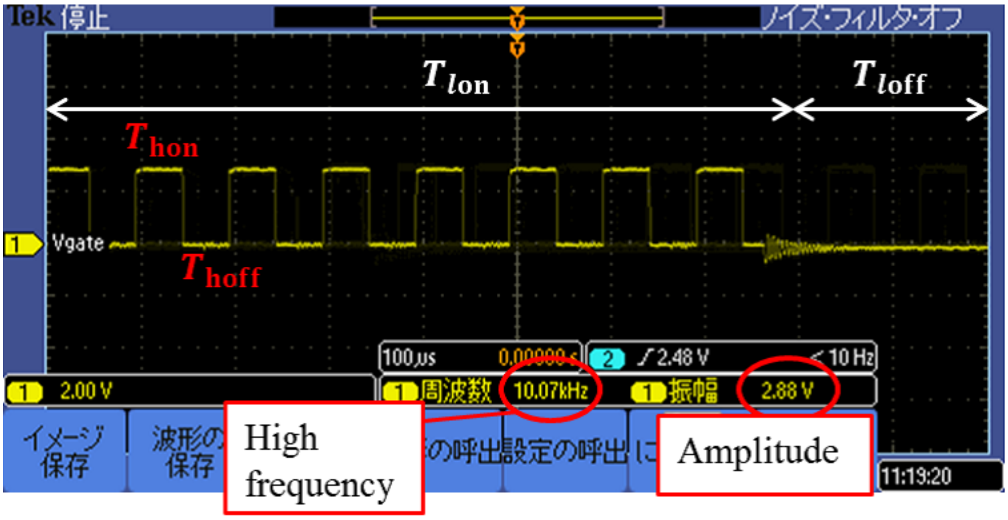

(b)

Figure 4.9: Experiment setup and measured waveform of the converter. (a) Experiment setup. (b) Measured waveform of V_{gate}.

versus the load changing from 100 Ω to 10 kΩ. Here, the input voltage of 3.5 V is selected to agree with the output voltage of the rectifying circuit when it performs maximum efficiency at the optimal load for an RF input power of 80 mW. Furthermore, the input power of the converter calculated to be 63 mW which almost agrees with the output DC power of the rectifying circuit calculated from Table 4.1. In the case of R'_{in}, the simulation and experimental results are in well agreement with the designed value of 187 Ω when the load is wide changing from 200 Ω to 10 kΩ. At the load of 100 Ω, when the load resistance is smaller than the input resistance, the buck-boost converter operates at the CCM which leads to the input current increasing. As a result, the input resistance is decreased. In the case of the efficiency, it increases at low load resistance and decreases at the high load resistance. The output current is decreasing as the load increases at a fixed input power. The major loss of the converter is dominated by the loss such as diode loss, switching loss, inductor and other resistance losses when the load resistance is below 3000 Ω. Whereas the major loss of the converter is dominated by the loss of the output capacitor that a part of the output current flows through the output capacitor as the load resistance is too big to neglect the impedance of the capacitor. The measured efficiency is over 85 % in the load range from 400 to 6000 Ω.

Similarly, Figure 4.10(b), at a fixed load resistance of 800 Ω, shows the efficiency and the input resistance R'_{in} versus the input voltage changing from 2.5 to 4.5 V. At this input voltage range, the input power is varying from 31 to 104 mW. Note that the R'_{in} is also almost steady at 190 Ω and is independent of the input voltage. As for the efficiency, the measured one is over 85 % at the whole input voltage range. In the case of the simulation, the efficiency is increasing as the input voltage increases. In the case of the experiment, the efficiency is increasing at the beginning and then slightly decreases as the input voltage increases. Because of the limitation from the operation voltage of HF and LF oscillators, the input voltage is restrained among the range of 2.5 to 6 V. The switching loss increases because of a low gate control voltage V_{gate} when the input voltage is low. The diode loss, inductor and other resistance loss will increase at a high input voltage due to current increasing. Additionally, as seen from Fig. 4.6(b), the power consumption of oscillators is increasing as the supplied voltage increases.

In addition, for both figures in Fig. 4.10, the measured R'_{in} is slightly bigger than the simulation results. The reason is that the wire resistance and the noise of real pulse wave cuts the on-state time which minimizes the input current. Furthermore, the experiment efficiency is approximately 5 point lower than the simulation one because the series resistance loss in capacitor and the wire resistance loss are not considered in simulation. In Chapter 4.3.1, we have discussed that the input resistance of this new buck-boost converter R'_{in} is the combination of the main circuit R_{in} and the control-pulse circuit Z_{sw} in parallel. In practice, using measurement circuit in Fig. 4.9(a), the input resistance, calculated from measured input voltage and input current, is the value of R'_{in} which already includes R_{in} and Z_{sw}. According to the simulation and experiment results reported above, the input resistance R'_{in} is almost equal to the value of R_{in}, which well agrees with the theory analysis. Consequently, that the new buck-boost converter has constant input resistance characteristic is verified both by simulation and experiment results.

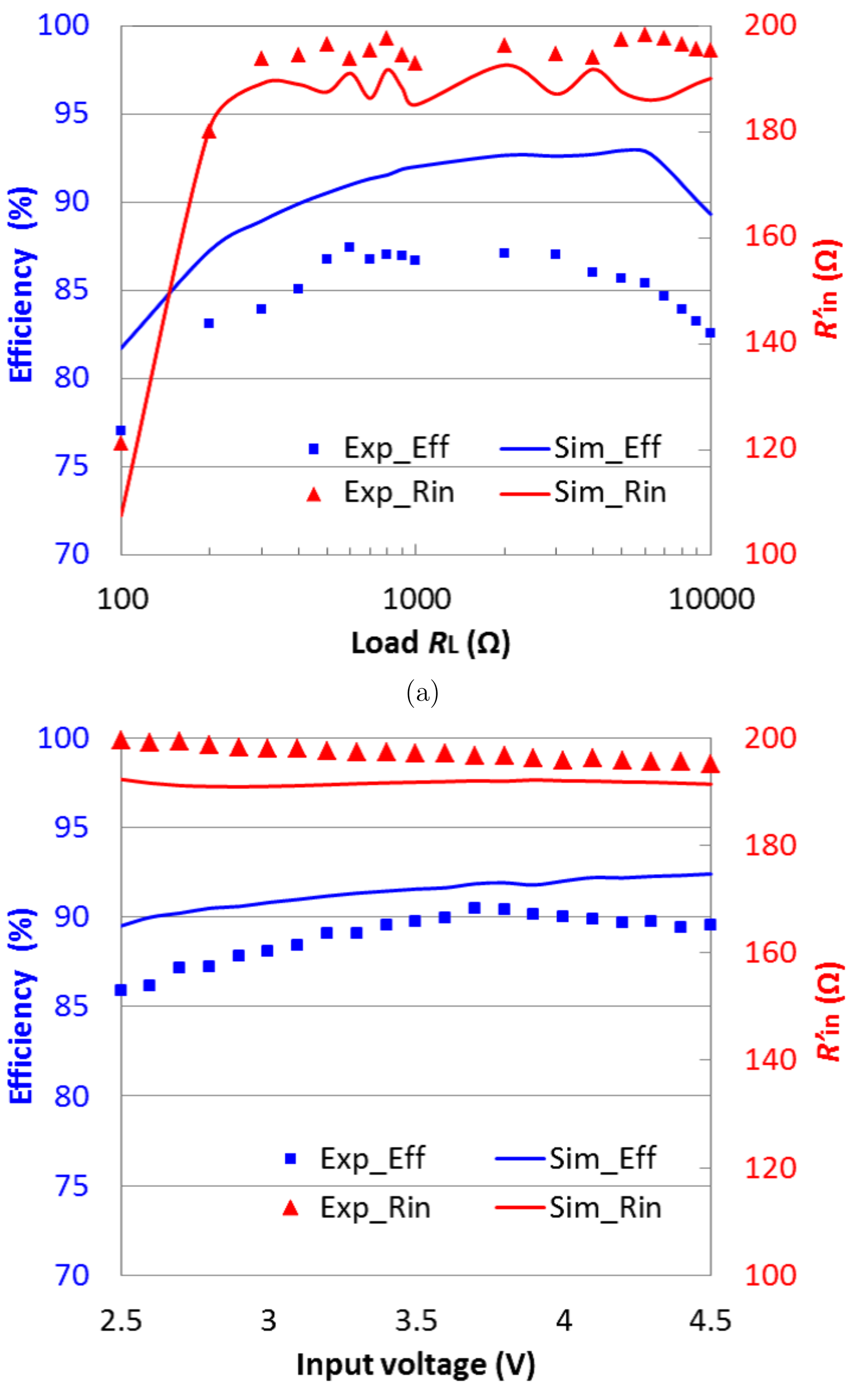

(a)

(b)

Figure 4.10: Simulation and experimental results of the self-powered buck-boost converter. (a) Efficiency and input resistance R'_{in} vs. load resistance for a fixed input voltage of 3.5 V. (b) Efficiency and input resistance R'_{in} vs. input voltage for a fixed load of 800 Ω.

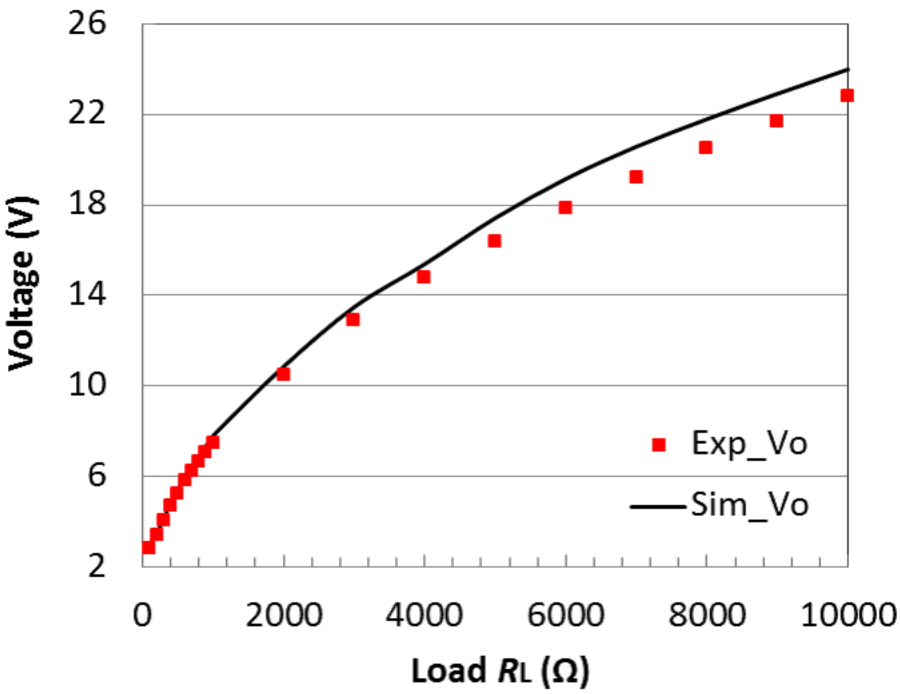

(a)

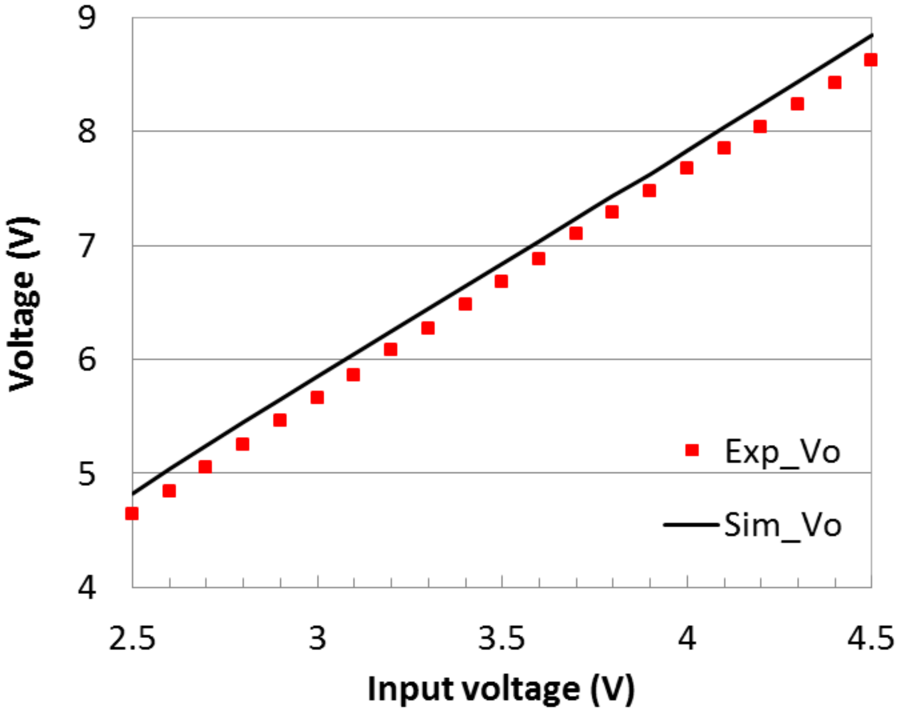

(b)

Figure 4.11: Simulation and experimental results about output voltage of the self-powered buck-boost converter. (a) Output voltage vs. load resistance for a fixed input voltage of 3.5 V. (b) Output voltage vs. input voltage for a fixed load of 800 Ω. Exp_V_o, Sim_V_o are the experiment result and simulation result, respectively.

With respect to the input/output voltage relationship of this buck-boost converter, apply the formula of $\frac{V_{\mathrm{o}}^2}{R_{\mathrm{L}}} = \frac{V_{\mathrm{in}}^2}{R_{\mathrm{in}}}$ to Eq. (3.37), it yields:

$$V_{\mathrm{o}} = \sqrt{\frac{D_{\mathrm{h}}^2 D_{\iota}}{2L f_{\mathrm{h}}} V_{\mathrm{in}}^2} \cdot R_{\mathrm{L}}^{\frac{1}{2}}, \tag{4.6}$$

$$V_{\mathrm{o}} = \sqrt{\frac{D_{\mathrm{h}}^2 D_{\iota}}{2L f_{\mathrm{h}}} R_{\mathrm{L}}} \cdot V_{\mathrm{in}}, \tag{4.7}$$

which indicates that the relationship between V_{o} and R_{L} is a parabolic curve with horizontal axis when the input voltage V_{in} is fixed. Similarly, the relationship between V_{o} and V_{in} is linear when the load resistance R_{L} is fixed. Figure 4.11 gives the simulation and experiment results about output voltage of the buck-boost converter. Figure 4.11(a) shows the output voltage versus load resistance for a fixed input voltage of 3.5 V where the output voltage is increasing as the load increases, and the shape of the curve well agrees with Eq. (4.6). Figure 4.11(b) shows the output voltage versus input voltage for a fixed load resistance of 800 Ω. Where the output voltage is linearly increasing as the input voltage increases, and the shape of the curve well agrees with Eq. (4.7). For both figures, the experiment results are in good agreement with the simulations. It is clear that the output voltage is boosted by the buck-boost converter, which indicates that this resistance conversion buck-boost converter only plays a booster role here.

4.4 Experiment on Self-powered RF-DC-DC Circuit

Similarly, summarize the efficiency-load relation of the rectifier and buck-boost converter as mentioned above in Table 4.2. As expected, the overall efficiency of the RF-DC-DC circuit should be steady and over 67 % in the load range of 200 Ω to 10 kΩ. Then,we conduct an experiment on the self-powered RF-DC-DC circuit using the experiment architecture in Fig. 4.12(a) with 2.45 GHz microwave power. Here, we can obtain a DC power at the load port with the incident microwave power where an extra DC power source is needless. The measured items are listed in Table 4.3. Using these measured items, the overall efficiency, the efficiency of

Table 4.2: Efficiency and load relationships of the high-efficiency rectifier and self-powered buck-boost converter in experimental results.

	R_{L}	R_{in}	Efficiency
High-efficiency rectifier	190 Ω		82.5 %
Self-powered buck-boost converter	200 Ω-10 kΩ	almost 190 Ω	over 82 %
Self-powered RF-DC-DC circuit	200 Ω-10 kΩ		predicted value 67 %

Table 4.3: Measured items of the self-powered RF-DC-DC circuit.

Item	Represent
Power sensor A	Input RF power of RF-DC-DC circuit
Power sensor B	Reflection RF power
Voltmeter A	Output voltage of rectifier V_{rec}
Voltmeter B	Output voltage of RF-DC-DC circuit I_{o}
Ammeter	Input current of buck-boost converter I_{in}

the RF-DC rectifier alone, the efficiency of the buck-boost converter alone, the tracking efficiency and the input resistance of the converter can be calculated.

Firstly, several efficiency curves are shown in Fig. 4.13 and each efficiency curve is explained by the block diagram in Fig. 4.14. The red RF-DC-DC curve is the overall efficiency of the RF-DC-DC circuit. The blue RF-DC (with converter) curve is the efficiency of the rectifier when it is connected to the converter. In contrast, the black RF-DC (without converter) curve is the efficiency of a general rectifier. The green DC-DC curve is the efficiency of the buck-boost converter when it is utilized in the RF-DC-DC circuit. With a fixed input RF power of 80 mW, the variation of overall efficiency of the RF-DC-DC circuit over a load range of 100 Ω to 10 kΩ is shown in Fig. 4.13(a). It is obvious that the efficiency of the rectifier (with converter) is almost constant over 80 % in that wide load range. Compared with the general rectifier (black), it seems that the rectifier

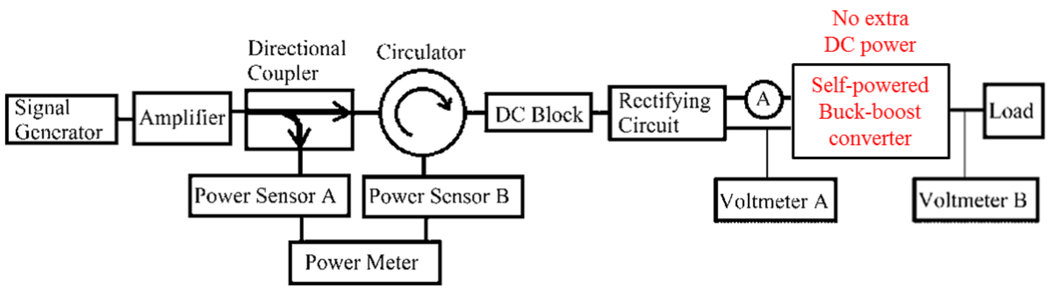

(a)

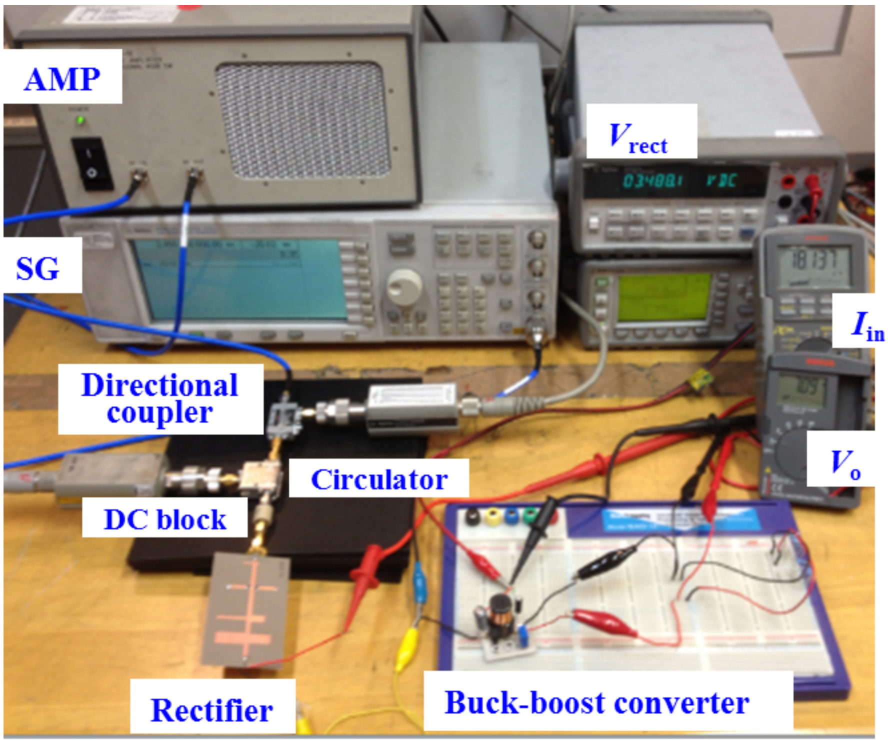

(b)

Figure 4.12: Experiment setup for measuring the efficiency of the self-powered RF-DC-DC circuit. (a) Experiment setup. (b) Experiment photograph.

(with converter) always operates at the peak efficiency despite the load resistance. The efficiency of the buck-boost converter (blue) is over 82 % in that wide load range. Consequently, the overall efficiency, which is the multiplication of previous two efficiencies, is almost constant over 66 % in this ultra-wide load range of 200 Ω to 10 kΩ (a ratio of 1:50). Specially, the overall efficiency is over 70 % in the load range of 400 to 4000 Ω (a ratio of 1:10). The overall efficiency is low at the load of 100 Ω because the input resistance of the converter is mismatching with the optimal load of the rectifier which reduces the rectifying efficiency. As the efficiency of the converter decreases at high load resistance as mentioned in Chapter 4.3.3, the overall efficiency is also slightly decreasing as the load resistance increases.

With a fixed load resistance of 800 Ω, Figure 4.13(b) shows the overall efficiency versus the input power changing from 20 to 120 mW. Note that the overall efficiency exceeds 66 % in the input power range of 40 to 120 mW. The overall efficiency is low when the input power is below 40 mW. Referring to Chapter 4.3.3, the output voltage of the rectifier is smaller than 2.5 V when the input power is lower than 40 mW at the load of 190 Ω. However, a necessary minimum operation voltage for control-pulse oscillators is also 2.5 V. Therefore, the buck-boost converter can not work well when the input power of the RF-DC-DC circuit is below 40 mW, which leads to a decrease in overall efficiency. When the input power exceeds 100 mW, the optimal load of the rectifier becomes lower than the designed value of R'_{in}. As a result, the impedance mismatching occurs between the rectifier and converter. Then the overall efficiency is decreasing as the efficiency of the rectifier decreases. In practice, if the input power is much higher, the output voltage of the rectifier probably reaches the overvoltage (6 V) of control-pulse oscillators which would decrease the efficiency of the converter even break the converter. However, the output DC voltage (V_{DC}) of the rectifier is restrained by the breakdown voltage (B_{V}) of the HF diode which satisfies the equation: $V_{\mathrm{DC}} \approx B_{\mathrm{V}}/2$. As the breakdown voltage of the HF diode is 7 V, the rectifying diode would breakdown first before the output voltage reaching 6 V. It means that the rectifying diode of the rectifier plays another important role in overvoltage protection for control-pulse circuits here. Thus, considering the efficiency and overvoltage, this RF-DC-DC circuit is suggested to be used in the power range of 30 to 140 mW.

The tracking efficiency η_{track}, as defined in Eq. (3.38), is also investigated.

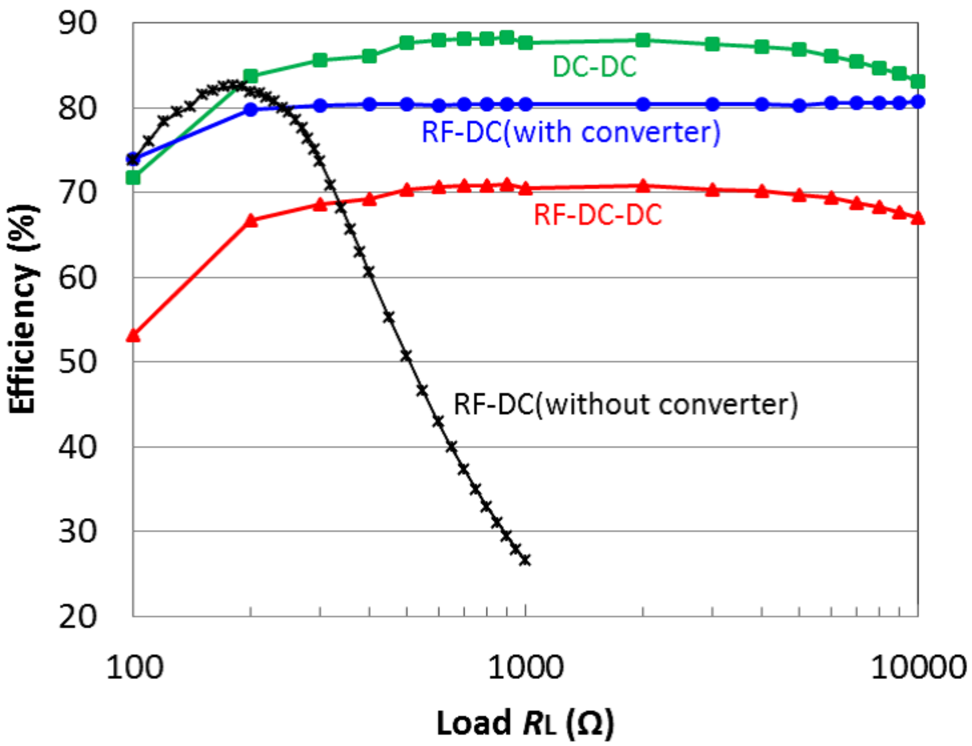

(a)

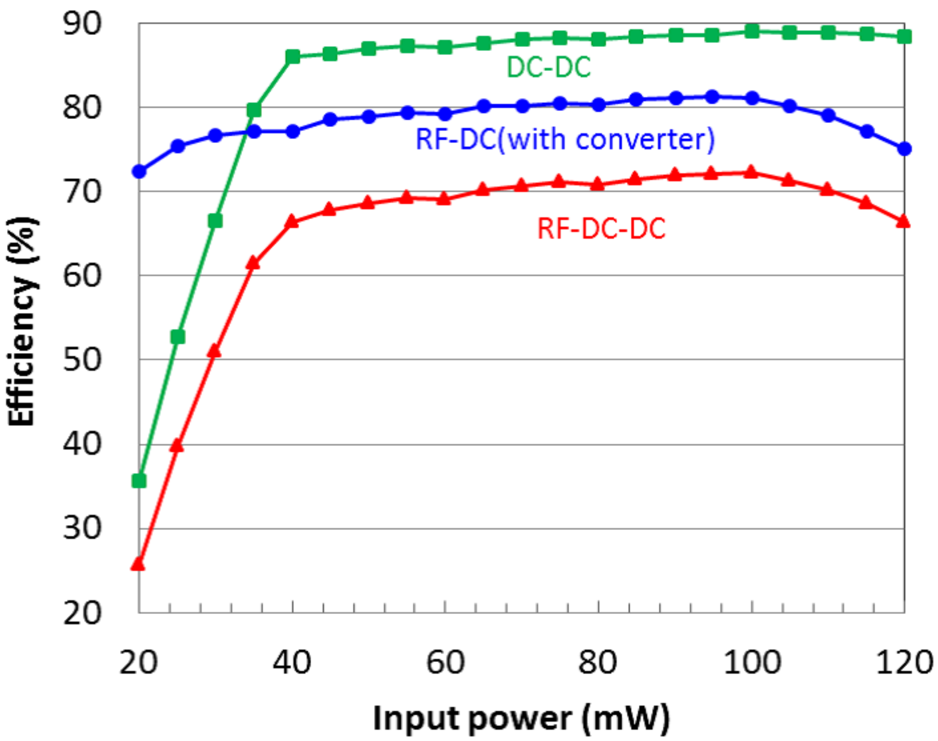

(b)

Figure 4.13: Measured overall efficiency of the self-powered RF-DC-DC circuit. (a) Efficiency comparison of the RF-DC-DC circuit and the general rectifier for a fixed input power of 80 mW. (b) Overall efficiency vs. input power for a fixed load of 800 Ω.

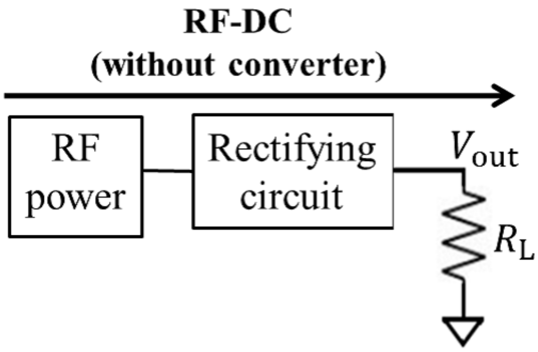

(a)

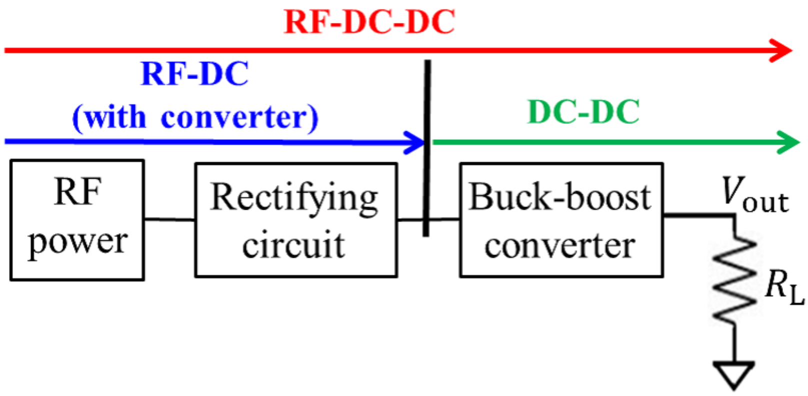

(b)

Figure 4.14: Illustration for the efficiency of each part in RF-DC-DC circuit. (a) General rectifier. (b) RF-DC-DC circuit.

Figure 4.15(a) shows the tracking efficiency and R'_{in} versus load resistance at a fixed input power of 80 mW. Note that the variation tendency of the tracking efficiency is in accord with the input resistance because the former heavily depends on the latter. Track_Eff1 and Track_Eff2 are the tracking efficiency of the externally-powered RF-DC-DC circuit (in Chapter 3.5) and self-powered RF-DC-DC circuit, respectively. It is obvious that Track_Eff2 is constant as high as 97 % in the load range of 200 Ω to 10 kΩ, and is almost 5 percentage points bigger than Track_Eff1 because the impedance matching of the self-powered RF-DC-DC circuit is completely implemented. The R'_{in} is almost constant at the designed value of 190 Ω when the load is over 300 Ω. While it is much smaller than 190 Ω as the load is below 300 Ω and the same phenomenon can be seen in the buck-boost converter from Fig. 4.10(a), where the reason has been explained. Therefore, the overall efficiency is low when the load is below 300 Ω as shown in Fig. 4.13(a).

On the other hand, Figure 4.15(b) shows the tracking efficiency η_{track} and input resistance R'_{in} versus input power at a fixed load resistance of 800 Ω. Similarly, the R'_{in} is almost constant at 190 Ω when the input power is over 40 mW whereas it strictly deviates from 190 Ω when the input power is below 40 mW. In practice, if the input microwave power is too low to obtain the output voltage of 2.5 V in the rectifier, the control-pulse oscillators could not be driven, and the gate voltage of the MOSFET becomes zero which causes the switching to be off. In this case, the input resistance of the buck-boost converter seems to be infinite since the switching is open. Then the output voltage of the rectifier is increasing up to 2.5 V so that it is able to drive the oscillators which leads to switching on. In this case, the input resistance of the buck-boost converter decreases and move to agree with the designed value. After that, the output voltage begins to decrease again until it is too low to drive oscillators, and the operation repeats like above again and again. At this operation condition, the efficiency of the converter is very low. Therefore, R'_{in} is bigger than 190 Ω when the input power is below 40 mW, which is the reason of that the overall efficiency is low at low input power level as shown in Fig. 4.13(b). As for tracking efficiency, Track_Eff2 is also higher than Track_Eff1 and keeps constant over 95 % in the power range of 20 to 100 mW. While it suddenly falls because the optimal load is much smaller than 190 Ω at the input power of 120 mW. This is also the reason of that the overall efficiency is decreased at 120 mW in Fig. 4.13(b).

Figure 4.16 shows the reflection comparison between the rectifier (without converter) and the RF-DC-DC circuit. The reflection of the rectifier heavily depends on the impedance of the rectifying diode which is affected by the output load resistance or the output voltage. In fact, the reflection of the RF-DC-DC circuit is as same as the rectifier, which is also directly related to the output voltage of the rectifier part and the input resistance of the converter. As seen from Fig. 4.16(a), the reflection of the RF-DC-DC circuit is almost constant and is much lower than that of the rectifier (without converter) because the R'_{in} is almost constant at this load range. In Fig. 4.16(b), the reflection of the RF-DC-DC circuit is much higher at low power level because of impedance mismatching as mentioned previously. Additionally, the reflection of the RF-DC-DC circuit is slightly higher (approximate 0.5 percentage point) than that of the rectifier (without converter) because of subtle differences between the actual R'_{in} and 190 Ω.

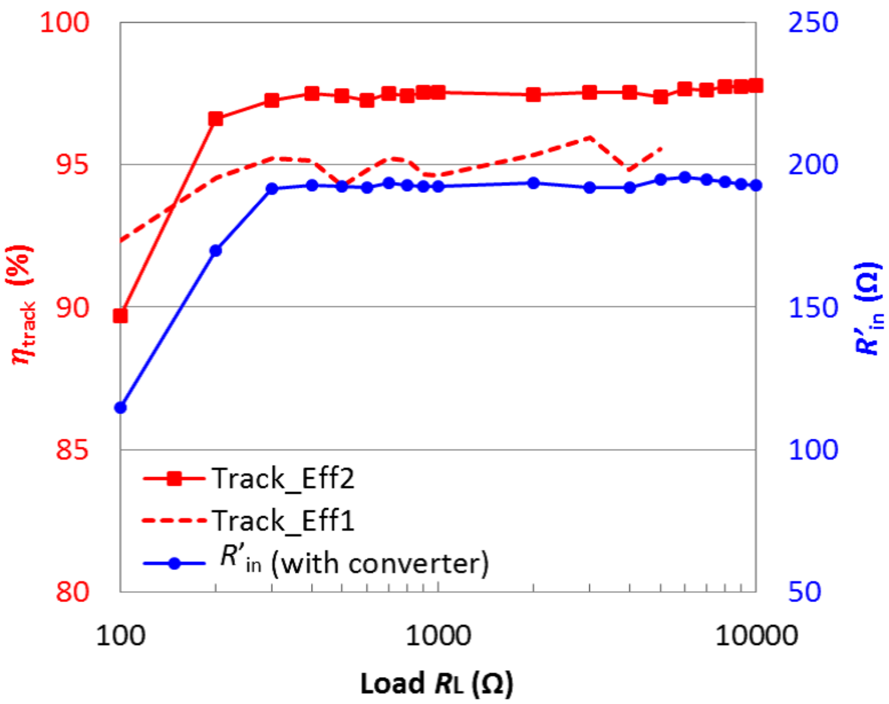

(a)

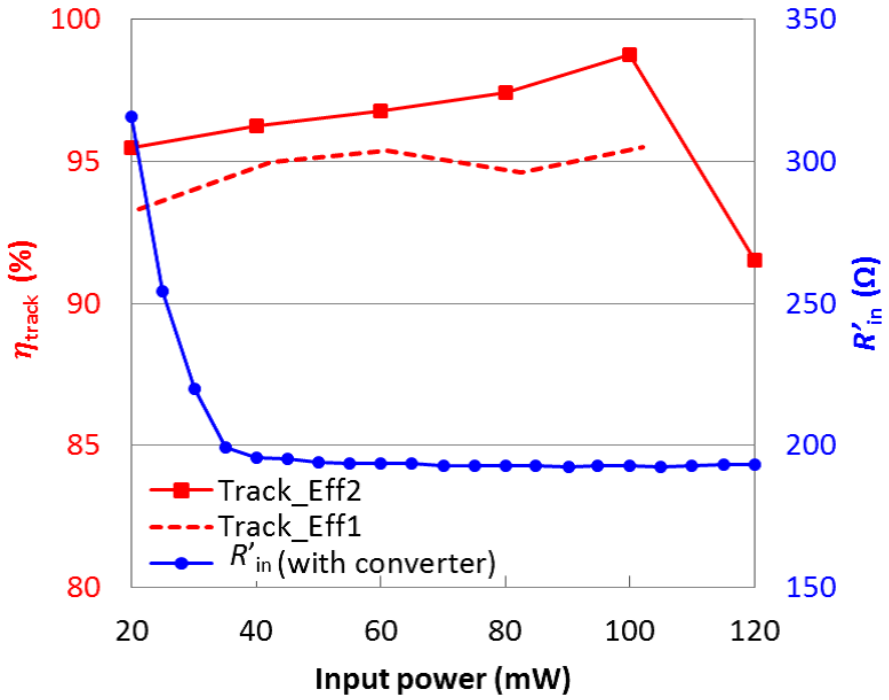

(b)

Figure 4.15: η_{track} comparison and R'_{in}. (a) η_{track} and R'_{in} vs. load resistance for a fixed input power of 80 mW. (b) η_{track} and R'_{in} vs. input power for a fixed load of 800 Ω. Track_Eff1 and Track_Eff2 are the tracking efficiency of the externally-powered and self-powered RF-DC-DC circuit, respectively.

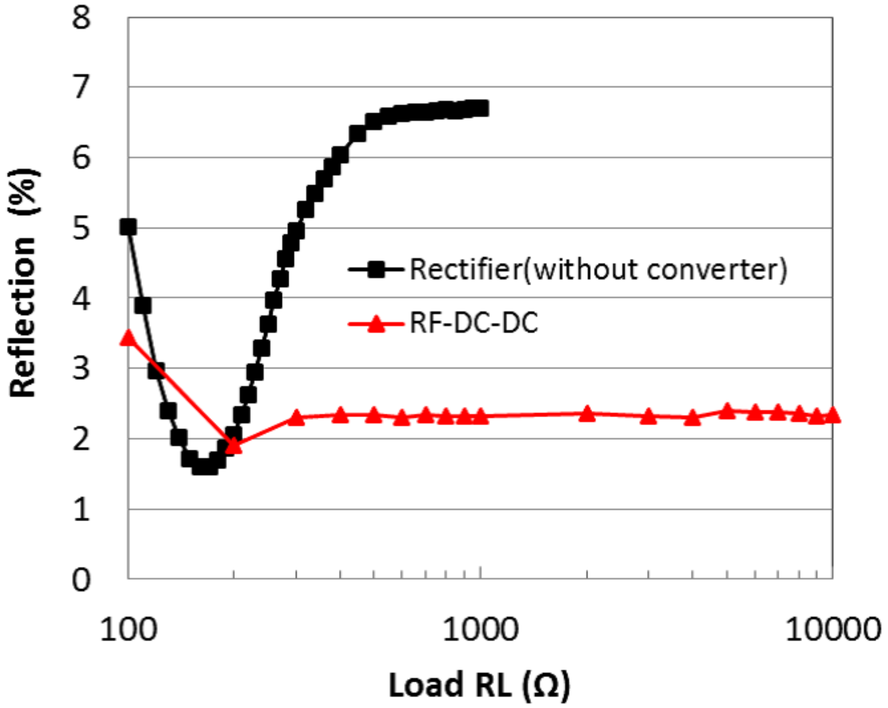

(a)

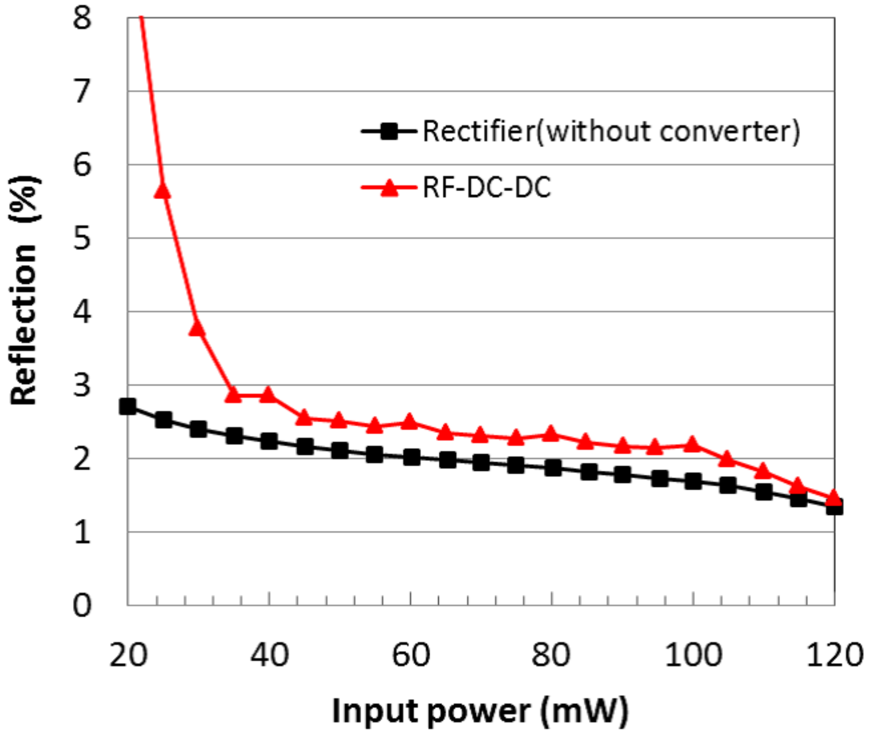

(b)

Figure 4.16: Reflection comparison between the general rectifier and the RF-DC-DC circuit. (a) Reflection vs. load resistance for a fixed input power of 80 mW. (b) Reflection vs. input power for a fixed load of 800 Ω.

Next, Figure 4.17 shows the output voltage of each single part of the RF-DC-DC circuit and rectifier (without converter). In Fig. 4.17(a), as expected, the V_{out} of the rectifier (with converter) is almost constant at 3.5 V because the variation of R'_{in} is sufficiently small. Observe that the V_{out} of the RF-DC-DC circuit, a boosted voltage, which well agrees with the curve in Fig. 4.11(a). In contrast, the V_{out} of the rectifier (without converter) is also given by the black point curve. In Fig. 4.17(b), the V_{out} of the rectifier (with converter) is increasing as the input power increases where the variation is as same as the one without converter, and the V_{out} of the RF-DC-DC circuit is increasing with the input power. Compared with the voltage conversion of the buck-boost converter (without rectifier), Figure 4.18 gives the output-input voltage curve of the buck-boost converter in the RF-DC-DC circuit. It is obvious that the two curves are in good agreement when the input voltage is higher than 2.5 V. The input voltage is boosted just a little by the converter because of a low efficiency at low input voltage level.

4.5 Summary

This chapter, firstly, a high-efficiency rectifying circuit used for 2.45 GHz microwave is designed and measured. Compared with the circuit designed in Chapter 3.4, this rectifier also uses a class-F load part while it reverses the polarity of the HF diode to obtain a positive output voltage and removes the DC block capacitor in the structure. The measured peak efficiency is 82.5 % at the optimal load of 190 Ω for an input microwave power of 80 mW.

Secondly, we design a self-powered non-inverting DCM buck-boost converter. Compared with the buck-boost converter designed in Chapter 3.3, there are mainly six improvements as follows. (1) It can obtain a positive output voltage with a positive input voltage just changing the position of MOSFET and diode. (2) An additional DC power source is needless because the control-pulse circuit is powered by the input voltage of the converter. (3) The input resistance of the buck-boost converter R'_{in} is designed to be equal to the optimal load of the rectifier (190 Ω). (4) The MOSFET gate driver is removed which attributes to a low power consumption of the control-pulse circuit. (5) A relatively big input capacitor (100 μF) is used to restrain the ripple of output voltage from the rectifier. (6) A variable resistance is used which makes the low frequency duty-on ratio be manual adjustable, then the input resistance R'_{in} is adjustable. Based on the simulation and experimental

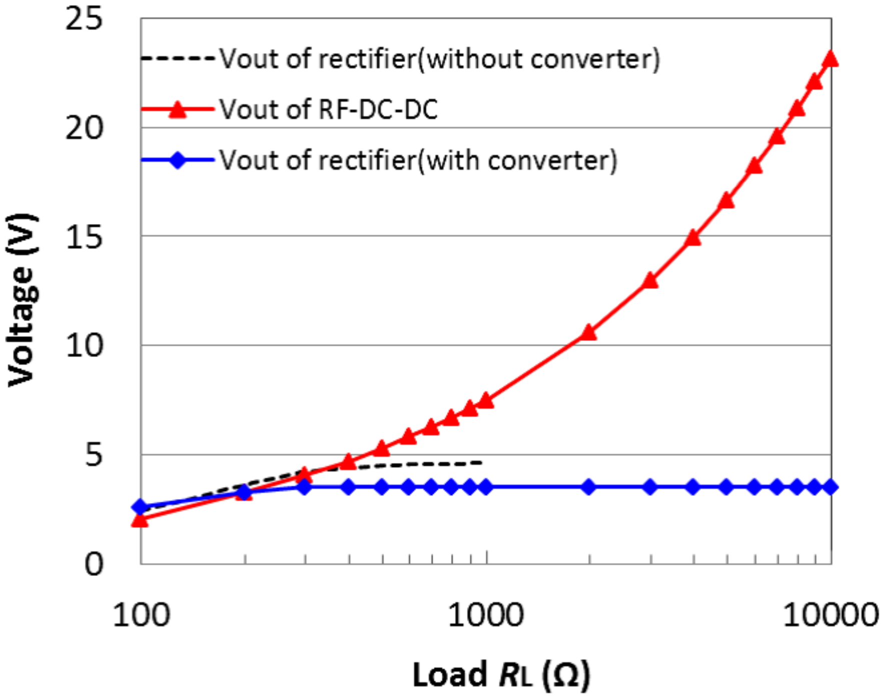

(a)

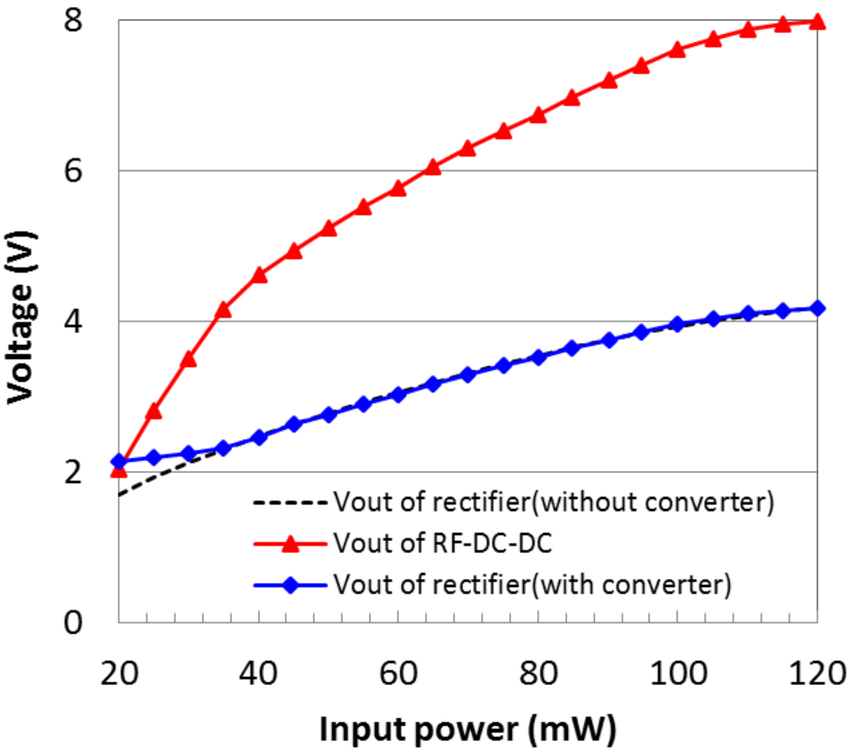

(b)

Figure 4.17: Output voltage of each part of the RF-DC-DC circuit. (a) Output voltage vs. load resistance for a fixed input power of 80 mW. (b) Output voltage vs. input power for a fixed load of 800 Ω.

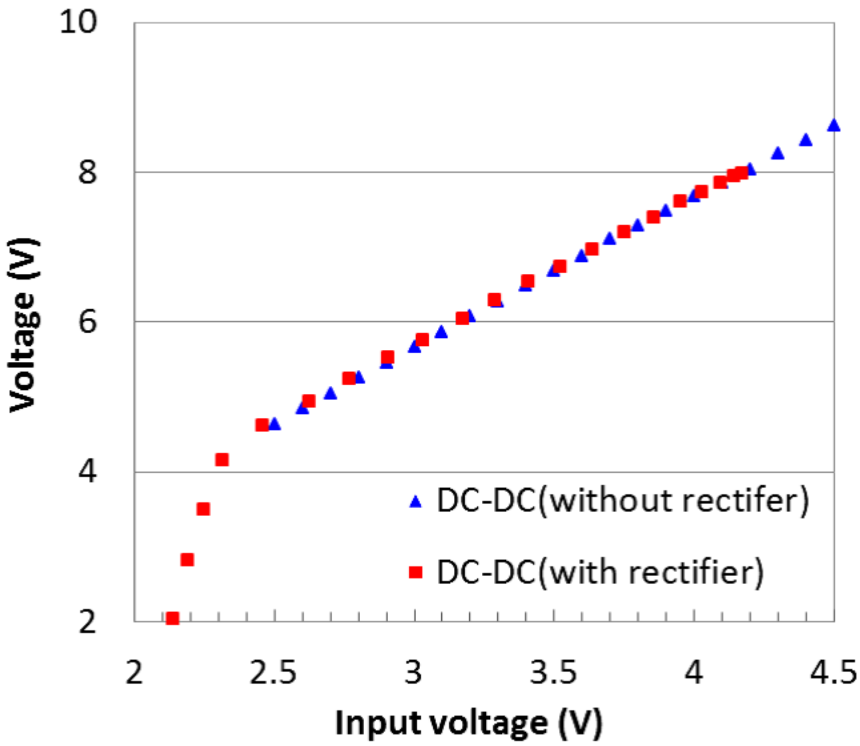

Figure 4.18: Input/output voltage relationships of the buck-boost converter in RF-DC-DC circuit.

results, the input resistance of the converter is almost constant at 190 Ω despite the changes of load resistances and input powers, which is in accordance with the theoretical analysis. Moreover, the measured efficiency of the converter exceeds 83 % for a wide load range of 200 Ω to 10 kΩ, and the input voltage is boosted by the buck-booster converter.

Finally, we conduct an experiment on RF-DC-DC circuit using the self-powered buck-boost converter and the rectifier. The conversion efficiency of the rectifier is approximately steady at 80 %, despite the load resistance varying from 200 Ω to 10 kΩ for an input microwave power of 80 mW. Compared with the peak efficiency of 82.5 % at the optimal load, the maximum power tracking efficiency is over 97 %. Furthermore, the overall efficiency of the RF-DC-DC circuit is constant over 66 % in an ultra-wide load range of 200 Ω to 10 kΩ (a ratio of 1:50). On the other hand, with a fixed load of 800 Ω, the overall efficiency of the RF-DC-DC circuit is also constant over 66 % for the input power of 40 to 120 mW. According to the experimental results, the proposed self-powered RF-DC-DC circuit exhibits a high efficiency in an ultra-wide load range.

A comparison between Figs. 3.14 and 4.13 shows that the varying ripple of the overall efficiency is small in the self-powered RF-DC-DC circuit. Similarly, the varying ripple of the input resistance is also small in the self-powered RF-DC-DC circuit by comparison with Figs. 3.15 and 4.15. Make a comparison between externally-powered RF-DC-DC circuit and self-powered RF-DC-DC circuit in Table 4.4 where the superiors of the self-powered RF-DC-DC circuit are obvious.

In this Chapter, a self-powered RF-DC-DC circuit as an improved rectifying circuit, which exhibits a high efficiency in an ultra-wide load range, is developed. However, there are still some problems to be solved such as: (1) As the supplied voltage limitation from control-pulse circuit, the input RF power of the RF-DC-DC circuit is limited in the power range of 30 to 140 mW. It is expected to be used for a much more wide power range. (2) The efficiency of the buck-boost converter is expected to be much more high (such as 95 %) to reduce the loss caused by the converter, which would make the overall efficiency of the RF-DC-DC circuit close to the peak efficiency of the general rectifying circuit as much as possible. (3) The RF-DC-DC circuit is expected to be adapted to much small load resistance such as the range of 100 mΩ to 10 Ω. (4) This resistance conversion buck-boost converter is also expected to be valuable for other WPT system such as inductive coupling and magnetic or electromagnetic resonant coupling.

Table 4.4: Comparison between externally-powered and self-powered RF-DC-DC circuits. Z_{opt} is the optimal load of the rectifier. P_{RF} is the input RF power.

Item	externally-powered RF-DC-DC circuit	self-powered RF-DC-DC circuit
Power supply	require an extra DC power	supplied by the input power
$\eta_{\max(\text{rf}-\text{dc})}$	79.2 %	82.5 %
Z_{opt} and R_{in}	$R_{\text{in}} = 133\ \Omega$; $Z_{\text{opt}} = 160\ \Omega$.	$R'_{\text{in}} \approx Z_{\text{opt}} = 190\ \Omega$
R_{in}	unadjustable	adjustable
V_{in} ripple	large	small
η_{track} vs. load	> 94 % in 200-5000 Ω (1:25)	> 97 % in 200-10000 Ω (1:50)
η_{track} vs. P_{RF}	> 93 % in 20-100 mW (1:5)	> 95 % in 20-100 mW (1:5)
η_{all} vs. load	> 60 % in 100-5000 Ω (1:50)	> 66 % in 200-10000 Ω (1:50)
η_{all} vs. P_{RF}	> 61 % in 40-100 mW (1:2.5)	> 66 % in 40-120 mW (1:3)

Chapter 5

Experiment on Driving a DC Motor Using MPT

5.1 Introduction

In this chapter, the RF-DC-DC circuit proposed previous is used to drive a dynamic load resistance device. We conduct several experiments on driving a low-power DC motor using microwave power transmission. As the self-powered buck-boost converter in Chapter 4 exhibits a low efficiency at low input power level, we design a relatively high output voltage rectifier and an improved buck-boost converter whose control-pulse circuit is supplied by the output voltage of the converter. By comparison, we also design a relatively low output voltage rectifier and an improved buck-boost converter whose control-pulse circuit is supplied by the input voltage of the converter. This chapter proposes a compact power-receiving device which consists of a rectenna array and the improved self-powered buck-boost converter. With the combination of two different rectenna arrays and two different converters, there are four different power-receiving devices. Finally, using those power-receiving devices, some MPT experiments on driving the DC motor using continuous-wave (CW) and pulsed-wave are conducted.

5.2 Background

The Mars Exploration Rover mission is part of NASA's Mars Exploration Program, a long-term effort of robotic exploration of the red planet. Primary among the mission's scientific goals is to search for and characterize a wide range of rocks and soils that hold clues to past water activity on Mars. The spacecraft are targeted to sites on opposite sides of Mars that appear to have been affected by liquid water in the past. NASA's twin robot geologists, the Mars Exploration Rovers, launched toward Mars on June 10 and July 7, 2003, in search of answers about the history of water on Mars. They landed on Mars January 3 and January 24 PST, 2004 [74]. Power supply technology for rovers is an important issue. So far, several means for electric power supply are used for Mars exploration rover, such as solar cells, lithium batteries and a radioisotope power system. However, there are some problems such as the increase of weight and the limitation of activity time and area. For example, using solar power limits the places on Mars that the rover can explore. They are restricted to landing and traveling around the equatorial region where they can get enough sunlight to re-energize their batteries. Therefore, MPT, an innovative way for powering moon or planet exploration rovers, is proposed [75]. Similarly, for a wide area and continuous Mars observation, MPT for Mars exploration airplane is also proposed [26].

Both rover and airplane proposed above are mainly actuated by DC motors. A static solar power station generates DC power and changes it into microwave power, then transmits microwave power to a distant rover or airplane. The rover or airplane, equipped with rectenna (or rectenna array), receives microwave power and changes it into DC power, which actuates DC motors of rover or a propeller of airplane. As we know, input V-I characteristic of DC motor exhibits variable which depends on its revolution speed and mechanical load. Therefore, the emulated input resistance of DC motor is variable. As a result, the rectifying efficiency is variable when the rectenna is connected to a DC motor. The motor would not work well even stop when it is changed from one operating condition to another because of power shortage caused by impedance mismatch.

Therefore, to solve the problems mentioned above, this chapter only focuses on the study of driving a DC motor using MPT. We design a power-receiving device which has capability of efficiently driving a dynamic load resistance device (such as a DC motor) in the MPT system.

5.3 Low-power DC Motor

If the load resistance characteristics of a DC motor match the optimal load of the rectenna, the output characteristics of the rectenna will be equivalent to those when the rectenna is loaded by a load resistance [38]. It means that a rectenna can drive a DC motor with the maximum efficiency when the load characteristic of the motor equals to the optimal load of the rectenna. However, powered by the microwave, a motor is difficult to maintain a steady revolution speed due to the change of mechanical loads, which leads to a decrease in efficiency of the rectenna. Therefore, if we insert a constant input resistance buck-boost converter between the rectenna and the DC motor, the output impedance of the rectenna maintains constant despite operating conditions of the motor. Consequently, the efficiency of the rectenna will keep constant. Hence, it is necessary to check the input V-I characteristics or the input resistance characteristics of a DC motor before designing a rectenna.

The DC motor used in this study is an RF-500TB-14415 motor made by Mabuchi Motor Co., Ltd as shown in Fig. 5.1(a). This type of motor is usually used for low-power household electrical appliances such as audio-video equipment. The operating voltage range is from 1.5 to 9 V and the output power is widely from 0.01 to 2 W [76]. A DC power source is used to measure the input load characteristics of the motor connected with a small fan as a reference mechanical load. The block diagram of the measurement circuit is shown in Fig. 5.1(b), where an ammeter and a voltmeter measure the input current I_{m} and the input voltage V_{m}, respectively. Then the emulated input resistance R_{m} and input power P_{m} can be calculated by $R_{\mathrm{m}} = V_{\mathrm{m}}/I_{\mathrm{m}}$ and $P_{\mathrm{m}} = V_{\mathrm{m}}I_{\mathrm{m}}$, respectively. To determine R_{m} and P_{m}, the input current is measured with a changed input voltage. The results are shown in Fig. 5.2, which indicates that the input resistance R_{m} increases from 36 to 140 Ω and the input power P_{m} increases from 10 to 645 mW when the input voltage increases from 0.6 to 9 V. Of course, instead of the small fan, if a heavy mechanical load was used, the input resistance would be lower because of a higher current consumption. As the same reason, R_{m} decreases at a higher input voltage. When the input voltage exceeds 5 V, the revolution speed of the fan becomes very fast which results in a heavy resistance of air, then the increase of the current consumption leads to the decrease of R_{m}.

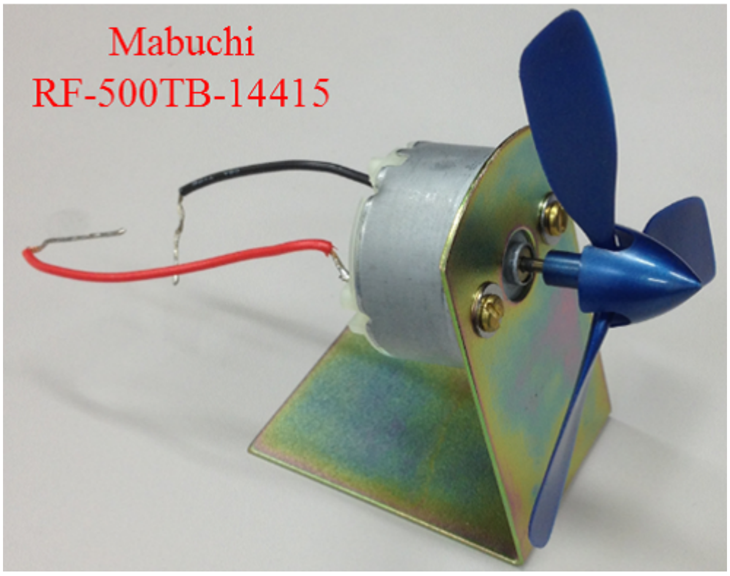

(a)

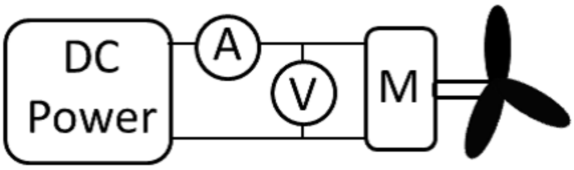

(b)

Figure 5.1: Photograph of the DC motor and measurement setup for input load resistance R_{m}. (a) Photograph. (b) Measurement setup. An ammeter and a voltmeter measure the input current I_{m} and the input voltage V_{m}, respectively.

5.4 Rectenna Design

5.4.1 Antenna Design

The rectenna is very important for converting wireless RF power into DC power. A rectenna usually contains a receiving antenna and a rectifying circuit. The receiving antenna collects microwave incident power and the rectifying circuit converts microwave power into DC power. In the previous chapters, we only focused on the discussion about rectifying circuits. This chapter will discuss about the design of an antenna.

An antenna is an electrical device for radiating or receiving radio waves. On transmission, an antenna accepts energy from a transmission line and radiates it into space, and on reception, an antenna gathers energy from an incident wave

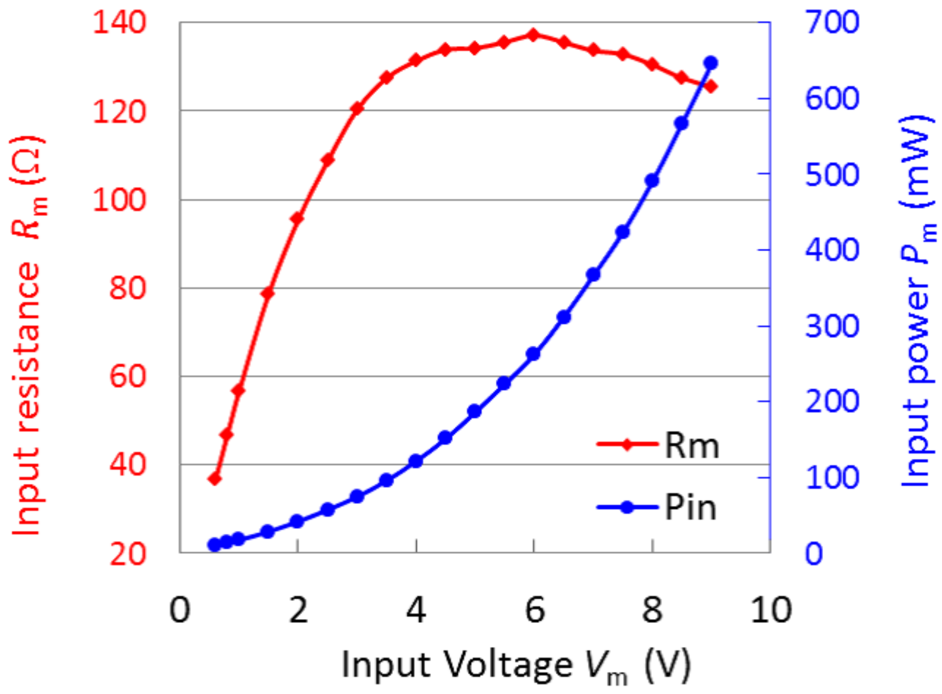

Figure 5.2: Measured input load characteristics of the DC motor.

and sends it down a transmission line. In this chapter, an antenna designed to receive microwave from transmission side. According to different shape and application, there are linear antenna, planar antenna, aperture antenna and so on. For microwave power transmission, a microstrip patch antenna (or array) is commonly used by many researchers [13]-[15]. Patch antenna, with a simple shape, performs a relatively high gain so that it can receive much more power in a limited microwave power density environment. In addition, microstrip patch antennas are excellent in low fabrication cost and readily amenable to mass production [77].

In this experiment, since a horn antenna is used as a microwave transmission antenna, we design a linear polarization circular patch antenna as a receiving antenna. With respect to the dielectric substrate for the rectifier circuit, we all use the same dielectric substrate of NPC-F260 as shown in Table 3.4, where the thickness of the substrate H is 0.8 mm in previous chapters. However, the thickness of the substrate decreases resulting in dielectric losses increasing so that the gain of the patch antenna will decrease, which has been reported in the literature [78][79]. In this experiment, it requires a high gain for receiving as much power as possible in a limited power density environment. Therefore, we design two antennas with two different thickness of dielectric substrates (NPC-F260). Here, these two antennas such as H = 1.6 mm and H = 0.8 mm are referred to as H16 and H08, respectively.

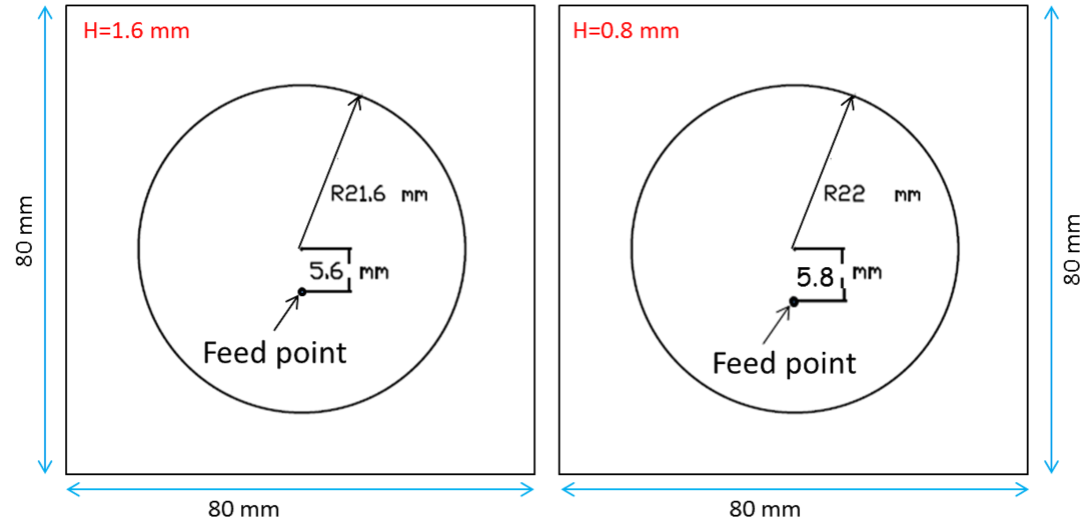

Figure 5.3: Designed antenna sizes.

We simulate two antennas by using HFSS simulator of ANSYS and fabricate them. Figure 5.3 shows the shape and sizes of antennas, where the whole size are both 80 mm × 80 mm, and the radius are 21.6, 22 mm, the distances from center to feed point are 5.6, 5.8 mm, respectively. Figure 5.4 shows the simulation and measured results of $|S_{11}|$. Note that the simulation results of two antennas are both a little different with the measured results. However, we make sure that the measured results are both resonant at the frequency of 2.45 GHz, where the $|S_{11}|$ of H16 and H08 are -28 dB and -24 dB, respectively.

The gain of an antenna is a very important factor in rectenna. The simulation results of antenna's gain are shown in Fig. 5.5, where the gain of H16 and H08 antennas are 7.04 dBi and 6.24 dBi, respectively. Then, as for measurement, compared to a standard half-wave dipole antenna with a known gain of 2 dBi, the gain of designed antenna can be calculated. We set the same power density condition to measure the receiving power of two designed antennas and the standard dipole antenna, then the gain of each antenna can be calculated referring to the receiving power. The effective aperture of the antenna A_e can be calculated by following:

$$A_\mathrm{e} = \frac{G_\mathrm{A}\lambda^2}{4\pi}, \tag{5.1}$$

where, G_A is the power gain, and λ is the free-space wavelength at 2.45 GHz. The results can be seen from Table 5.1. Note that the effective aperture of the H16 antenna is bigger than that of the H08 antenna. This means one H16 antenna can

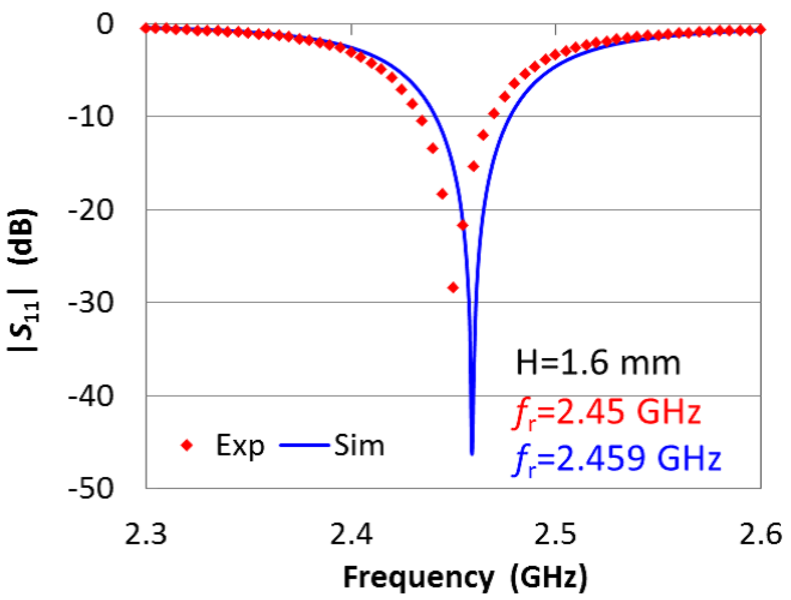

(a)

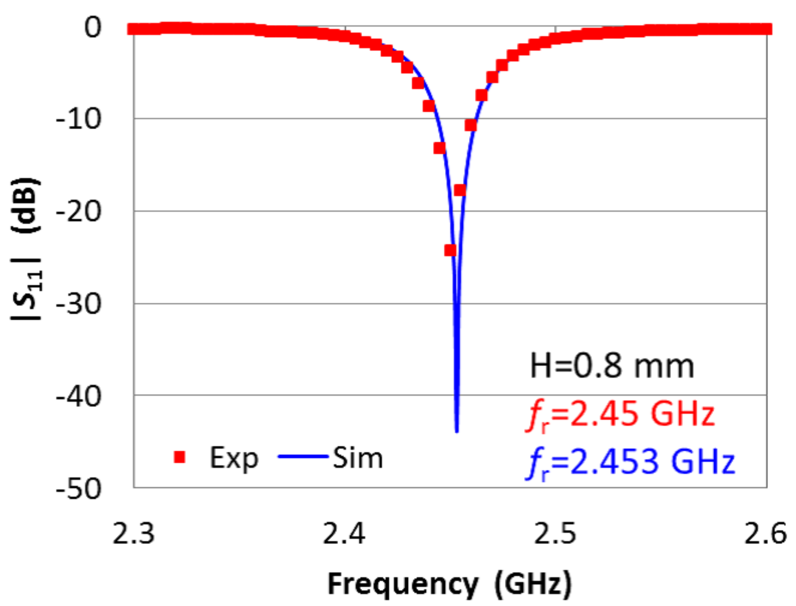

(b)

Figure 5.4: Simulated and measured $|S_{11}|$ of antennas. (a) Antenna H16 $|S_{11}|$ = -28 dB. (b) Antenna H08 $|S_{11}|$ = -24 dB.

Table 5.1: Comparison of H16, H08 and standard antennas for receiving power, gain and effective aperture.

Antenna	H16	H08	Standard
Receiving power (mW)	13.53	11.1	4.92
Gain (dBi)	6.39	5.53	2
Effective aperture (cm^2)	51.6	42.3	18.8

receive approximately 52 mW while H08 antenna can receive approximately 42 mW at the same microwave density of 1 mW/cm^2 which is the standard value of the radiation protection guidance. Consequently, we choose the H16 antenna as a receiving antenna because it is superior in capability of receiving power.

5.4.2 Small Rectifying Circuit

In order to make a compact rectenna, we design a small rectifying circuit to match with the size of antennas. As mentioned in Chapter 4.5, the output voltage of the rectifying circuit supplies voltage for the control-pulse circuit of the buck-boost converter. The overall efficiency of the RF-DC-DC circuit is low when the input power is below 40 mW because the output voltage of the rectifier is low so that it results in a low efficiency of the buck-boost converter. Therefore, it demands a higher output voltage in a lower input power level. On the other hand, a higher RF-DC conversion efficiency is also required. Considering all requirements mentioned above, we design a small rectifier A with a higher optimal load resistance to get a higher output voltage at the same power level. Compared with rectifier A, a small rectifier B with a normal optimal load resistance is also designed.

We use the same dielectric substrate of NPC-F260 and the thickness is 0.8 mm which is the same as the previous design. Similarly, an input matching circuit and two HSMS286F HF diodes are used in the rectifier, while the output filter consists of several open stubs without $\lambda/4$ line. Here, with respect to 2.45 GHz microwave in the NPC-F260 substrate, $\lambda/4$ line is approximate 21 mm which is almost the half length of the whole circuit as shown in Fig. 3.11. $\lambda/4$ line mainly addresses the fundamental frequency content of the output voltage. If we sufficiently deal with the other high order harmonics, the overall high frequency

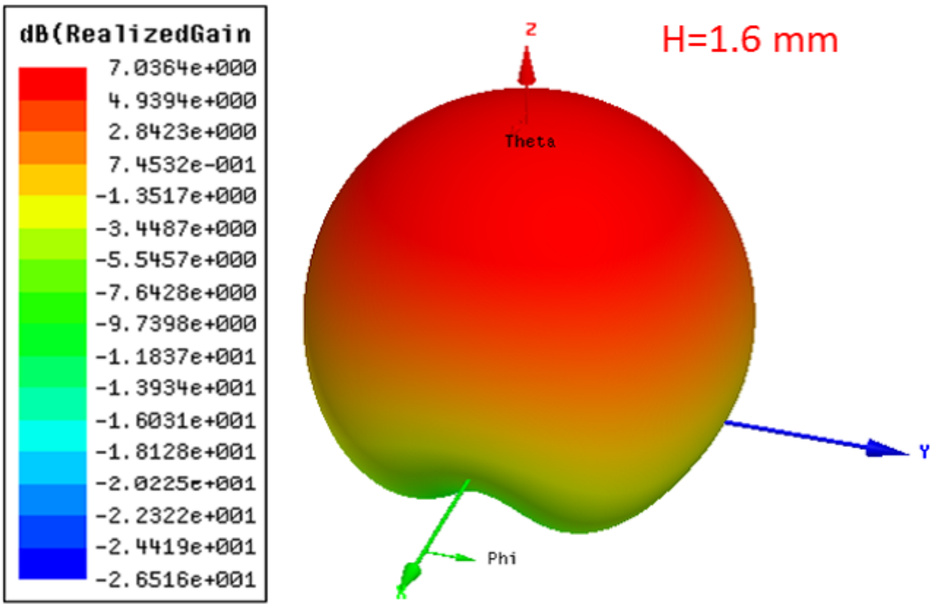

(a)

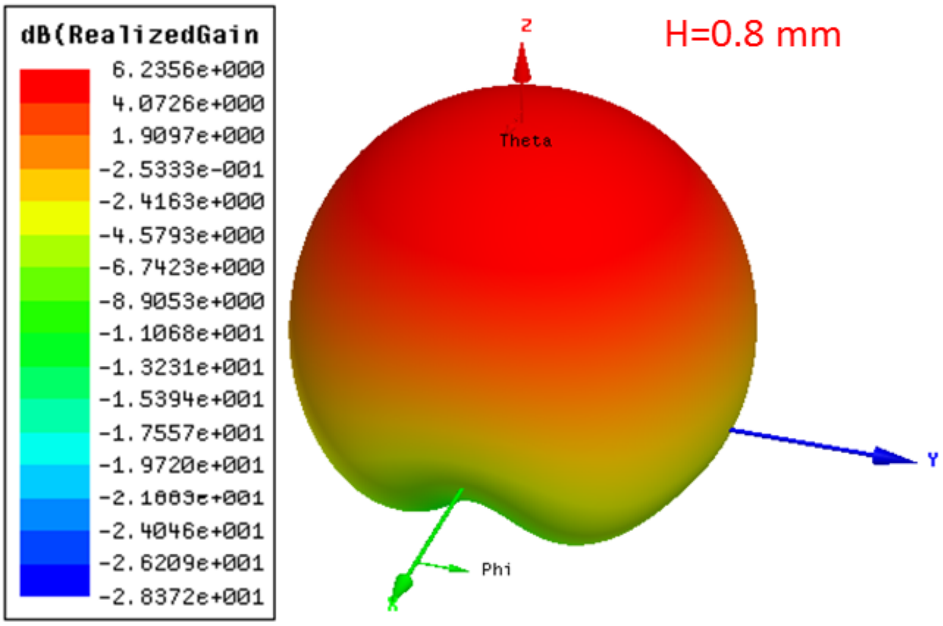

(b)

Figure 5.5: Simulated gains of antennas. (a) The gain of H16 antenna is 7.04 dBi. (b) The gain of H08 antenna is 6.24 dBi.

harmonic loss also can be restrained at a low level even without $\lambda/4$ line. Furthermore, the losses of high frequency harmonic contents are small for 2.45 GHz microwave. Figure 5.6 shows the simulation results of output voltage spectrum of four rectifiers. In Fig. 5.6(a), Ch3_rectifier and Ch4_rectifier are the rectifiers designed in Chapter 3 and Chapter 4, respectively. Figure 5.6(b) shows the results of the rectifier A and B. Observe that the fundamental frequency content in A and B are bigger than that in Ch3_rectifier and Ch4_rectifier, while the high order harmonics of the former is smaller than the latter one. As a result, the overall high frequency harmonic loss of the former is approximately equivalent to the latter one.

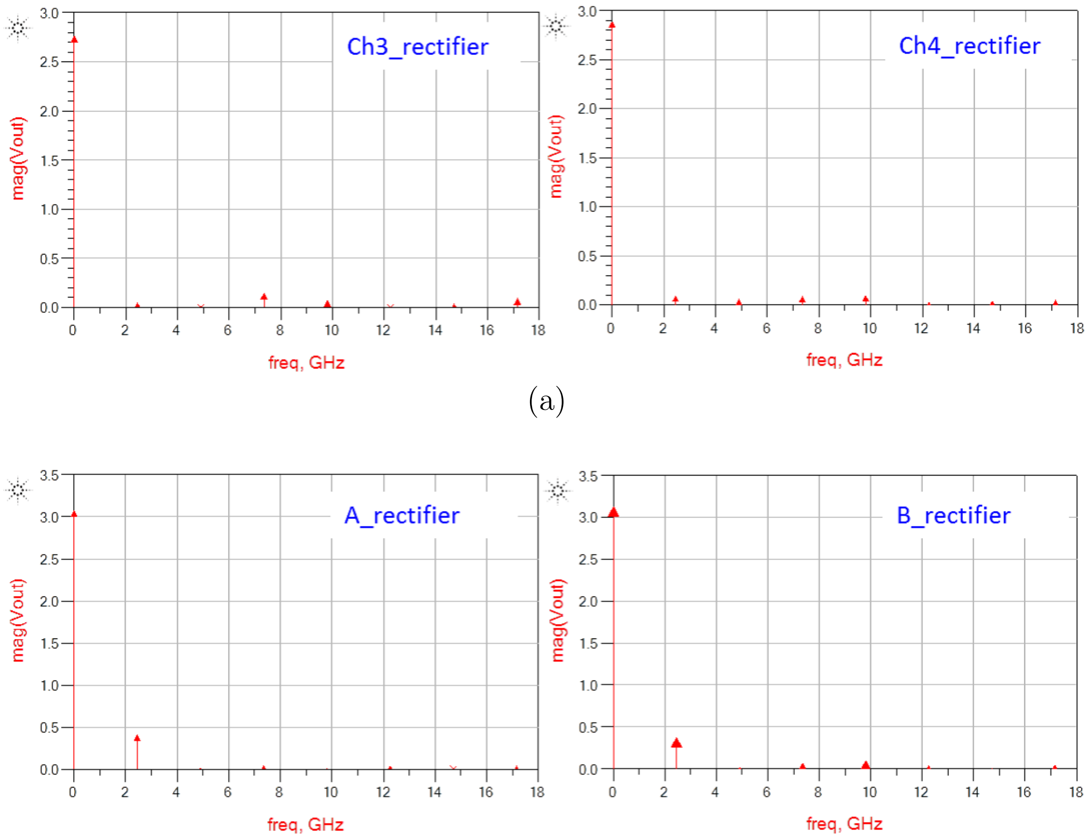

Figure 5.6: Simulated output voltage spectrum of rectifiers. (a) Ch3_rectifier and Ch4_rectifier are the rectifiers (with $\lambda/4$ line) designed in Chapter 3 and Chapter 4, respectively. (b) A_rectifier and B_rectifier are the rectifiers (without $\lambda/4$ line) designed in this chapter.

Figure 5.7 shows the photograph of the designed rectifier A, B and Ch4_rectifier as a contrast. The size of both rectifier A and B are 35 mm×50 mm, which is almost the half size of the Ch4_rectifier. Figure 5.8 shows the measured efficiency-load characteristics of the rectifier A and B at different input power levels. The results clearly indicate that the efficiency of the rectifier depends on the connected load and the input power. As for rectifier A, the optimal load is almost constant at 300 Ω in the input power range of 10 to 60 mW. The maximum efficiency is 80.8 % for a load of 300 Ω and an input power of 60 mW. As for rectifier B, the optimal load is almost constant at 160 Ω in the input power range of 10 to 60 mW. The maximum efficiency is 80 % for a load of 160 Ω and an input power of 80 mW. It is clear that the optimal load of the rectifier A is almost twice as big as that of the rectifier B.

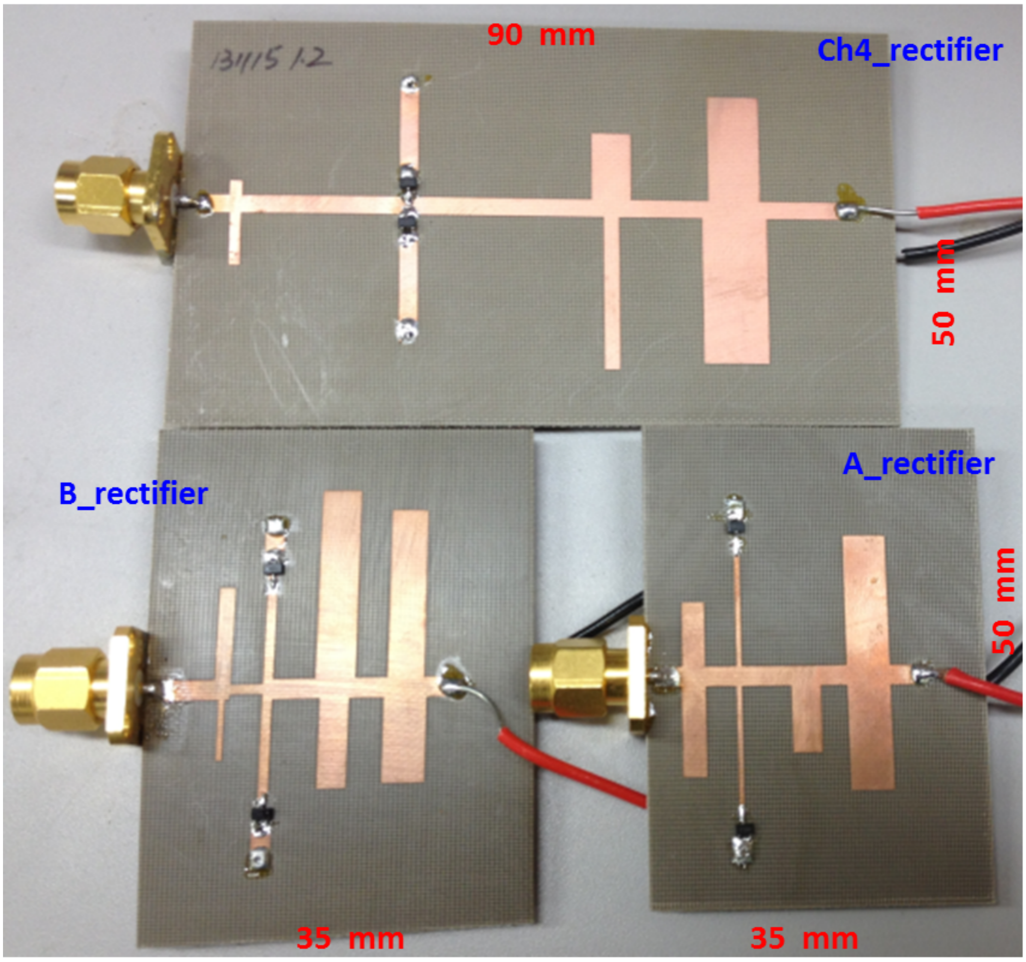

Figure 5.7: Photograph of designed rectifiers: A, B and Ch4_rectifier.

We also investigate the output voltage of both rectifiers and compare them in Fig. 5.9, where A_Eff, A_Vo are the efficiency and output voltage of the rectifier A, B_Eff, B_Vo are the efficiency and output voltage of the rectifier B. Figure 5.9(a) compares the efficiency and output voltage versus load resistance at a fixed input

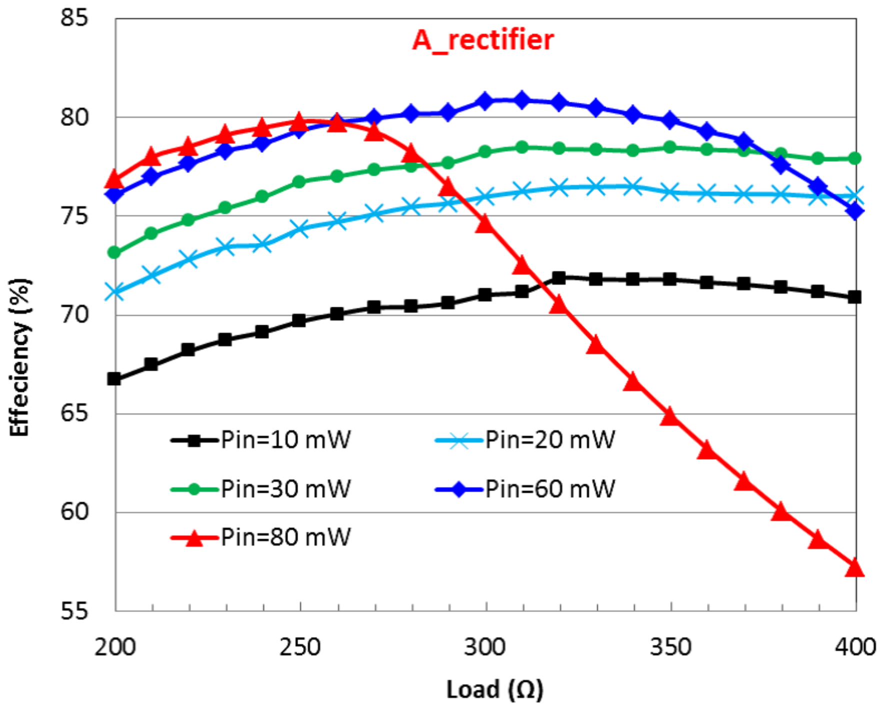

(a)

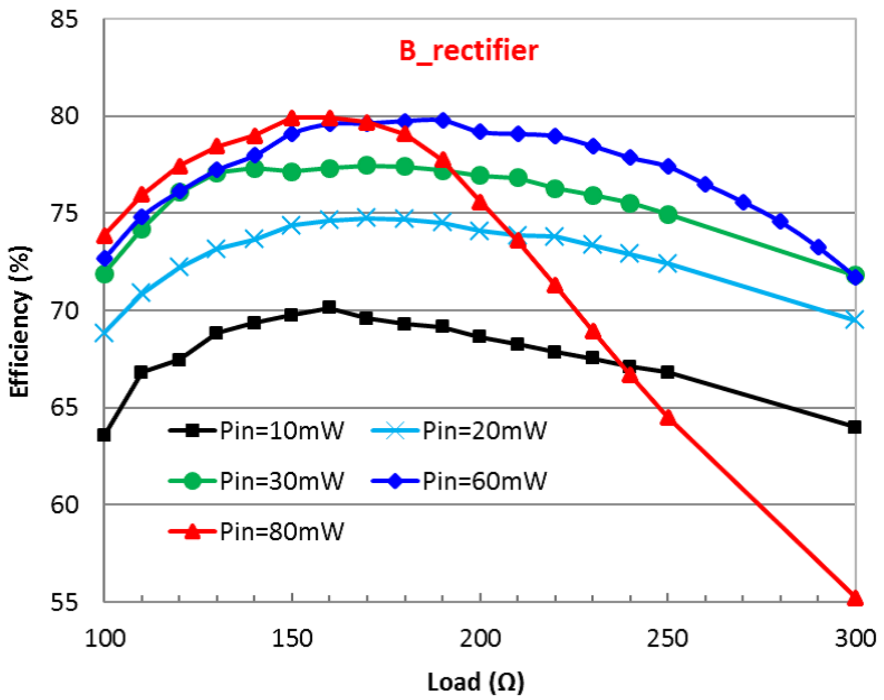

(b)

Figure 5.8: Measured efficiency results of the rectifier A and B for different input powers. (a) Efficiency-load characteristics of the A rectifier. The optimal load is almost 300 Ω. (b) Efficiency-load characteristics of the B rectifier. The optimal load is almost 160 Ω.

Table 5.2: Comparison of four rectifiers. Z_{opt} presents the optimal load of the rectifier. V_{out} (80 mW and Z_{opt}) means the output voltage of the rectifier at the optimal load for the same input power of 80 mW. −3.2 V means that the Ch3_rectifier obtains a negative output voltage which has been mentioned in Chapter 3.

Rectifier	Ch3	Ch4	A	B
Peak efficiency	79.2 %	82.5 %	80.8 %	80 %
Z_{opt} (Ω)	160	190	300	160
V_{out} (80 mW and Z_{opt}) (V)	−3.2	3.5	4.3	3.2
Size (mm)	90×50	90×50	35×50	35×50

power of 50 mW. Observe that the rectifier A presents a higher efficiency and output voltage at a higher load resistance while the rectifier B exhibits a higher efficiency and output voltage at a lower load resistance. In Fig. 5.9(b), when the input power is changing from 10 to 80 mW, the output voltage of both rectifiers are increasing while rectifier A obtains a higher output voltage than rectifier B, the efficiency of the rectifier B is increasing and levels off, while the efficiency of the rectifier A is increasing at the beginning and decreases at a higher power level. The reason is as following. Rectifier A obtains a higher output voltage which leads to a higher reverse voltage applied on the rectifying diode. Consequently, the reverse voltage applied on the diode exceeds the breakdown voltage at a lower input power level which results in efficiency decreasing of the rectifier A.

Until now, we have designed and measured four rectifiers which have each merits and demerits as summarized in Table 5.2. Note that the higher optimal load rectifier obtains a higher output voltage and the output voltage of the A rectifier is 1 V bigger than that of the B rectifier. Ch3_rectifier and rectifier B have almost the same peak efficiency and the same optimal load while the size of the rectifier B is half smaller than Ch3_rectifier. Compared to Ch4_rectifier, the efficiency of the rectifier A is slightly lower but it obtains a higher output voltage with a half small size.

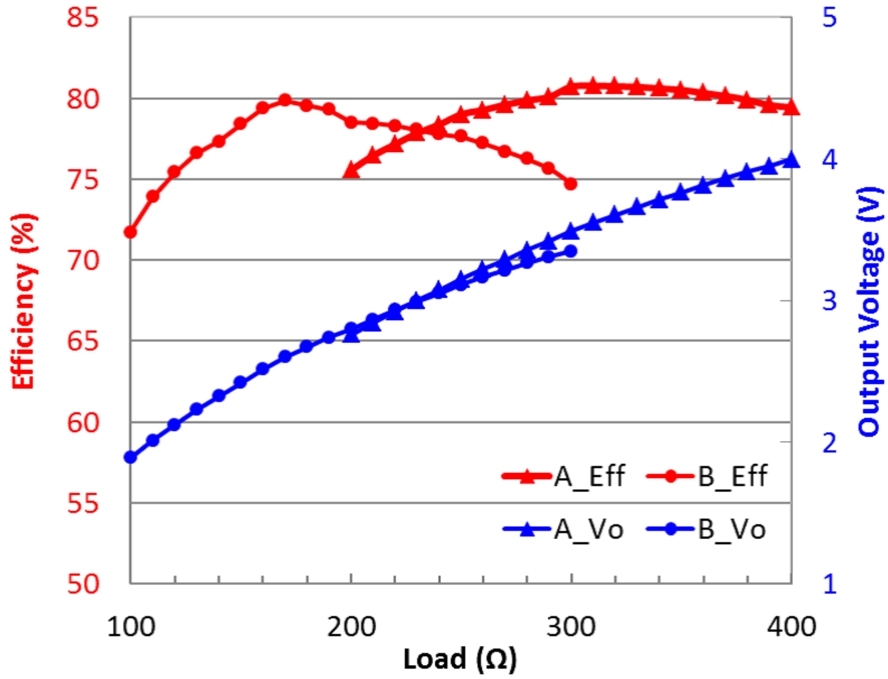

(a)

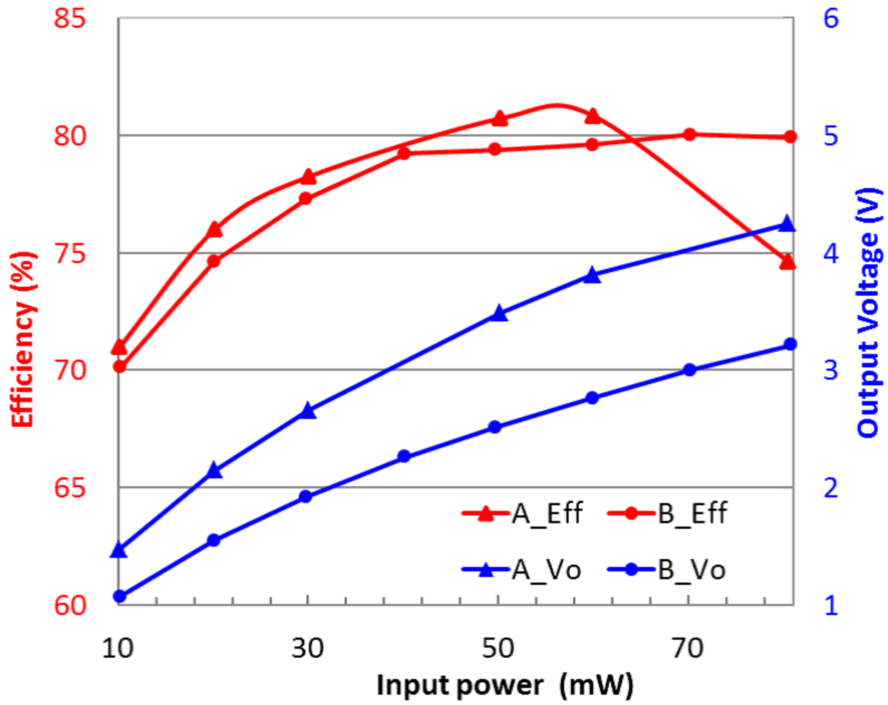

(b)

Figure 5.9: Comparison of the measured efficiency and the output voltage. (a) Efficiency and output voltage vs. load for a fixed input power of 50 mW. (b) Efficiency and output voltage vs. input power for the optimal load of 300 Ω (rectifier A) and 160 Ω (rectifier B), respectively. A_Eff, A_Vo are the efficiency and output voltage of the rectifier A; B_Eff, B_Vo are the efficiency and output voltage of the rectifier B.

5.5 Compact Power-receiving Device

5.5.1 Improved Buck-boost Converter

A buck-boost converter with a constant input resistance is previously proposed to improve the efficiency-load characteristics of the rectifier in Chapter 4.3. However, the converter operates at low efficiency for input power levels below 40 mW, because the control-pulse oscillator can not be powered by the input voltage of the converter at such low power levels. To overcome this issue, an improved buck-boost converter is designed as shown in Fig. 5.10. Compared to the previous one in Chapter 4.3, the improved buck-boost converter is smaller and simpler because it uses only HF oscillator and a small inductor L (220 μH). As seen the operating waveforms from Fig. 5.10(b), the operating condition has no sleep-state. More importantly, the power for the control-pulse oscillator is supplied by the output voltage of the converter, which is referred to as O-type. By comparison, the control-pulse oscillator is powered by the input voltage of the converter is also designed, which is referred to as I-type. As we have mentioned, the buck-boost converter designed in Chapter 4.3 exhibits a boost converter where the output voltage is larger than input voltage. Therefore, O-type converter is suitable for lower power level because of a higher supplied voltage for the control-pulse oscillator.

Similarly, the input resistance of the converter R_{in} can be calculated using Eq. (3.37). The other parameters are as follows: $L = 220$ μH, f_{h}=20 kHz, D_{h}=0.5, D_{ι} should equal 1 because there is no low-frequency oscillator in this case. This gives an R_{in} value of 35 Ω. According to Eq. (3.37), the input resistance R_{in} of this buck-boost converter will remain a constant value of 35 Ω even though the connected load resistance is above 35 Ω. Hence, when the DC motor described in Chapter 5.3 is connected to the buck-boost converter as a load, its input load resistance of 36 to 140 Ω satisfies the load requirements of the buck-boost converter. The components of the circuit used in this converter are given in Table 5.3 and the photograph of fabricated circuits are shown in Fig. 5.11, which has a size of 25 mm×25 mm. For both converters, the components of the circuit used are the same and the only difference is the connection method.

Similarly, we use the measurement circuit in Fig. 4.9(a) to evaluate the efficiency and R_{in} of the buck-boost converter with a DC power source, and the

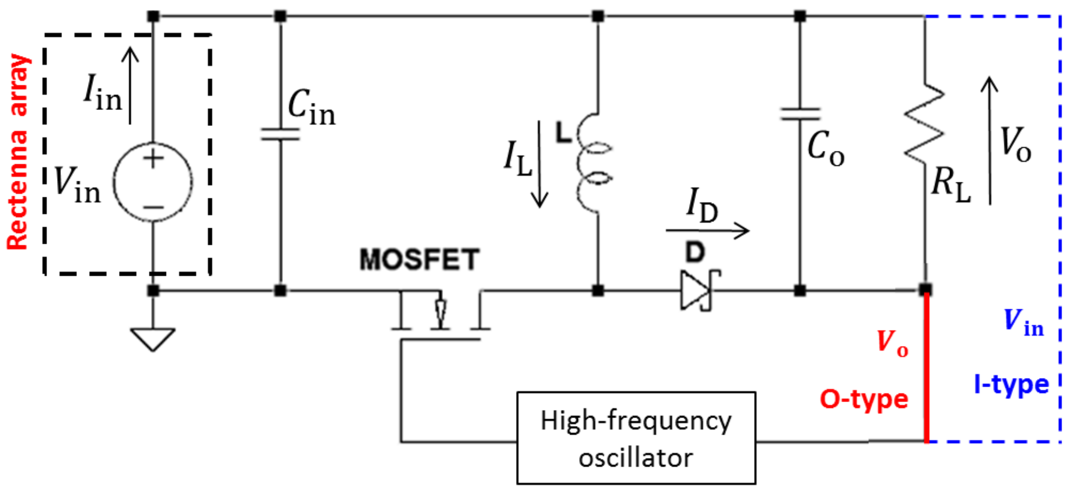

(a)

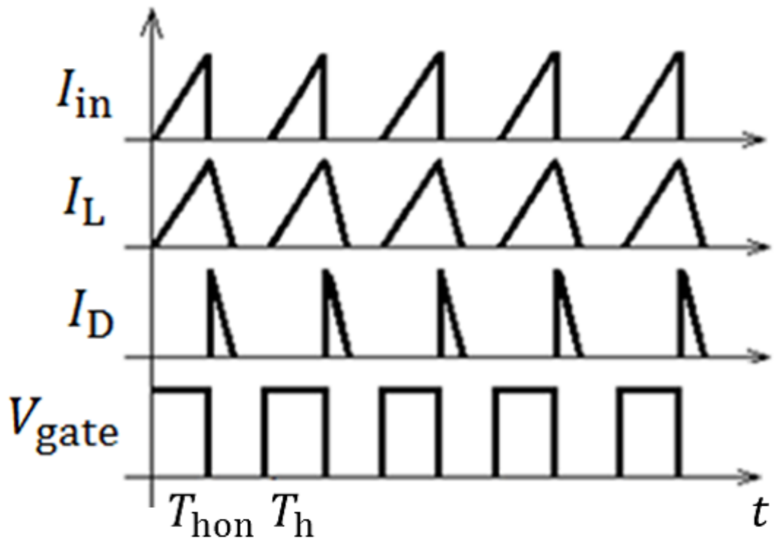

(b)

Figure 5.10: Block diagram and operating waveforms of the improved buck-boost converter. (a) Block diagram. (b) Operating waveforms. O-type: oscillator is powered by output voltage; I-type: oscillator is powered by input voltage.

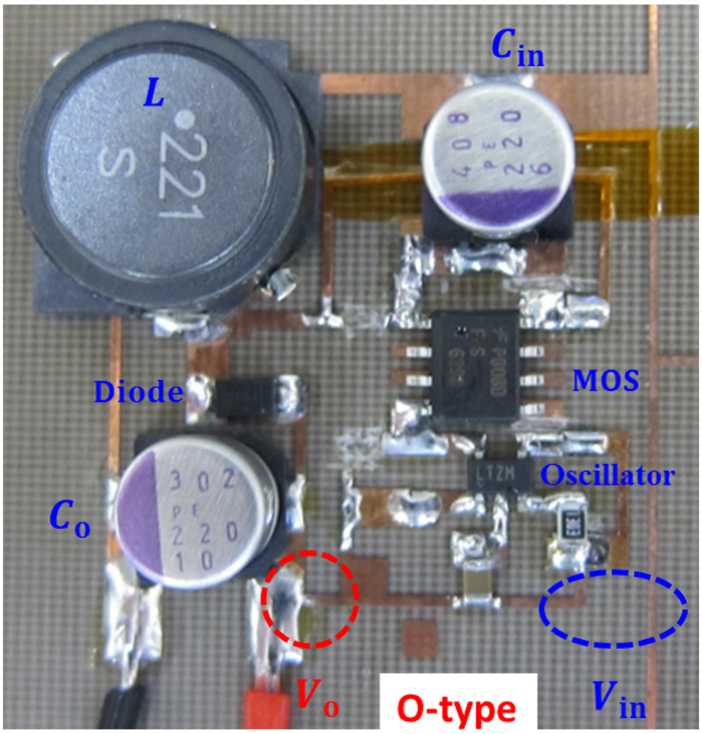

(a)

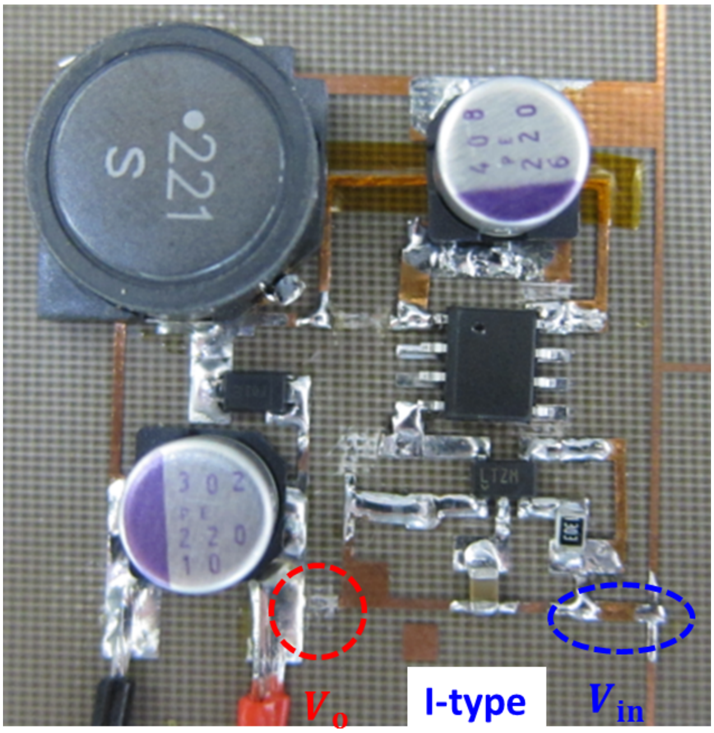

(b)

Figure 5.11: Photograph of fabricated buck-boost converters. (a) O-type: V_o line is connected to the oscillator and V_{in} line is open. (b) I-type: V_o line is open and V_{in} line is connected to the oscillator.

Table 5.3: Components of the improved buck-boost converters.

Component	Maker	Part NO.	Description
High-frequency oscillator	Linear Technology	LTC6900	$I_{\mathrm{SS}} = 0.5$ mA ($f = 3$ MHz); $V_{\mathrm{SSmin}} = 2.7$ V
N-MOS	Fairchild	FDS6298	$V_{\mathrm{DSS}} = 30$ V; $R_{\mathrm{DS(on)}} = 12$ mΩ ($V_{\mathrm{GS}} = 4.5$ V)
Schottky Diode	Diodes Incorporated	DFLS130L	$V_{\mathrm{RRM}} = 30$ V; V_{FM}= 0.21 V
Inductor	Taiyo Yuden	NS12555T221	$L = 220$ μH; $R_{\mathrm{dc}} = 0.27$ Ω; I_{dc} = 1 A
Capacitor C_{in}	Panasonic	6SVPE220M	220 μF ($V_{\mathrm{rated}} = 6.3$ V)
Capacitor C_{o}	Panasonic	10SVPE220M	220 μF ($V_{\mathrm{rated}} = 10$ V)

comparison results of two type converters are shown in Fig. 5.12. Here, O_Eff, I_Eff are the efficiency of O-type and I-type converters, respectively. O_Rin, I_Rin are the input resistance of O-type and I-type converters, respectively. In Fig. 5.12(a), at a fixed input voltage of 3 V, the efficiency and R_{in} of the I-type are measured with load changing from 10 to 500 Ω, while those of the O-type are measured with load changing from 10 to 200 Ω in order to avoid the oscillator of the O-type over-voltage. The efficiency and R_{in} variation tendencies are approximately the same. The efficiency of the O-type is slightly better than the one of the I-type when the load is below 50 Ω and that relation is inverted when the load is over 100 Ω because the supplied voltage for oscillator is simultaneously varying with the output voltage of the O-type converter. As expected, the R_{in} is constant to be 38 Ω which is close to the designed value of 35 Ω when the load is over 40 Ω. In Fig. 5.12(b), at a fixed load of 50 Ω, the efficiency and R_{in} of the I-type are measured with input voltage changing from 2.1 to 5 V, while that of O-type is measured with input voltage changing from 1.1 to 3 V. It is obvious that the O-type converter has the capability of handing lower input voltage and the I-type converter has the capability of handing higher input voltage. Additionally, the R_{in} of both type converters are constant and independent of the input voltage.

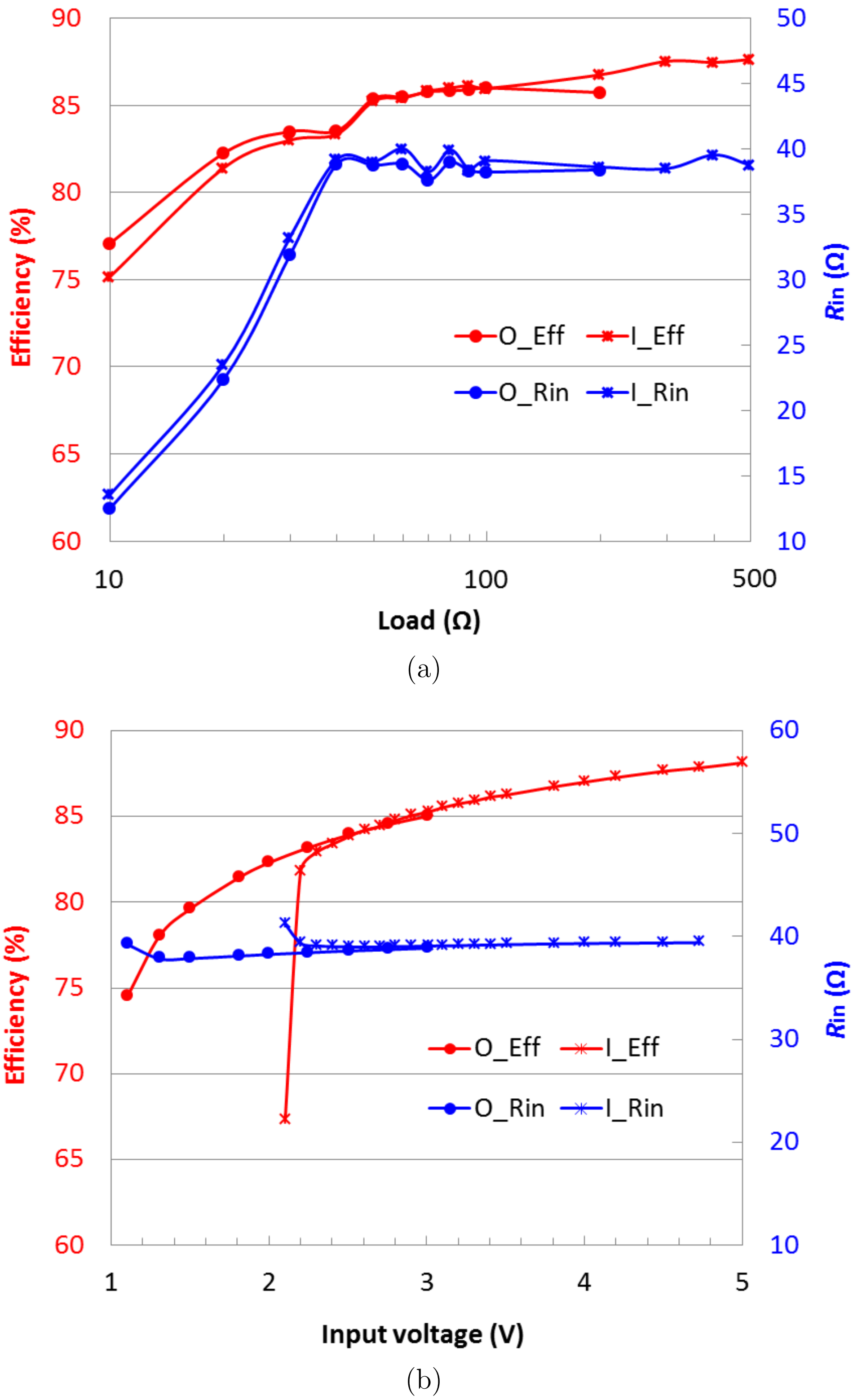

Figure 5.12: Comparison of measured results between O-type and I-type buck-boost converters. (a) Efficiency and R_{in} vs. load for a fixed input voltage of 3 V. (b) Efficiency and R_{in} vs. input voltage for a fixed load of 50 Ω.

Table 5.4: Comparison of four buck-boost converters such as the converter in Chapter 3, Chapter 4 and O-type, I-type converters in this chapter.

Converter	Ch3	Ch4	I-type	O-type
Power supply	extra DC power source	input voltage	input voltage	output voltage
Voltage polarity	inverting	non-inverting	non-inverting	non-inverting
Control circuit	HF, LF oscillators and gate driver	HF, LF oscillators	HF oscillator	HF oscillator
Size	large	medium	small	small

Until now, we have designed and measured four buck-boost converters which have each merits and demerits as summarized in Table 5.4. Those four converters all operate at discontinuous conduction mode with constant input resistance characteristic and play a boost converter role in the application. The O-type and I-type have the small size and O-type has the capability of handing lower power without extra DC power supply.

5.5.2 Compacting Rectenna Array and Buck-boost Converter

A single rectenna consists of the antenna designed in Chapter 5.4.1 and the rectifier as shown in Fig. 5.13. The optimal load of the A rectifier and B rectifier described in Chapter 5.4.2 are 300 Ω and 160 Ω, respectively. While the input resistance of the buck-boost converter described in Chapter 5.5.1 is almost 35 Ω. Therefore, in order to match the input resistance of the buck-boost converter, a common method that several rectennas are connected in parallel as a rectenna array is usually applied to decrease the optimal load of the rectenna [80]. Then we set 9 A_rectennas connected in parallel as A rectenna array and 4 B_rectennas connected in parallel as B rectenna array, respectively. The optimal load of the A rectenna array and the B rectenna array can be calculated to be approximately 33 Ω and 40 Ω, respectively.

Additionally, in order to make the rectenna array in a compact board, we use a multilayer substrate with the antennas in the upper layer and the rectifiers in the lower layer and GND in the middle layer. The buck-boost converter is also in the lower layer, and is connected to the output of the rectenna array. We connect the feed point of the antenna and the input port of the rectifier by a through hole which is isolated from the middle layer. The GND in rectifiers and buck-boost converter are all connected to the middle layer by other through holes. Figure 5.14 shows a side-view diagram of the multilayer substrate. In the upper layer, antennas are arranged in an equilateral triangle position with the separation between two near antennas of 75 mm, which is almost 0.61 λ (λ is a free-space wavelength at 2.45 GHz). The rectenna array has two types such as A and B, and the buck-boost converter also has two types such as O-type and I-type. With those different types, there are four different combinations of the rectenna array and the buck-boost converter such as A rectenna array + O-type converter (9AO), A rectenna array + I-type converter (9AI), B rectenna array + O-type converter (4BO) and B rectenna array + I-type converter (4AI), respectively. The rectenna and converter combination is referred to as compact power-receiving device here. The photograph of the 9AO and 4BI power-receiving devices are shown in Fig. 5.15.

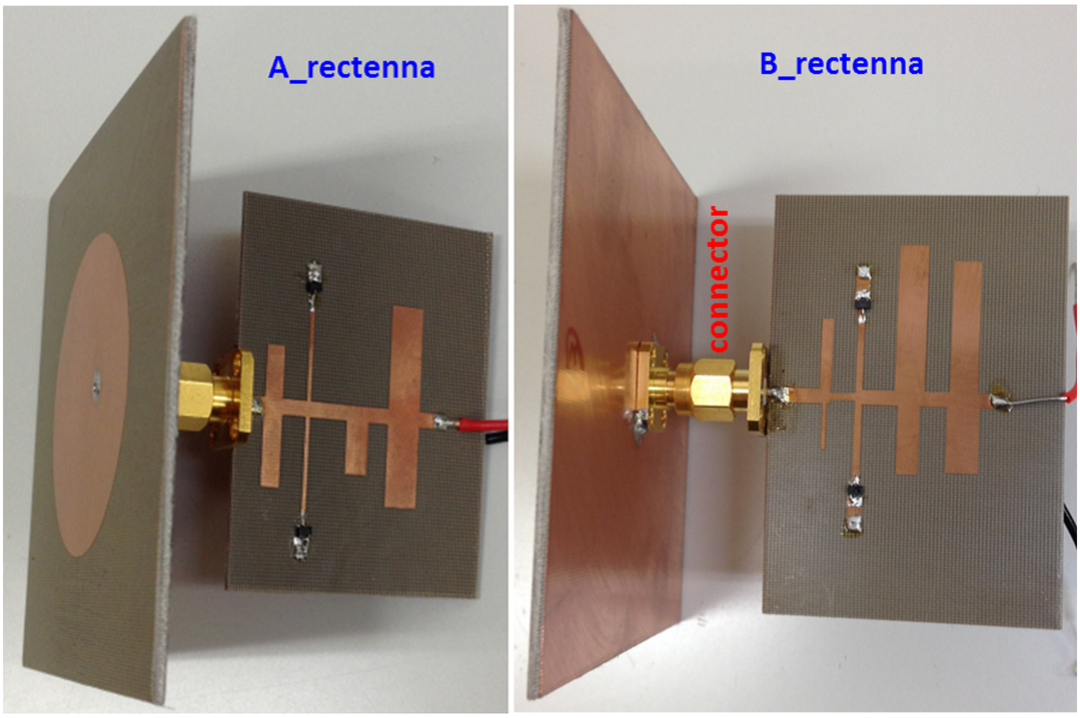

Figure 5.13: Photograph of a single A rectenna and B rectenna.

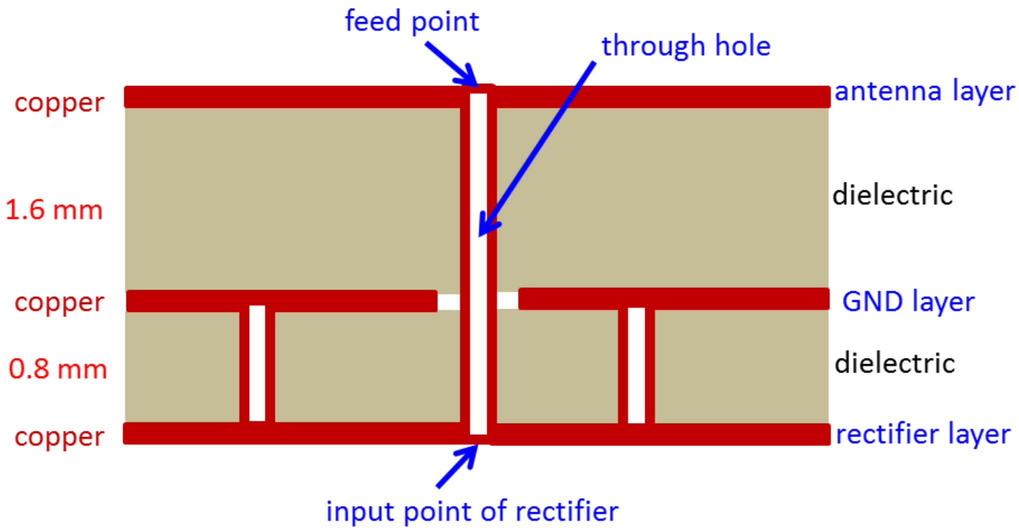

Figure 5.14: Side-view diagram of the multilayer substrate.

5.6 MPT Experiment Using Continuous-wave

5.6.1 Power Received by Antenna Array

In order to evaluate the overall efficiency of the compact power-receiving device, it is first necessary to measure the power received by the antenna array P_{rall}. Figure 5.16(a) shows a block diagram of the experimental setup used to measure P_{rall} of 9 antennas. It consists of a signal generator (SG), an amplifier, a directional coupler, a horn antenna and the receiving antenna array (without the rectifying circuits or buck-boost converter). The SWH-22 horn antenna of ARA Technologies Inc. we used has an aperture size of 36 mm×25 mm and a gain of 16.3 dBi. According to the antenna far field distance d_{f} calculation, $d_{\mathrm{f}} = 2D^2/\lambda$, where D is the largest dimension of the aperture, the far field distance d_{f} is calculated to be 21 cm. Hence, we set the microwave power transmission distance at 3 m which is much longer than d_{f}.

The power meter measures the input power of the transmission antenna through power sensor A, and measures the received power of each individual antenna one by one through power sensor B. In order to eliminate the influence from the reflection of near antennas, the other eight antennas are all connected to a 50 Ω dummy load as one antenna is being measured. The example of 9 antennas measurement is shown in Fig. 5.16(b). For comparison, the power received by just

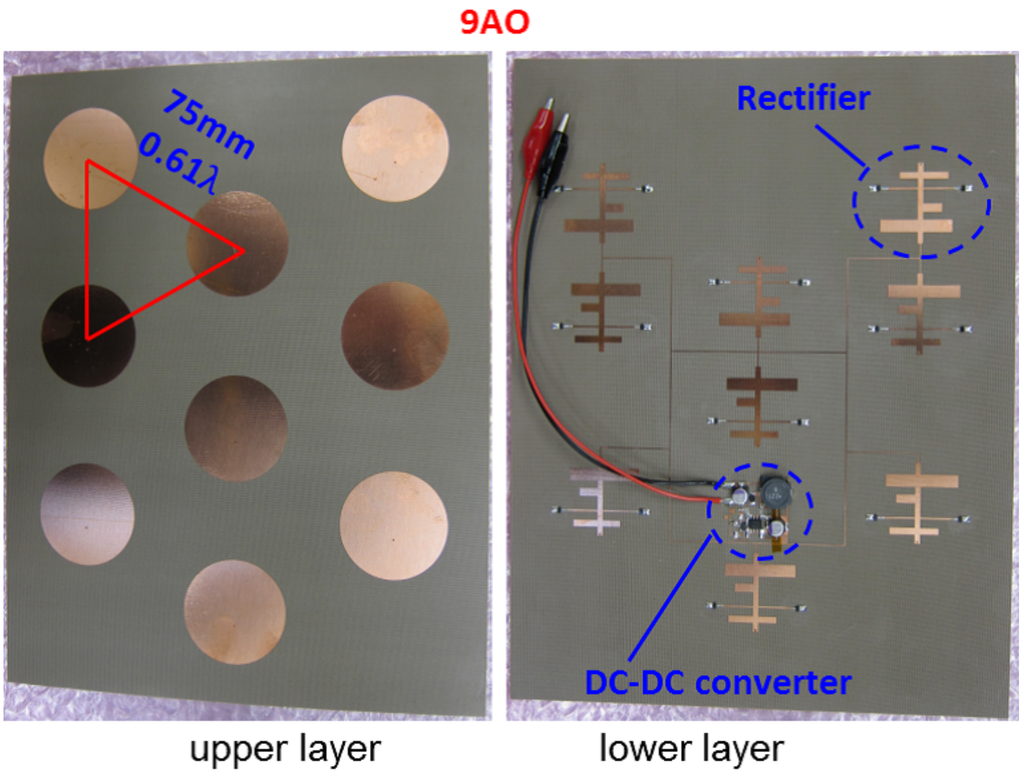

(a)

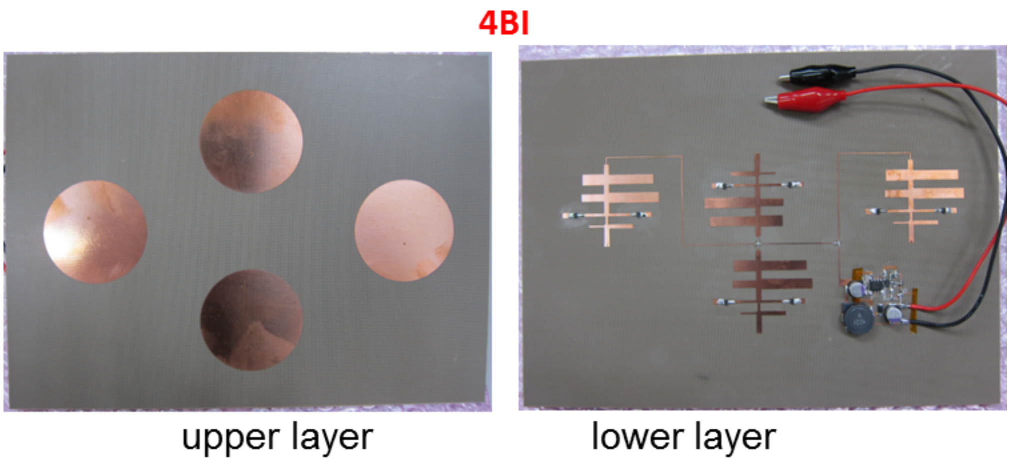

(b)

Figure 5.15: Photograph of the compact rectenna array and buck-boost converter. (a) 9AO power-receiving device. (b) 4BI power-receiving device.

Table 5.5: Relative power received by 9 antennas array and a single antenna vs. power density (P_{den}).

P_{den} (mW/cm^2)	0.25	0.5	0.74	0.98	1.22	1.46	1.67	1.89	2.09
a1	0.879	0.882	0.882	0.881	0.877	0.883	0.881	0.877	0.89
a2	0.828	0.831	0.83	0.833	0.829	0.829	0.828	0.828	0.839
a3	0.738	0.737	0.736	0.736	0.735	0.735	0.735	0.735	0.745
b1	0.691	0.692	0.692	0.691	0.689	0.69	0.691	0.689	0.698
b2	0.774	0.77	0.772	0.771	0.768	0.768	0.772	0.772	0.781
b3	0.955	0.956	0.956	0.957	0.955	0.954	0.956	0.956	0.965
c1	0.856	0.86	0.86	0.859	0.857	0.854	0.858	0.857	0.868
c2	0.843	0.844	0.843	0.846	0.846	0.847	0.844	0.842	0.854
c3	0.731	0.735	0.734	0.736	0.732	0.732	0.73	0.731	0.744

a single antenna, placed at the center position, is also measured, and power received by each antenna of nine antennas are expressed relative to this as shown in Fig. 5.17. These power proportion relation should be constant at different power densities because the gain of antennas are changeless. As shown in Table 5.5, it is obvious that the relative power proportion between a single antenna and antenna array is independent of the power density. The power received by the individual antennas in the array is lower than that received by the single antenna because of overlapping of the effective apertures in the antenna array. Similarly, using the same measurement method, the receiving power of 4 antennas array is also measured. Figure 5.18 shows that the overall power received by the 9 antennas array P_{Aall} and 4 antennas array P_{Ball} in different power densities P_{den}. P_{Aall} increases linearly from 95 to 800 mW and P_{Ball} increases linearly from 45 to 376 mW as the power density is increased from 0.25 to 2.08 mW/cm^2.

5.6.2 Experiment on Driving DC Motor Using Continuous-wave

Figure 5.19 shows a block diagram of the experimental setup used to drive the DC motor by MPT with Continuous-wave power. It consists of the same transmitting

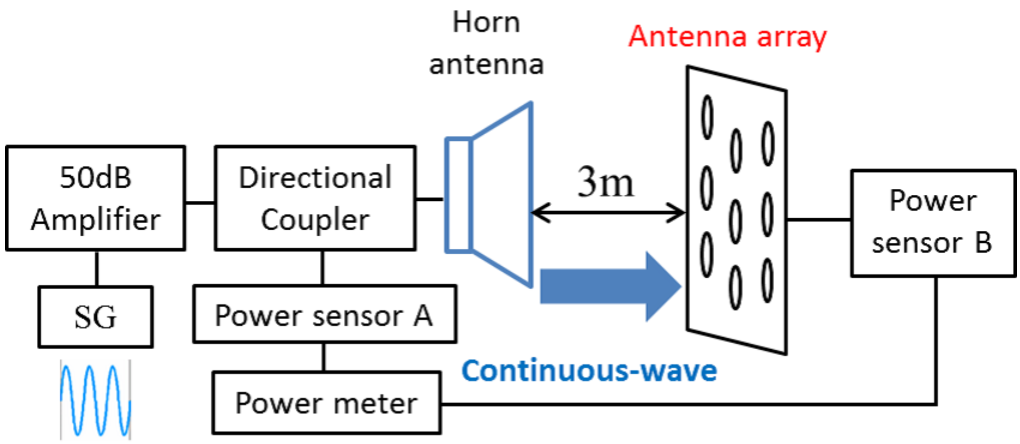

(a)

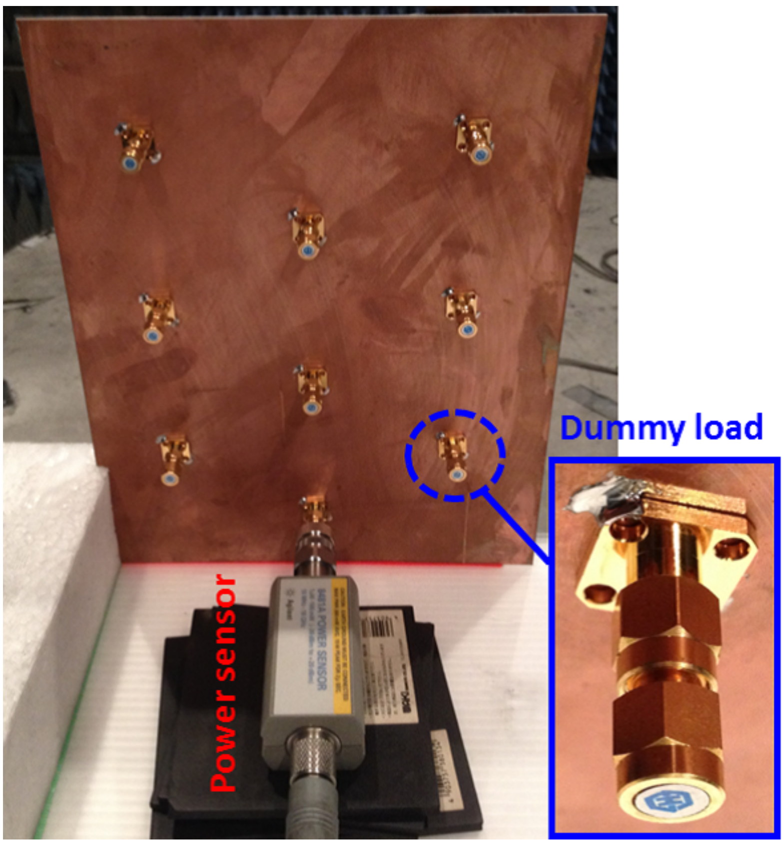

(b)

Figure 5.16: Experiment setup for measuring the receiving power of the antenna array. (a) Experiment setup. (b) Photograph of the antenna array setup. Power sensor measures the receiving power of each antenna with all other antennas connected to a 50 Ω dummy load.

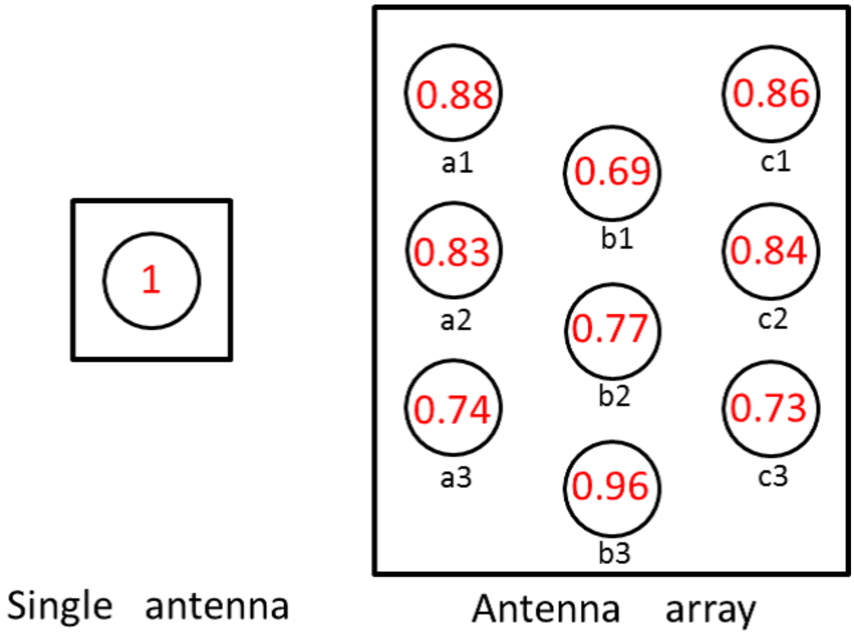

Figure 5.17: Relative power received by 9 antennas array and a single antenna.

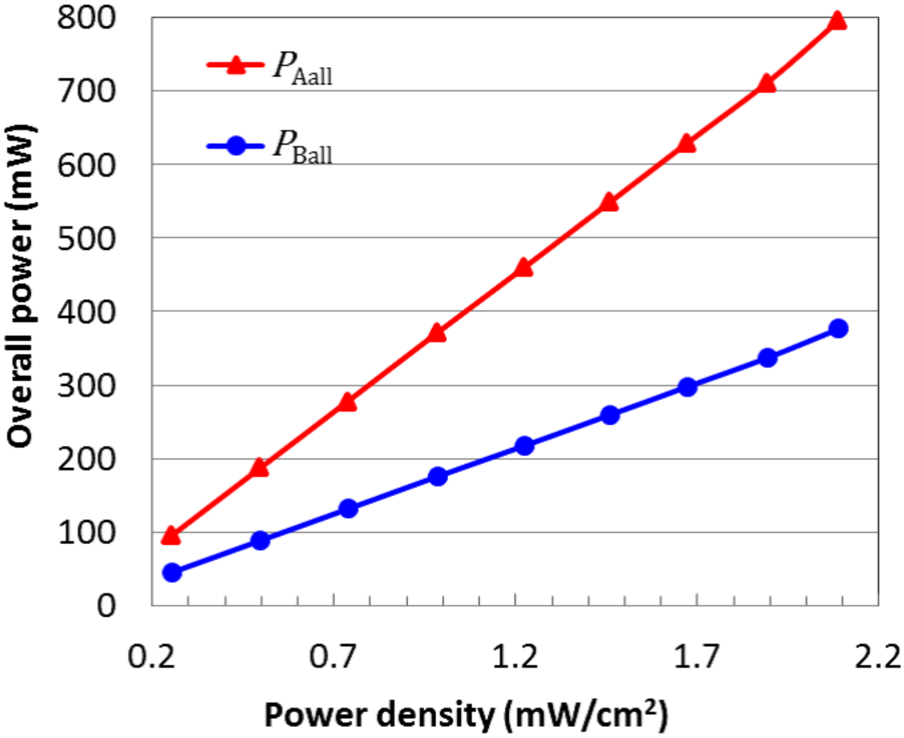

Figure 5.18: Overall powers received by 9 and 4 antennas array such as $P_{\rm Aall}$ and $P_{\rm Ball}$.

setup as Fig. 5.16, the compact power-receiving device and the DC motor. Of cause, the microwave power transmission distance is also 3 m. The power meter measures the input power of the transmission antenna through a power sensor. An ammeter and a voltmeter measure the input current I_{m} and the input voltage V_{m} of the DC motor, respectively. Firstly, we replace the DC motor with load resistances in Fig. 5.19 to test the compact power-receiving device using CW. Here, the overall efficiency η_{prd} is defined as the ratio of the power output from the buck-boost converter to the power received by the antenna array:

$$\eta_{\mathrm{prd}} = \frac{V_{\mathrm{m}} I_{\mathrm{m}}}{P_{\mathrm{rall}}} \times 100\,\%. \tag{5.2}$$

Figure 5.20(a) shows the overall efficiency η_{prd} of four types power-receiving devices such as 9AO, 9AI, 4BO, 4BI, for load resistances of 10 to 100 Ω with power density P_{den} of 0.98 mW/cm^2. As the load is changing from 30 to 100 Ω, the η_{prd} of the 9AO and 9AI are constant above 70 %, which is slightly higher than that of the 4BO and 4BI of 61 %. This is because that the P_{den} of 0.98 mW/cm^2 reaches the peak efficiency power level for A_rectifier while it is a lower level for B_rectifier according to the results in Chapter 5.4.2. As the load is below 30 Ω, the η_{prd} of four types are low due to the efficiency decrease of the buck-boost converter as shown in Fig. 5.12(a). Figure 5.20(b) shows the output voltage of the power-receiving device, which is also the input voltage of the DC motor V_{m}. Observe that the V_{m} of the 9AO and 9AI are higher than that of the 4BO and 4BI because the former exhibit a higher efficiency than the latter at the same input power and the same load resistance.

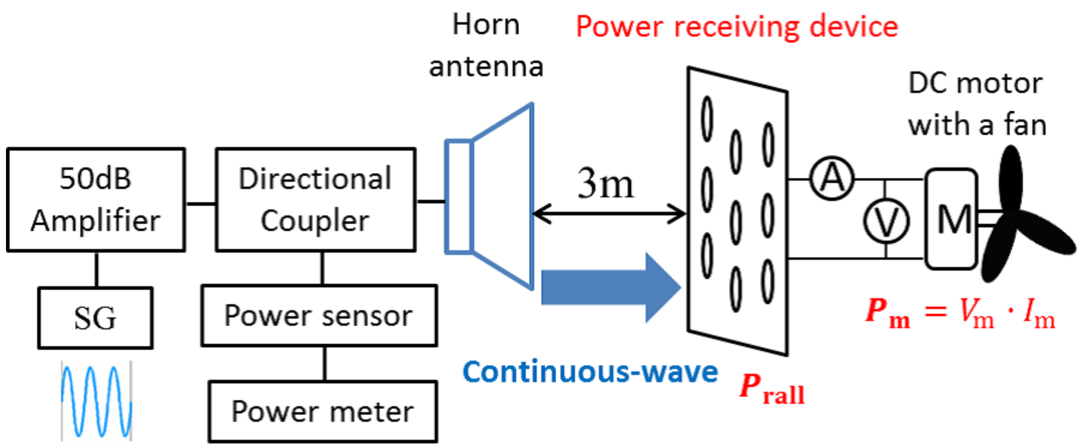

Figure 5.19: Experiment setup for driving DC motor by MPT using CW.

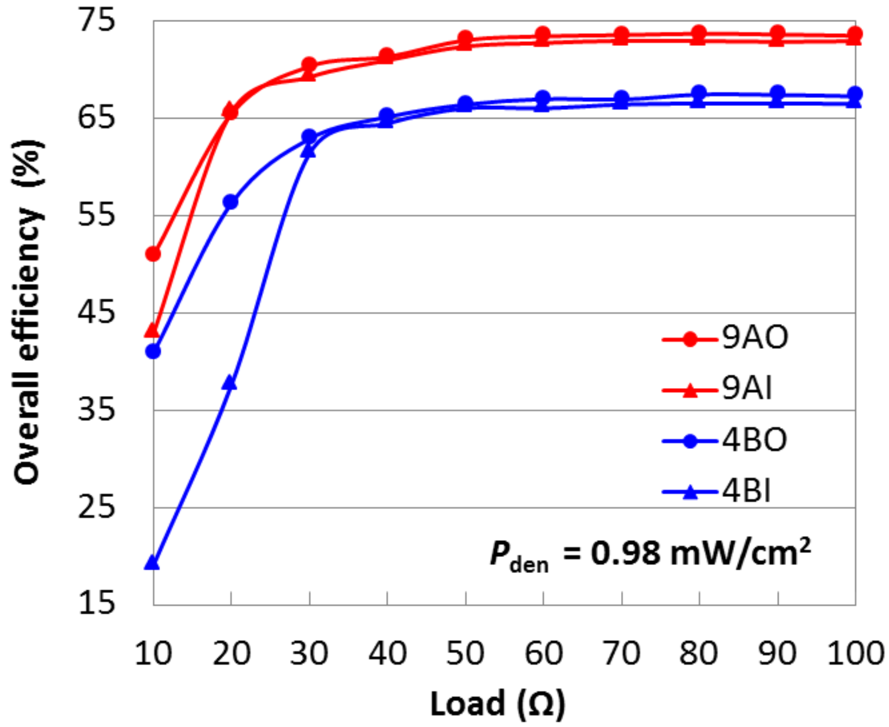

(a)

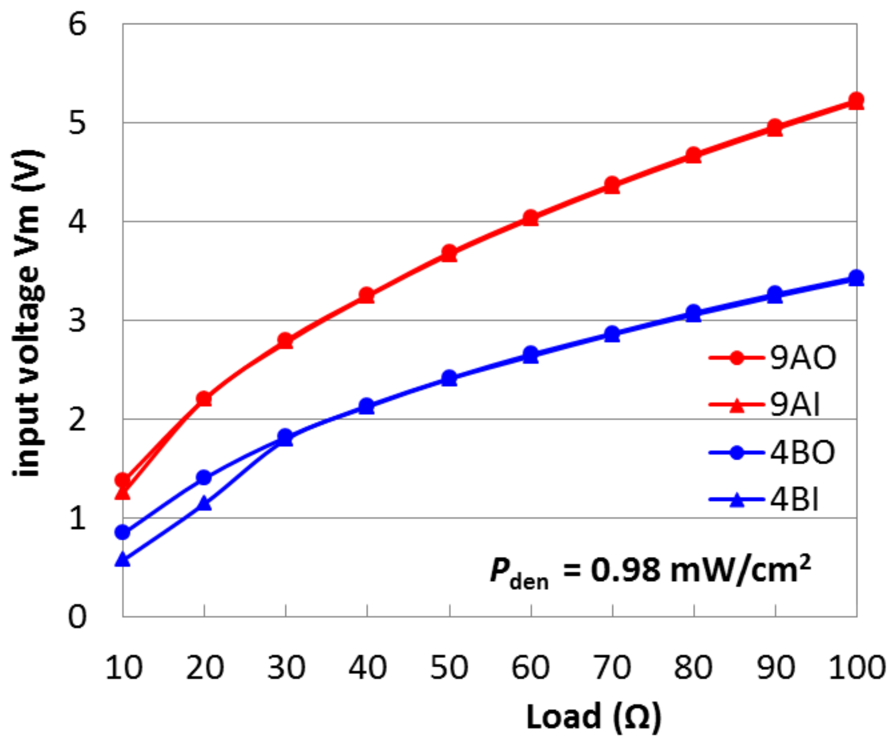

(b)

Figure 5.20: Comparison of measured overall efficiency and V_{m} for a fixed power density of 0.98 mW/cm^2. (a) Overall efficiency vs. load resistance. (b) V_{m} vs. load resistance.

Figure 5.21(a) shows the overall efficiency η_{prd} at load resistance of 30 Ω for P_{den} changing from 0.25 to 2.08 mW/cm^2. It is obvious that the η_{prd} of the O-type is higher than that of the I-type both in A_rectifier and B_rectifier for a lower power density level. Compared with 9AI, 9AO performs a higher efficiency when P_{den} is below 0.98 mW/cm^2 while it performs a lower efficiency as P_{den} over 0.98 mW/cm^2. However, compared with 4BI, 4BO performs a higher efficiency when P_{den} is below 0.98 mW/cm^2 while it performs approximately the same efficiency level with the 4BI when P_{den} is over 0.98 mW/cm^2. This is because that the A rectifier obtains a higher output voltage than B rectifier even at the same power density level resulting in efficiency decrease of the O-type converter when the power density is up to a higher level. As for 4BO, the output voltage of the rectifier B is not too large to lead to efficiency decrease of the converter even P_{den} is up to 2.08 mW/cm^2. As shown in Fig. 5.21(b), the V_{m} of the 4BI and 4BO are both below 3 V.

Next, we test the DC motor using MPT in CW power and the measurement overall efficiency results are shown in Fig. 5.22. Similarly, as the power density changing from 0.25 to 2.08 mW/cm^2, the four types overall efficiency are shown in Fig. 5.22(a). Compared with the case of 30 Ω load resistance, the η_{prd} of the 9AO and 9AI almost perform the same variation tendency while the η_{prd} of the 4BO and 4BI perform a little difference in the case of the DC motor. The reason is as following: The input load resistance of the motor R_{m} is increasing as the power density increases which leads to a higher V_{m} and the R_{m} is much larger than 30 Ω in the case of the DC motor. The larger R_{m} leads to V_{m} increase again which results in a higher efficiency of the 4BO because the efficiency of the O-type converter is increasing as the gate voltage increases. The overall efficiency of the 9AO is over 50 % as P_{den} is changing from 0.25 to 2.08 mW/cm^2 while the overall efficiency of the 9AI is over 61 % as P_{den} is changing from 0.5 to 2.08 mW/cm^2. As seen from Fig. 5.22(b), the V_{m} of the 4BO is slight higher than that of the 4BI. Compared with Fig. 5.21(b), V_{m} in Fig. 5.22(b) is higher because the R_{m} is much larger than 30 Ω. In conclusion, 9AO is better for a lower power density level as below 0.98 mW/cm^2 and 9AI is better for a medium power density level as below 1.9 mW/cm^2 and 4BO is better for a higher power density level as over 1.9 mW/cm^2.

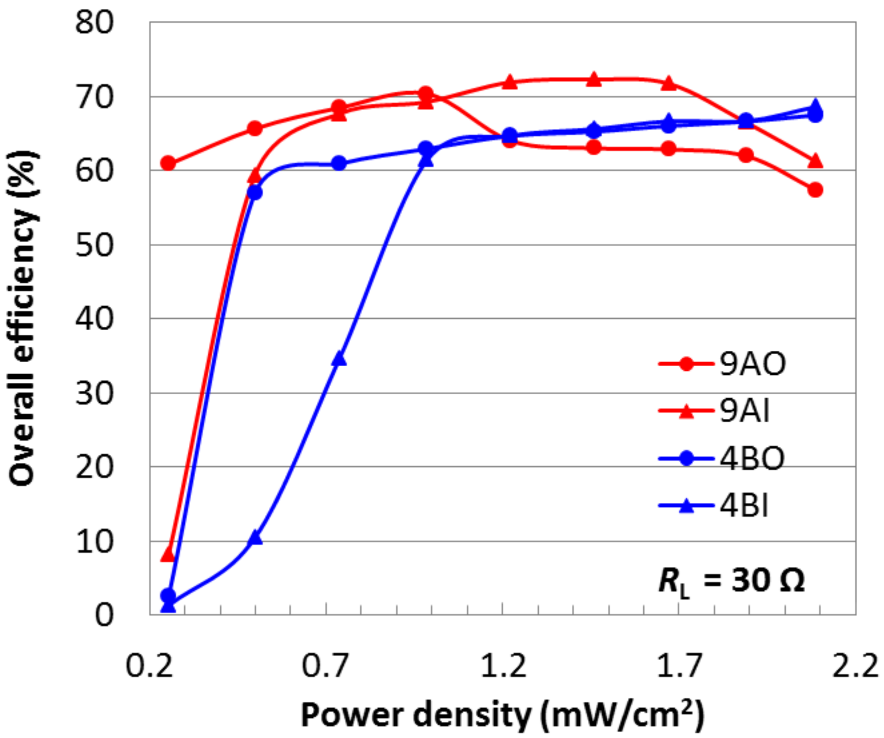

(a)

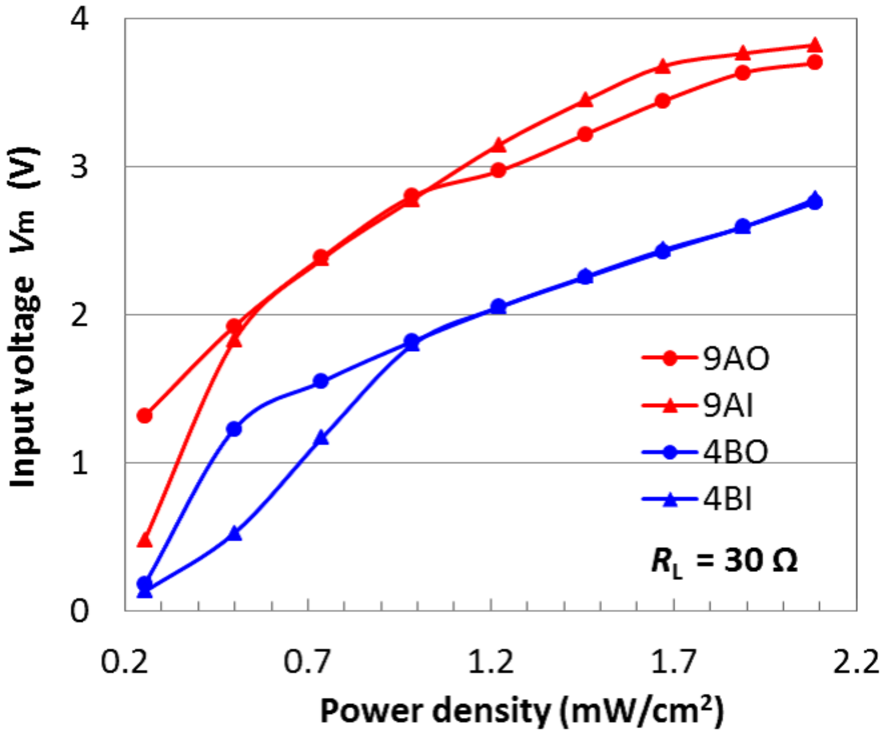

(b)

Figure 5.21: Comparison of measured overall efficiency and V_{m} for a fixed load resistance of 30 Ω. (a) Overall efficiency vs. power density. (b) V_{m} vs. power density.

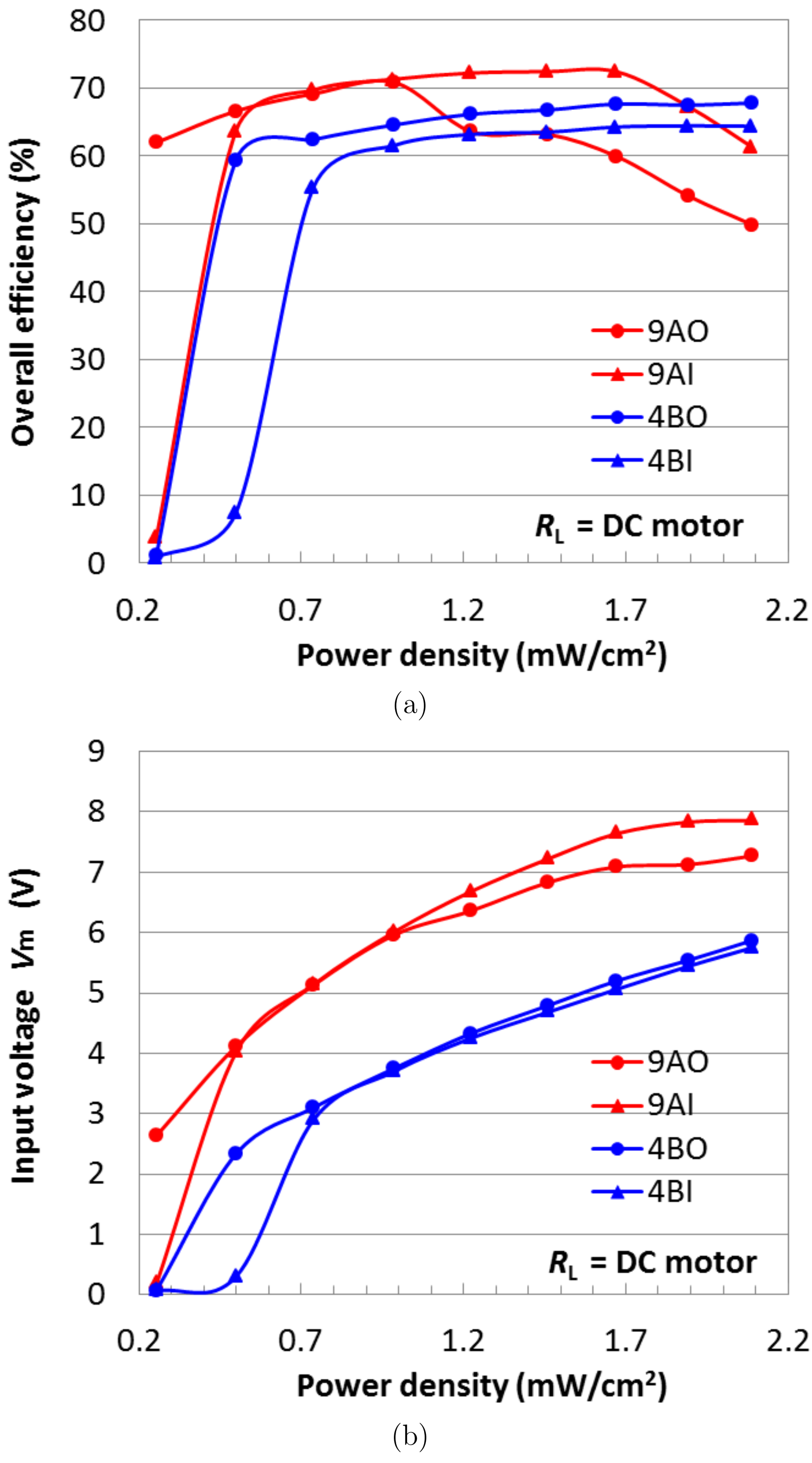

Figure 5.22: Comparison of measured overall efficiency with DC motor in CW power. (a) Overall efficiency vs. power density. (b) Input voltage of the motor vs. power density.

5.7 MPT Experiment Using Pulsed-wave

Recently, the simultaneous use of MPT and wireless communication has been proposed for ZigBee sensor devices and wireless LAN devices [32]-[34]. The authors proposed that scheduled pulsed-wave power transmission would eliminate or reduce interference between microwave power transmission and communication. Accordingly, we also test the compact power-receiving device using a pulsed-wave power transmission as shown in Fig. 5.23. Similarly, we test it using both load resistances and the DC motor. Here, we set the duty ratio of the pulsed-wave as D_{pw}. Then, the overall efficiency η'_{prd} presents as follows:

$$\eta'_{\mathrm{prd}} = \frac{V_{\mathrm{m}} I_{\mathrm{m}}}{P_{\mathrm{rall}} D_{\mathrm{pw}}} \times 100\,\%. \tag{5.3}$$

Figure 5.24(a) shows the overall efficiency of the 9AO versus the duty ratio of the pulsed-wave when it is loaded by a 30 Ω resistance or the DC motor. The measurement condition is that the power density is 0.98 mW/cm^2 and the pulsed-wave frequency is 25 kHz. Except for a duty ratio of 0.2, similar results are seen for both types of load. A bigger duty ratio leads to a higher input power so that the efficiency of the rectenna is increased. Therefore, the overall efficiency generally increases as the duty ratio is increasing from 0.2 to 1. Furthermore, the overall efficiency for driving the DC motor is over 44 % even though the duty ratio is widely changed from 0.2 to 1. Figure 5.24(b) shows the overall efficiency versus the frequency of the pulsed-wave for driving the DC motor at the power density of 0.98 mW/cm^2 and the duty ratio of 0.5. In this case, the overall efficiency performs a small variation, almost constant at 59 % in the frequency range of 0.33 to 41.7 kHz. As seen from the Eq. (5.3), the overall efficiency is independent of the frequency of the pulsed-wave, which is in agreement with the experiment results. Therefore, the proposed power-receiving device is also suitable for MPT in pulsed-wave power.

5.8 Summary

In this chapter, we conduct several experiments on driving a DC motor using MPT system both in CW and pulsed-wave. Firstly, the background of the study

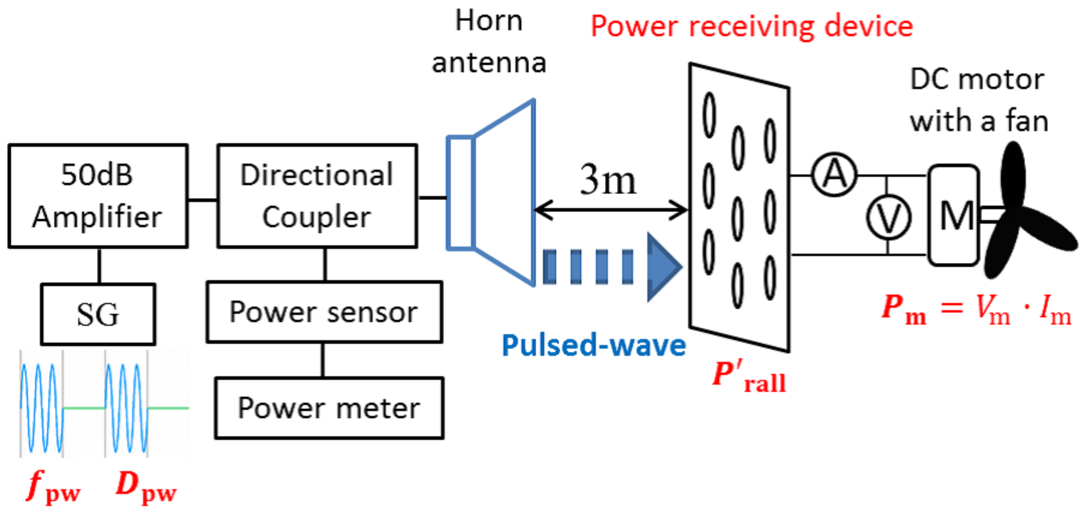

Figure 5.23: Experiment setup for driving DC motor by MPT using pulsed-wave.

that a DC motor is driven by MPT system is introduced. Then, as a test model, we choose a low-power DC motor and the input resistance of the motor is measured. Secondly, we design two antennas with different thicknesses of dielectric substrate of 1.6 and 0.8 mm, and the gain of two antennas are evaluated. We choose the thicker one as the receiving antenna because it exhibits a high gain. Thirdly, to make a compact rectenna array, we design two relatively smaller size rectifiers (A and B) with the measured peak conversion efficiencies of 80.8 % and 80 % at the optimal loads of 300 and 160 Ω, respectively. Fourthly, we design two improved buck-boost converters such as I-type and O-type converters according to the control-pulse oscillator supplied by the input voltage or the output voltage. Fifthly, we compact the antenna array and the rectifier array with the improved buck-boost converter in a multilayer substrate as a power-receiving device. Using those two rectifiers and two converters, there are four combinations of power-receiving devices such as 9AO, 9AI, 4BO, 4BI. Sixthly, we conduct several experiments on driving the DC motor with MPT in CW power using those four combination devices. The overall efficiency of the 9AO is above 60 % in the power density range of 0.25 to 0.98 mW/cm^2 and the overall efficiency of the 9AI is above 60 % in the power density range of 0.5 to 2.08 mW/cm^2. Finally, that the DC motor driven by MPT in pulsed-wave power using 9AO combination device is also tested. In the pulsed-wave case, the overall efficiency is above 44 % in the duty ratio range of 0.2 to 1 for a power density of 0.98 mW/cm^2. Additionally, at a fixed duty ratio of 0.5, the overall efficiency is almost constant at 59 % for the pulsed-wave frequency changing from 0.33 to 41.7 kHz. In conclusion, by

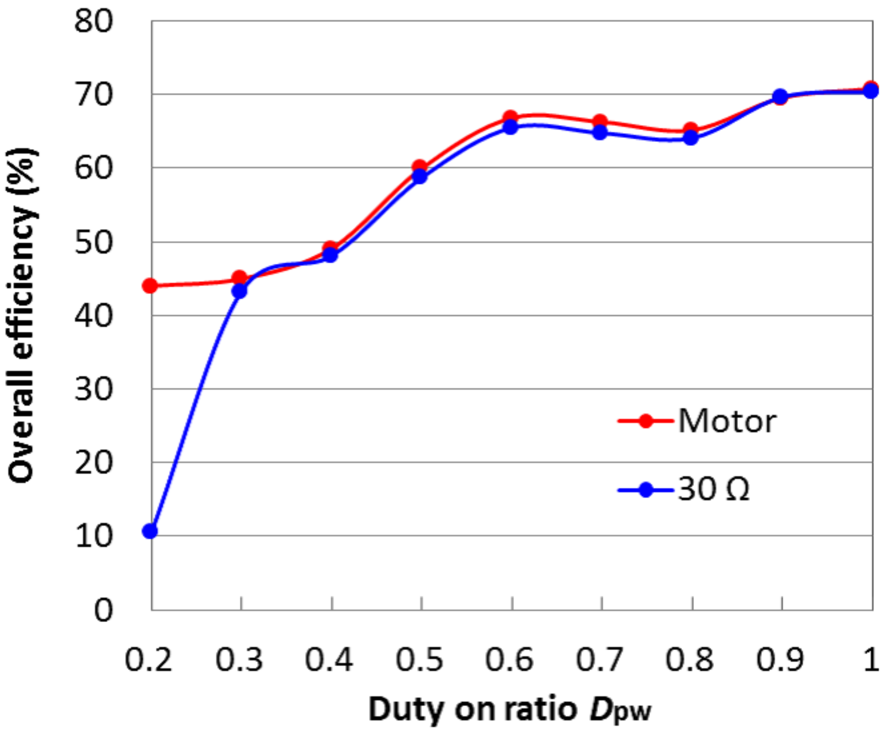

(a)

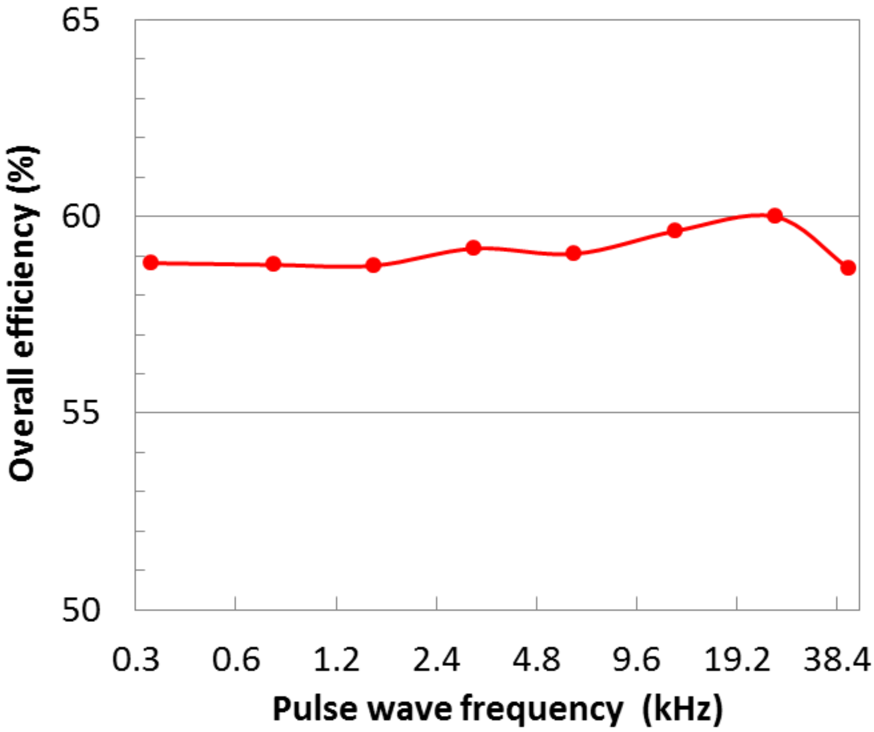

(b)

Figure 5.24: Measured overall efficiency in pulsed-wave mode. (a) Overall efficiency vs. duty ratio of the pulsed-wave. (b) Overall efficiency vs. frequency of the pulsed wave.

both CW and pulsed-wave power, the designed compact power-receiving device performs a relatively high efficiency for driving the DC motor. It is also expected to be valuable for other wireless power transmission applications.

Chapter 6

Conclusion

6.1 Summary and Conclusion

Many researchers are always perplexed by the problem of efficiency-load characteristics in rectenna. This thesis develops a rectenna adapted to ultra-wide load range for microwave power transmission system. We propose a novel resistance conversion DC-DC converter which plays an impedance matching role in rectenna. Connected to this special DC-DC converter, the rectenna seems to operate in a steady load resistance condition despite a varying load resistance connected to the converter. Consequently, when we set the input resistance of the DC-DC converter equal to the optimal load of a general rectenna, the rectenna can keep operating at the peak efficiency point independent of load resistances of the converter.

In Chapter 1, the history of wireless power transmission and microwave power transmission are introduced. An overview of rectenna researches in the world is summarized and the objectives of this thesis are expressed.

In Chapter 2, after giving an overview of efficiency improvement methods in rectenna researches and a comparison of impedance matching methods in WPT studies, we test a PWM controlled boost converter for impedance matching in rectifying circuit. We build a model of a RF-DC-DC circuit which consists of a rectifying circuit and a boost converter, and simulate it using harmonic balance analysis of ADS. Based on the simulation results, the RF-DC-DC circuit obtains a steady high overall efficiency (over 70 %) for a load range from 370 to 1300 Ω, which is wider than that of the rectifier at the same efficiency level. The boost converter connected to the RF-DC rectifier can limit the maximum reverse voltage of the rectifying diode under breakdown voltage at a wide range of load resistances. The simulation results clearly explain the principle of a DC-DC converter exhibiting as an impedance matching application for rectifying circuit. Therefore, an RF-DC-DC circuit is verified to be available for improving efficiency-load relation of rectenna in this chapter. However, the simulated PWM controlled boost converter just compresses a wide output load range into a narrow input resistance range in some degree. It is insufficient for impedance matching in rectenna.

In Chapter 3, from a new viewpoint, the input/output voltages and input/output resistances relationships of three basic topologies DC-DC converters are discussed. Based on the discussion results, a DCM inverting buck-boost converter, whose input resistance is independent of the load resistance or input power, is chosen for impedance matching in rectenna. We design a negative input voltage buck-boost converter to track the maximum efficiency of the rectifying circuit because the input resistance of the converter can match with the optimal load of the rectifying circuit. As expected, the measured input resistance of the buck-boost converter is approximately 133 Ω despite the changes of the load resistance and input power. Moreover, the measured efficiency of the converter exceeds 80 % for a wide range of loads or input powers. Then we design a rectifying circuit with negative output voltage and obtain a maximum RF-DC conversion efficiency of 79.2 % at an optimal load of 160 Ω with the 2.45 GHz microwave power of 82 mW. Next, we verify that the proposed converter successfully tracks the maximum efficiency of the rectifying circuit. The conversion efficiency of the rectifier is approximately steady at 75 %, despite the load resistance varying from 100 to 5000 Ω for an input microwave power of 82 mW. This means that the maximum power tracking efficiency is over 94 %, compared to the maximum efficiency of 79.2 % at the optimal load. Additionally, the overall efficiency of the RF-DC-DC circuit is approximately steady over 60 %, despite the load resistance changing from 100 to 5000 Ω. According to the experimental results, the proposed RF-DC-DC circuit is an effective MPPT method for low power rectenna. However, the proposed buck-boost converter is difficult for practical applications because of the requirement of an extra DC power supply. Additionally, owing to the loss of the buck-boost converter, the overall efficiency of the RF-DC-DC circuit is much lower than the maximum efficiency of the general rectifying circuit. Therefore, it is necessary to improve the efficiencies both of the rectifying circuit and the converter.

In Chapter 4, firstly, a relatively high-efficiency rectifying circuit is designed and measured. The measured peak efficiency is 82.5 % at the optimal load of 190 Ω for an input RF power of 80 mW. Secondly, we design a self-powered non-inverting DCM buck-boost converter. Compared with the buck-boost converter designed in Chapter 3, it is much superior in capability of handling variable load. Based on the simulation and experimental results, the input resistance of the converter is almost constant at 190 Ω despite the changes of load resistances and input powers, which is in accordance with the theoretical analysis. Moreover, the measured efficiency of the converter exceeds 83 % for a wide load range of 200 Ω to 10 kΩ, and the input voltage is boosted by the buck-booster converter. Finally, we conduct an experiment on RF-DC-DC circuit consisting of the self-powered buck-boost converter and the rectifier. The conversion efficiency of the rectifier is approximately steady at 80 % despite the load resistance varying from 200 Ω to 10 kΩ for an input microwave power of 80 mW. Compared with the peak efficiency of 82.5 % at the optimal load, the maximum power tracking efficiency is over 97 %. Furthermore, the overall efficiency of the RF-DC-DC circuit is constant over 66 % in this ultra-wide load range of 200 Ω to 10 kΩ (a ratio of 1:50). On the other hand, for a fixed load of 800 Ω, the overall efficiency of the RF-DC-DC circuit is also constant over 66 % for the input power of 40 to 120 mW. According to the experimental results, the proposed self-powered RF-DC-DC circuit exhibits a high efficiency in an ultra-wide load range.

In Chapter 5, we conduct several experiments on driving a DC motor using MPT system both in CW and pulsed-wave. Firstly, the background of the study that a DC motor is driven by MPT system is introduced. Then, as a test model, we choose a low-power DC motor and measure the input resistance of it. Secondly, we design two types antenna with dielectric substrate's thickness of 1.6 and 0.8 mm and evaluate them. We choose the thicker one as the receiving antenna because it exhibits a high gain. Thirdly, to make a compact rectenna array, we design two relatively smaller size rectifiers (A and B) with the measured peak conversion efficiencies of 80.8 % and 80 % at the optimal loads of 300 and 160 Ω, respectively. Fourthly, we design two improved buck-boost converters such as I-type and O-type according to the control-pulse oscillator supplied by the input voltage or the output voltage. Fifthly, we compact antenna array and rectifier array with the improved buck-boost converter in a multilayer substrate as a power-receiving device. Using those two rectifiers and two converters, there are four combinations of power-receiving devices such as 9AO, 9AI, 4BO, 4BI. Sixthly, we conduct several experiments on driving the DC motor with MPT in CW power using those four combination devices. The overall efficiency of the 9AO is above 60 % in the power density range of 0.25 to 0.98 mW/cm^2 and the overall efficiency of the 9AI is above 60 % in the power density range of 0.5 to 2.08 mW/cm^2. Finally, we also test the DC motor driven by MPT in pulsed-wave power using 9AO combination device. In the pulsed-wave case, the overall efficiency is above 44 % in the duty ratio range of 0.2 to 1 for a power density of 0.98 mW/cm^2. Additionally, at a fixed duty ratio of 0.5, the overall efficiency is almost constant at 59 % for the pulsed-wave frequency changing from 0.33 to 41.7 kHz. In conclusion, by both CW and pulsed-wave power, the designed compact power-receiving device performs a relatively high efficiency for driving a load resistance variable device such as a DC motor.

6.2 Thesis Contributions

The contributions of this thesis can be summarized as follows: (1) A relatively high-efficiency rectifier for low-power (80 mW) is developed in Chapter 4. (2) A relatively small size and high-efficiency rectifier for low-power (50 mW) is developed in Chapter 5. (3) The input/output resistance relationships of three topologies DC-DC converters in both CCM and DCM are discussed in Chapter 3, which is expected to be a valuable reference for impedance matching in WPT system. (4) A self-powered buck-boost converter as a resistance conversion circuit whose input resistance is constant and independent of load resistances or input powers. It has been successfully used in rectenna for maximum power point tracking in Chapter 4. It is also expected to be used in other WPT system and energy harvesting system because its constant input resistance characteristics are independent of the operating frequency. (5) A rectenna adapted to pulsed-wave MPT system is firstly discussed here in Chapter 5 and it is expected to be used in coexistent power transmission and communication system. (6) A power-receiving device is developed to effectively drive a DC motor by MPT in Chapter 5, which will be a good reference for researches on airplane or robot powered by WPT system.

6.3 Suggestion for Future Work

This thesis has solved several issues in MPT system. However, a lot work remains to be done and some of the possible future research directions are suggested as follows: (1) In order to effectively simulate the rectifier, a precise HF diode model in ADS or other simulator such as microwave office is required. (2) Because of the supplied voltage limitation from the control-pulse circuit, the input RF power of the RF-DC-DC circuit is limited in the power range of 30 to 140 mW. It is expected to be improved for a much more wide power range. (3) It is necessary to develop a high efficiency (up to 95 %) of the buck-boost converter which can reduce the loss caused by the converter to make the overall efficiency of the RF-DC-DC circuit close to the peak efficiency of the general rectifying circuit. (4) A rectenna, adapted to much small load resistance such as the range of 100 mΩ to 10 Ω, is necessary for charging a battery or driving a high power motor. (5) The impedance conversion buck-boost converter is also expected to be used for other WPT system such as inductive coupling and resonant coupling system. (6) RF harvesting technology and multi-method of energy harvesting technologies are expected to be developed for the application of powering sensor network nodes.

Bibliography

[1] Tesla, N., "The Transmission of Electrical Energy Without Wires," *The Thirteenth Anniversary Number of the Electrical World and Engineer.* Mar. 1904.

[2] Tesla, N., "Experiments with Alternate Current of High Potential and High Frequency," *Journal of the Institution of Electrical Engineers.* Vol.21, No.97, Apr. 1892.

[3] Brown, W. C., "The history of the development of the rectenna," in *Proc. SPS Microwave Systems Workshop at JSC-NASA,* pp.271-280, 1980.

[4] Brown, W. C., "The history of power transmission by radio waves," *IEEE Trans. Microw. Theory Tech.,* Vol.32, pp.1230-1242, Sept. 1984.

[5] Brown, W. C., "An experimental microwave-powered helicopter," *IRE International Convention Record,* Vol.13, pp.225-235, Mar. 1966.

[6] Glaser, P. E., "Power from the Sun: Its Future," *Science,* Vol.162, No.3856, pp.857-886, Nov. 1968

[7] Matsumoto, H., "Microwave Power Transmission from Space and Related Nonlinear Plasma Effects," *The Radio Science Bulletin,* No.273, pp.11-35, 1995

[8] Matsumoto, H., "Research on Solar Power Station and Microwave Power Transmission in Japan: Review and Perspectives," *IEEE Microwave Magazine,* pp.36-45, Dec. 2002

[9] Matsumoto, H., Hirata, H., Hashino, Y. and Shinohara, N., "Theoretical Analysis of Nonlinear Interaction of Intense Electromagnetic Wave and Plasma Waves in the Ionosphere," *Electronics and Communications in Japan,* Part3, Vol.78, No.11, pp.104-114, Nov. 1995.

[10] Shinohara, N., "Power without wires," *IEEE Microw. Mag.,* Vol.12, No.7, pp.S64-S73, Dec. 2011.

[11] Kurs, A., Karalis, A. Moffatt, R., Joannopoulos, J. D., Fisher, P. and Soljacic, M., "Wireless power transfer via strongly coupled magnetic resonances," *Science,* Vol.317, No.5834, pp.83-86, July 2007.

[12] Ogawa, K., Ozaki, K., Yamada, M. and Honda, K., "High Efficiency Small-Sized Rectenna Using a High-Q LC Resonator for Long Distance WPT at 950 MHz," in *Proc. IMWS-IWPT2012,* Kyoto, pp.255-258, May 2012.

[13] Suh, Y. H. and Chang, K., "A high-efficiency dual-frequency rectenna for 2.45- and 5.8-GHz wireless power transmission," *IEEE Trans. Microw. Theory Tech.,* Vol.50, No.7, pp.1784-1789, July 2002.

[14] Shinohara, N., "Beam efficiency of wireless power transmission via radio waves from short range to long range," *J. Electromagn. Eng. Sci.,* Vol.10, No.4, pp.224-230, Dec. 2010.

[15] Fujino, Y., Fujita, M., Kaya, N., Kunimi, S., Ishii, M., Ogihata, N., Kusaka, N. and Ida, S., "A Dual Polarization Microwave Power Transmission System for Microwave propelled Airship Experiment," in *Proc. of ISAP ' 96,* Chiba, Japan, pp.393-396, 1996.

[16] Lee, W. Y., Huh, J., Choi, S. Y., Thai, X. V., Kim, J. H., Al-Ammar, E. A., El-Kady, M. A. and Rim, C. T., "Finite-width magnetic mirror models of mono and dual coils for wireless electric vehicles," *IEEE Trans. Power Electron.,* Vol.28, No.3, pp.1413-1428, Mar. 2013.

[17] Matias, R., Cunha, B., Martins, R., "Modeling Inductive Coupling for Wireless Power Transfer to Integrated Circuits," in *Proc. WPTC2013,* Perugia, Italy, pp.198-201, May 2013.

[18] Waffenschmidt, E. and Staring, T., "Limitation of Inductive Power Transfer for Consumer Applications," in *Proc. 13th Eur. Conf. on Power Electron. App.,(EPE 2009),* Barcelona, Spain, pp.1-10,Sept. 2009.

[19] Lee, S. H. and Lorenz, R. D., "Development and Validation of Model for 95 % Efficiency, 220 W Wireless Power Transfer over a 30 cm Air-gap," in *Proc. 2010 IEEE Energy Conversion Congress and Exposition (ECCE),* Atlanta, GA, pp.885-892, Sept. 2010.

[20] Koh, K. E., Beh, T. C., Imura, T., Hori, Y., "Impedance Matching and Power Division Using Impedance Inverter for Wireless Power Transfer via Magnetic Resonant Coupling," *IEEE Trans. Ind. Appl.,* Vol.50, No.3, pp.2061-2070, Oct. 2013.

[21] Cheon, S., Kim, H., Kang, S. Y., Lee, M. L., Lee, J. M. and Zyung, T., "Circuit-model-based analysis of a wireless energy-transfer system via coupled magnetic resonances," *IEEE Trans. Ind. Electron.,* Vol.58, No.7, pp.2906-2914, July 2011.

[22] Moriwaki, Y., Imura, T. and Hori, Y., "Basic study on reduction of reflected power using DC/DC converters in wireless power transfer system via magnetic resonant coupling,"in *IEEE 33rd Int. Telecommun. Energy Conf.,* Amsterdam, Netherlands, pp.1-5, Oct. 2011.

[23] Fu, M., Zhang, T., Zhu, X. and Ma, C., "A 13.56 MHz wireless power transfer system without impedance matching networks," in *Proc. WPTC2013,* Perugia, Italy, pp.222-225, May 2013.

[24] Shinohara, N., Wireless Power Transfer via Radiowaves, Wiley-ISTE, Jan. 2014.

[25] Shinohara, N., "Beam Control Technologies With a High-Efficiency Phased Array for Microwave Power Transmission in Japan," *Proceeding of IEEE,* Vol.101, No.6, pp.1448-1463, June 2013.

[26] Iwashimizu, M., Mitani, T., Shinohara, N., Sasaki, G., Hiraoka, K., Matsuzaki, K. and Yonemoto, K., "Study on direction detection in a microwave power transmission system for a Mars observation airplane," in *Proc. WPTC2014,* Jeju, Korea, pp.146-149, May 2014.

[27] Hasegawa, N., Yoshida, S., Furuta, S., Moriguchi, Y. and Kawasaki, S., "The 20W C-Band Lightweight GaN HPA for Wireless Sensor and Power Transmission in a Spacecraft," in *Proc. WPTC2014,* Jeju, Korea, pp.21-23, May 2014.

[28] Takano, T., "Wireless Power Transfer from Space to Earth," *IEICE Trans. Commun.,* Vol.E96-C, No.10, pp.1218-1226, Oct. 2013.

[29] Sasaki, S., Takaaki, K., Maki, K., "Microwave Power Transmission Technologies for Solar Power Satellites," *Proc. IEEE,* Vol.101, No.6, pp.1438-1447, June 2013.

[30] Yoshino, J., Shinohara, N. and Mitani, T., "Estimation of beam forming accuracy for satellite experiment toward SPS," in *Proc. WPTC2014,* Jeju, Korea, pp.28-31, May 2014.

[31] Ishikawa, T. and Shinohara, N., "Study on panel gradient estimation system for panel-structure solar power satellite/station," in *Proc. WPTC2013,* Perugia, Italy, pp.143-146, May 2013.

[32] Imoto, N., Yamashita, S., Ichihara, T., Yamamoto, K., Nishio, T., Morikura, M. and Shinohara, N., "Experimental Investigation of Co-channel and Adjacent Channel Operations of Microwave Power and IEEE 802.11g Data Transmissions," in *IEICE Trans. Commun.,* Vol.E97-B, No.9, pp.1835-1842, Sept. 2014.

[33] Yamashita, S., Imoto, N., Ichihara, T., Yamamoto, K., Nishio, T., Morikura, M. and Shinohara, N., "Implementation and Feasibility Study of Co-channel Operation System of Microwave Power Transmissions to IEEE 802.11-Based Batteryless Sensor," *IEICE Trans. Commun.,* Vol.E97-B, No.9, pp.1843-1852, Sept. 2014.

[34] Shinohara, N. and Ichihara, T., "Coexistence of Wireless Power Transfer via Microwaves and Wireless Communication for Battery-less ZigBee Sensors," in *Int. Sym. on. EMC'14,* Tokyo, Japan, 15A-H7, May 2014.

[35] Goto, H., Shinohara, N., Mitani, T., Dosho, H. and Mizuno, M., "Study on microwave power transfer to sensors in car engine compartment," in *Proc. WPTC2014,* Jeju, Korea, pp.150-153, May 2014.

[36] Shinohara, N., Kubo, Y., Tonomura, H., "Wireless charging for electric vehicle with microwaves," in *Proc. 3rd Int. Electric Drives Production Conf. (EDPC),* Nuremberg, Germany, pp.1-4, Oct. 2013.

[37] Shibata, T., Aoki, Y., Otsuka, M., Idogaki, T. and Hattori, T., "Microwave Energy Transmission System for Microrobot," *IEICE Trans. Electr.,* Vol.E80-C, No.2, pp.303-308, Feb. 1997.

[38] Fujino, Y., Ito, T., Fujita, M., Kaya, N., Matsumoto, H., Kawabata, K., Sawada, H. and Onodera, T., "A driving test of a small DC motor with a rectenna array," *IEICE Trans. Commun.,* Vol.E77-B, No.4, pp.526-528, Apr. 1994.

[39] Fujino, Y., Fujita, M., Y., Ito, Matsumoto, H., Kaya, N., Fujiwara, T. and Sato, T., "Driving test of a small DC motor with a rectenna array and MILAX flight experiment (in Japanese)," *Review of the Communications Research Laboratory,* Vol.44, No.3, pp.113-120, Sept. 1998.

[40] Karacolak, T., Hood, A. Z. and Topsakal, E., "Design of a Dual-Band Implantable Antenna and Development of Skin Mimicking Gels for Continuous Glucose Monitoring," *IEEE Trans. Microw. Theory Tech.,* Vol.56, No.4, pp.1001-1008, Apr. 2008.

[41] Hagerty, J. A., Helmbrecht, F., McCalpin, W., Zane, R. and Popovic, Z., "Recycling ambient microwave energy with broadband antenna arrays," *IEEE Trans. Microw. Theory Techn.,* Vol.52, No.3, pp.1014-1024, Mar. 2004.

[42] Paing, T., Morroni, J., Dolgov, A., Shin, J., Brannan, J., Zane, R. and Popovic, Z., "Wirelessly powered wireless sensor platform," in *Proc. 37th IEEE Eur. Microw. Conf.,* Munich, Germany, pp.241-244, Oct. 2007.

[43] Dolgov, A., Zane, R. and Popovic, Z., "Power Management System for Online Low Power RF Energy Harvesting Optimization," *IEEE Trans. Circuits Syst.,* Vol.57, No.7, pp.1802-1811, July 2010.

[44] Yoo, T. W. and Chang, K., "Theoretical and Experimental Development of 10 and 35 GHz Rectennas," *IEEE Trans. Microw. Theory Tech.,* Vol. 40, No.6, pp.1259-1266, June 1992.

[45] Nihon Dengyo Kosaku Co., Ltd. Product Information: http://www.den-gyo.com/english/products/index.html (90 % efficiency is described on website in Japanese : http://www.den-gyo.com/special01/01.html)

[46] Yo, T. C., Lee, C. M., Hsu, C. M. and Luo, C. H., "Compact circularly polarized rectenna with unbalanced circular slots," *IEEE Trans. Antennas Propag.,* Vol.56, No.3, pp.882-886, Mar. 2008.

[47] Chou, J. H., Lin, D. B., Weng, K. L. and Li, H. J., "All Polarization Receiving Rectenna With Harmonic Rejection Property for Wireless Power Transmission," *IEEE Trans. Antennas Propag.,* Vol.62, No.10, pp.5242-5249, Oct. 2014.

[48] Douyere, A., Lan Sun Luk, J. D. and Alicalapa, F., "High efficiency microwave rectenna circuit: modelling and design," *Electr. Lett.,* Vol.44, No.24, pp.1409-1410, Nov. 2008.

[49] Takhedmit, H., Cirio, L., Merabet, B., Allard, B., Costa, F., Vollaire, C. and Picon, O., "Efficient 2.45 GHz rectenna design including harmonic rejecting rectifier device," *Electr. Lett.,* Vol.46, No.12, pp.811-812, June 2010.

[50] Park, J. Y., Han, S. M. and Ito, T., "A rectenna design with harmonic-rejecting circular-sector antenna," *IEEE Antennas and Wireless Propag. Lett.,* Vol.3, No.1, pp.52-54, Dec. 2004.

[51] Umesao, N., Ida, J., Kawabata, K., Tashino, S., Noguchi, K. and Itoh, K., "High Efficiency Rectification by SOI based Gate Controlled Diode for RF Energy Harvesting," in *Proc. WPTC2013,* Perugia, Italy, pp.91-94, May 2013.

[52] Kotani, K. and Ito, T., "Self-Vth-Cancellation High-Efficiency CMOS Rectifier Circuit for UHF RFIDs," *IEICE Trans. Electr.,* Vol.E92-C, No.1, pp.153-160, Jan. 2009.

[53] Yehui, H., Leitermann, O., Jackson, D. A., Rivas, J.M. and Perreault, D.J., "Resistance compression networks for radio-frequency power conversion," *IEEE Trans. Power Electron.,* Vol.22, No.1, pp.41-53, Jan. 2007.

[54] Godoy, P. A., Perreault, D. J. and Dawson, J. L., "Outphasing energy recovery amplifier with resistance compression for improved efficiency," *IEEE Trans. Microw. Theory Techn.,* Vol.57, No.12, pp.2895-2906, Dec. 2009.

[55] Xu, J. and Ricketts, D. S., "An efficient, watt-level microwave rectifier using an impedance compression network (ICN) with applications in outphasing energy recovery systems," *IEEE Microw. Compon. Lett.,* Vol.23, No.10, pp.542-544, Oct. 2013.

[56] Georgiadis, A., Collado, A. and Niotaki, K., "Dual-band electromagnetic energy harvester with resistance compression network," in *URSI 2014 General*

Assembly and Scientific Symposium (GASS), Beijing, China, pp.1-4, Aug. 2014.

[57] Falkenstein, E., Roberg, M. and Popovic, Z., "Low-Power Wireless Power Delivery," *IEEE Trans. Microw. Theory Techn.,* Vol.60, No.7, pp.2277-2286, July 2012.

[58] Gutmann, R. J. and Borrego, J. M., "Power Combining in an Array of Microwave Power Rectifiers," *IEEE Trans. Microw. Theory Techn.,* Vol. MTT-27, No.12, pp.958-968, Dec. 1979.

[59] Hatano, K., Shinohara, N., Mitani, T., Nishikawa, K., Seki, T. and Hiraga, K., "Development of Class-F Load Rectennas," in *Proc. IMWS-IWPT2011,* Kyoto, Japan, pp.251-254, May 2011.

[60] Avago HSMS286x series diode datasheet. http://www.efo.ru/components/avago/catalog/files/pdf/5989-4023EN.pdf

[61] Richelli, A., Colalongo, L., Quarantelli, M., Carmina, M. and KovacsVajna, Z. M., "A 0.2-1.2 V DC-DC Boost Converter for Power Harvesting Applications," *IEEE Transactions on power electronics,* Vol.24, No.6, pp.1541-1546, June 2009.

[62] Skvarenina, T. L., The Power Electronics Handbook,CRC press, Boca Raton London New York Washington, D.C., 2002, chap. 2.

[63] Erickson, R. W., DC-DC Power Converters, Article in Wiley Encyclopedia of Electrical and Electronics Engineering, 2004

[64] Kazimierczuk, M. K. and Massarini, A., "Feedforward control of DC-DC PWM boost converter," *IEEE Trans. Circuits Syst. I, Fundam.Theory Appl.,* Vol.44, No.2, pp.143-148, Feb. 1997.

[65] Chen, H. M., Chang, R. C. and Lei, P. S., "An exact, high-efficiency PFM DC-DC boost converter with dynamic stored energy," in *15th IEEE Int. Conf. on Electron., Circuits and Syst.,* pp.622-625, Aug. 2008.

[66] Wang, J., Gong, W. C. and He, L. N., "Design and implementation of high-efficiency and low-power DC-DC converter with PWM/PFM modes," in *7th Int. Conf. on ASIC,* Guilin, China, pp.596-599, Oct. 2007.

[67] Rashid, M. H., Power Electronics Handbook, ACADEMIC PRESS, A Harcourt Science and Technology Company, 2001, chap. 13.

[68] Roberg, M., Reveyrand, T., Ramos, I., Falkenstein, E. A. and Popovic, Z., "High-Efficiency Harmonically Terminated Diode and Transistor Rectifiers," *IEEE Trans. Microw. Theory Techn.,* Vol.60, No.12, pp.4043-4052, Dec. 2012.

[69] Honjo, K., "A simple circuit synthesis method for microwave class-F ultra-high-efficiency amplifiers with reactance-compensation circuits," *Solid State Electron.,* Vol.44, No.8, pp.1477-1482, Aug. 2000.

[70] Shinohara, N., Solar Power Satelite/Station, Ohmsha press, 2012, Chapter 3.2.4.

[71] LTC6992 Data Sheet, Linear Technology.
http://cds.linear.com/docs/jp/datasheet/j69921234fc.pdf.

[72] LTC6900 Data Sheet, Linear Technology.
http://cds.linear.com/docs/en/datasheet/6900fa.pdf.

[73] FDS6298 Data Sheet, Fairchild Semiconductor.
https://www.fairchildsemi.com/datasheets/FD/FDS6298.pdf.

[74] Jet Propulsion Laboratory (JPL), NASA.
http://mars.nasa.gov/mer/overview/

[75] Sayuri, S., Yoshiro, K., Masatsugu, O., Ryo, M., Tomohiro, O., Shigeo, K., Satoshi, Y. and Naoki, H., "Basic Research on Microwave Power Transmission to Exploration Rover (in Japanese)," in *IEICE Technical Report,* WPT2013-41, Mar. 2014.

[76] RF-500TB. Mabuchi Motor. http://www.mabuchi-motor.co.jp
/cgi-bin/catalog/j_catalog.cgi?CAT_ID=rf_500tb.

[77] Garg, R., Bhartia, P., Bahl, I. and Ittipiboon, A., Mictrostrip Antenna Design Handbook, Artech House, 2001.

[78] Salman, J. W., Ameen, M. M. and Hassan, L. S. O., "Effects of the Loss Tangent, Dielectric Substrate Permittivity and Thickness on the Performance of Circular Microstrip Antennas," *Journal of Engineering and Development,* Vol.10, No.1, pp.1-13, Mar. 2006.

[79] Derneryd, A. G., "Analysis of the Microstrip-Disk Antenna Elements," *IEEE Trans. on Antennas and Propagation,* Vol.AP-27, No.5, pp.660-664, Sept. 1979.

[80] Shinohara, N. and Matsumoto, H., "A Study of Dependence of DC Output of Rectenna Array on the Method of Inter-connection of Its Array Element," *IEEJ Trans. on Power and Energy,* Vol.117-B, No.9, pp.1254-1261, Sept. 1997.

Publication List

Related Publications

Major Publications

1. Huang, Y., Mitani, T., Ishikawa, T. and Shinohara, N., "Experiment on Driving a Low-power DC Motor by Microwave Power Transmission in Continuous-wave and Pulsed-wave," *IEICE Transactions on Electronics* (conditional acceptance).

2. Huang, Y., Shinohara, N. and Mitani, T., "Development of a Rectifying Circuit of Rectenna Adapted to Ultra-Wide Load Range with Self-Powered DC-DC Converter," *IEICE Transactions on Electronics C,* Vol.J97-C, No.9, pp.342-351, Sept. 2014 (in Japanese).

3. Huang, Y., Shinohara, N. and Mitani, T., "A Constant Efficiency of Rectifying Circuit in an Extremely Wide Load Range," *IEEE Trans. Microw. Theory Techn.,* Vol.62, No.4, pp.986-993, April 2014.

4. Yamashita, S., Sakaguchi, K., Huang, Y., Yamamoto, K., Nishio, T., Morikura, M. and Shinohara, N., "Rate Adaptation Based on Exposure Assessment Using Rectenna Output for WLAN Station Powered with Microwave Power Transmission," *IEICE Transactions on Communication* (under review).

Proceedings of International Conference

1. Sakaguchi, K., Yamashita, S., Huang, Y., Yamamoto, K., Nishio, T., Morikura, M. and Shinohara, N., "Experiment of Power Supply Method for WLAN Sensor Using Both Energy Harvesting and Microwave Power Transmissions," in *Proc. PowerMEMS2014,* Hyogo, Japan, Nov. 2014.

2. Huang, Y., Shinohara, N. and Mitani, T., "Improve the Efficiency-Load Characteristic of Rectifying Circuit Using a Self-Powered DC-DC Converter," in *Proc. WPTC2014,* Jeju, Korea, May 2014, pp.197-200.

3. Huang, Y., Shinohara, N. and Mitani, T., "A Study on Low Power Rectenna Using DC-DC Converter to Track Maximum Power Point," in *Proc. APMC2013,* Soule, Korea, Nov. 2013, pp.83-85.

4. Huang, Y., Mitani, T., Ishikawa, T. and Shinohara, N., "Experiments on Driving a Low-power DC Motor by Microwave Power Transfer," in *Proc. WPTC2015* (under review).

Proceedings of Domestic Conference

1. Huang, Y., Ishikawa, T., Shinohara, N. and Mitani, T., "A Study of Driving Low Power DC Motor Using Microwave Power Transfer," in *IEICE Technical Report,* WPT2014-61, Kyoto, Nov. 2014 (in Japanese).

2. Ishikawa, T., Huang, Y., Matsumuro, T., Tsukamoto, Y., Nishimura, T., Goto, H., Mitani, T. and Shinohara, N., "Small Demonstration Model of the Microwave Power Transfer System to Electric Vehicle," in *Proceedings of the 2014 IEICE Society Conference,* BI-8-3, Tokushima, Sept. 2014 (in Japanese).

3. Sakaguchi, K., Yamashita, S., Huang, Y., Yamamoto, K., Nishio, T., Morikura, M. and Shinohara, N., "Experiment of Power Supply Method for WLAN Sensor Operated by Microwave Power Transmission and Energy Harvesting," in *Proceedings of the 2014 IEICE Society Conference,* B-21-14, Tokushima, Sept. 2014 (in Japanese).

4. Huang, Y., Shinohara, N. and Mitani, T., "Development of a DC-DC Converter with Constant Input Resistance to Improve the Efficiency of Rectenna,"

in *IEEE AP-S & MTT-S Kansai Young Engineers' Meeting 2013,* Kyoto, Dec. 2013 (in Japanese).

5. Huang, Y., Shinohara, N. and Mitani, T., "Improve the Efficiency-Load Characteristic of a Low Power Rectenna Using a DC-DC Converter," in *IEICE Technical Report,* MW2013-170, Saitama, Dec. 2013 (in Japanese).

6. Huang, Y., Shinohara, N. and Mitani, T., "Development of a DC Power-supply Circuit for Low Power Rectenna II," in *The 16th Space Solar Power System Symposium,* Hamamatsu, Oct. 2013 (in Japanese).

7. Ichihara, T., Mitani, T., Shinohara, N. and Huang, Y., "Study on an Intermittent Microwave Power Transmission to a ZigBee device II," in *IEICE Technical Report,* WPT2012-49, Uji, Mar. 2013 (in Japanese).

8. Huang, Y., Shinohara, N. and Mitani, T., "Development of a DC Power-supply Circuit for a Low Power Rectenna," in *IEICE Technical Report,* MW2012-108, Utsunomiya, Oct. 2012.

Other Publications

Major Publications

1. Sakui, M., Huang, Y., Amei, K. and Ohji, T., "A Method of 2 Pulses Switching for Single-Phase Voltage-Double PFC Converter with Partial Switching Circuit," *IEEJ Transactions on Industry Applications,* Vol.131, No.6, pp.862-863, June 2011 (in Japanese).

Proceedings of Domestic Conference

1. Sakui, M., Huang, Y., Amei, K. and Ohji, T., "A Method of 2 Pulses Switching for Single-Phase Voltage-Double PFC Converter with Partial Switching Circuit," in *The 28th National Conference of the Institute of Electrical Installation Engineers of Japan,* Shinjuku, Aug. 2010 (in Japanese).

Awards

1. 「2013 KDDI Scholarship for International Students」
2. 「2014 Chinese Government Award for Outstanding Self-financed Students Abroad」

Appendix A

Single Shunt Rectifying Circuit

Figure A.1 shows a block diagram of a general rectenna which usually contains an antenna, an input filter, a rectifying component, an output filter and a load. A rectifying circuit is a rectenna circuit without antennas. Many researchers usually discuss the antenna and the rectifying circuit separately. A single shunt rectifying circuit is often used in the rectenna because it performs a high efficiency with a simple circuit structure. The single shunt rectifying circuit has full-wave rectifying capability with one single diode. As shown in Fig. A.2, a single shunt rectifying circuit usually contains an input filter, a rectifying diode, a $\lambda_g/4$ line, a capacitor and a load. Referring to [58], the theory of the single shunt rectifying circuit can be explained as follows.

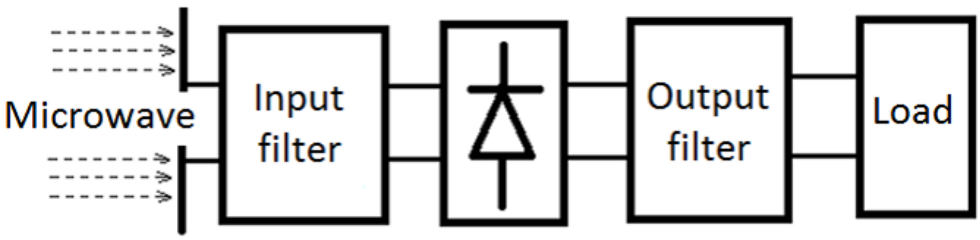

Figure A.1: Block diagram of a general rectenna. It usually contains an antenna, an input filter, a rectifying component, an output filter and a load.

As shown in Fig. A.2, the current $I_1(t)$ is still the high frequency sine wave which can be expressed with Eq. (A.1) and the waveform is shown in Fig. A.3.

$$I_1(t) = I_0 \sin(\omega t). \tag{A.1}$$

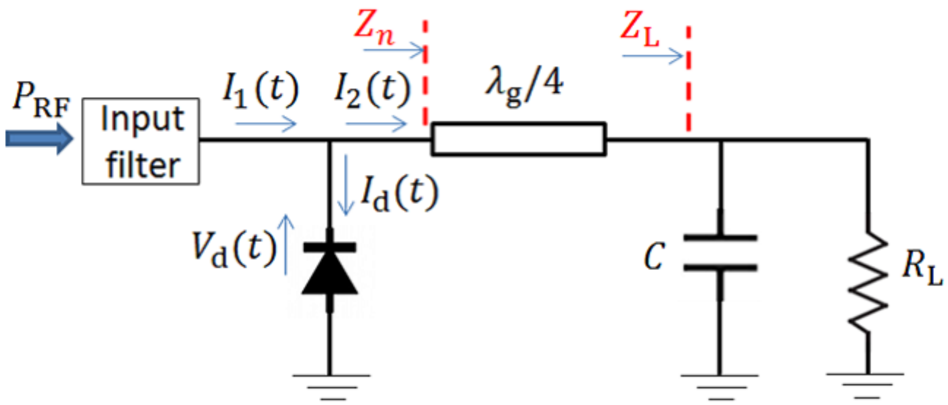

Figure A.2: Block diagram of a single shunt rectifying circuit. It usually contains an input filter, a rectifying diode, a $\lambda_g/4$ line, a capacitor and a load.

Suppose the rectifying diode is ideal, then the diode is open at half period of $0 \leq \omega t < \pi$. It yields the current $I_2(t)$ as following:

$$I_2(t) = I_0 \sin(\omega t), (0 \leq \omega t < \pi). \tag{A.2}$$

Additionally, for rectifying circuit, the impedance of the output filter Z_n seems to be open for odd harmonics and short for even harmonics. It means that only even harmonics current flows through $I_2(t)$. Therefore, $I_2(t)$ satisfies:

$$I_2(\omega t + \pi) = I_2(\omega t). \tag{A.3}$$

Combine Eqs. (A.2) and (A.3), $I_2(t)$ can be rewritten as following:

$$I_2(t) = I_0 |\sin(\omega t)|, (0 \leq \omega t < 2\pi), \tag{A.4}$$

and the waveform of $I_2(t)$ is shown in Fig. A.4 which is a full-wave rectified waveform.

As for the diode current I_d, it satisfies $I_\mathrm{d} = I_1 - I_2$. Then:

$$I_\mathrm{d}(t) = I_0 \sin(\omega t) - I_0 |\sin(\omega t)|, \tag{A.5}$$

which indicates that the diode current I_d is a half-wave rectified waveform. As for the diode voltage V_d, it is 0 when the diode is on. When diode is off, the voltage applied on the diode includes the DC voltage at the load port (V_L) and the odd harmonics components. Therefore, the diode voltage V_d can be written as:

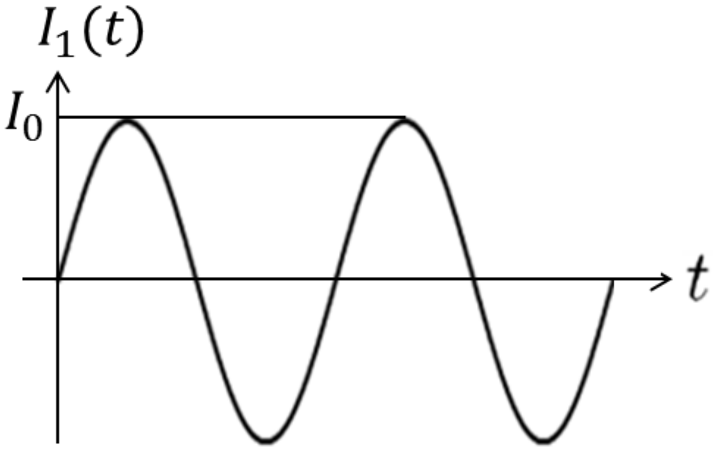

Figure A.3: Current waveform of I_1.

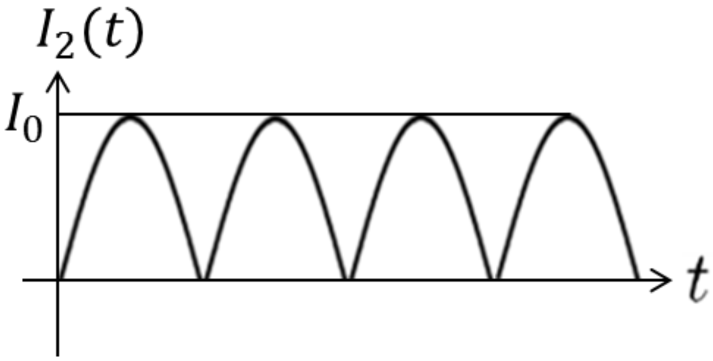

Figure A.4: Current waveform of I_2.

$$V_{\mathrm{d}}(t) = \begin{cases} 2V_{\mathrm{L}}, (0 \leq \omega t < \pi) \\ 0, (\pi \leq \omega t < 2\pi) \end{cases} \tag{A.6}$$

Figure A.5 shows the waveform of V_{d} and I_{d}.

As shown in Fig. A.2, the impedance of Z_{L} and Z_{n} can be written as following:

$$Z_{\mathrm{L}} = \frac{1}{j\omega C + \frac{1}{R_{\mathrm{L}}}}, \tag{A.7}$$

$$Z_{\mathrm{n}} = \frac{Z_{\mathrm{L}} + jZ_0 \tan(\beta_{\mathrm{n}}\lambda_{\mathrm{g}}/4)}{Z_0 + jZ_{\mathrm{L}} \tan(\beta_{\mathrm{n}}\lambda_{\mathrm{g}}/4)} Z_0. \tag{A.8}$$

where Z_0 is the characteristic impedance and β_{n} is the phase velocity. ωC is close to infinity as capacitance C is large enough for high frequency. As a result, Z_{L}

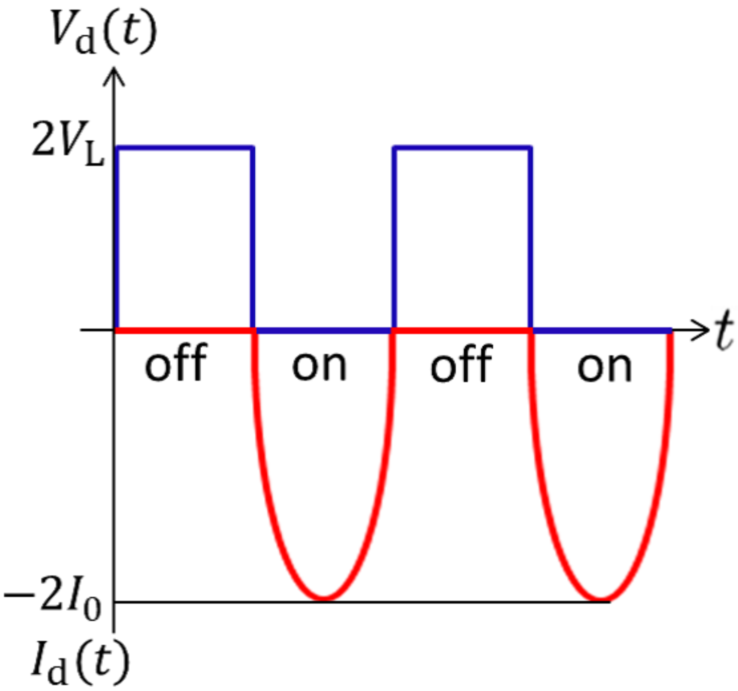

Figure A.5: Voltage and current waveforms of the diode: V_d, I_d.

is close to 0 when ωC is close to infinity. In this case, the impedance Z_n can be rewritten as follows:

$$Z_n = \begin{cases} Z_L, \text{close to } 0 \text{ (even harmonics)} \\ \frac{Z_0^2}{Z_L}, \text{close to } \infty \text{ (odd harmonics)}, \end{cases} \tag{A.9}$$

which indicates that the impedance of the output filter Z_n is open for odd harmonics and is 0 for even harmonics. Thus, the single shunt rectifying circuit is similar to the class-F amplifier in addressing harmonics problems. Consequently, the single shunt rectifying circuit is also named as class-F rectifier.